CHAPTER 1

Introduction

1.1. Background

1.1.1 The greenhouse gas methane (CH_4)

Methane (CH_4) is an important greenhouse gas as it contribute to approximately 32% of the radiative forcing of the global climate, because it has 28 times as much global warming potential (i.e., the ratio of warming that occurs as a result of radiative absorption by a gas) as CO_2 in a 100-year time horizon (IPCC 2014). CH_4 concentration in the atmosphere has nearly tripled since pre-industrial times, but the rate of increase has reduced to nearly zero since the 1990s (Dlugokencky et al., 2011). Surface-based observations from four networks (National Oceanic and Atmospheric Administration, NOAA; Advanced Global Atmospheric Gases Experiment, AGAGE; Commonwealth Scientific and Industrial Research Organization, CSIRO; and University of California Irvine, UCI) showed that the concentration was stabilized from 1999 to 2006 to 1773 ± 3 ppb. Since 2007, CH_4 levels have been rising again at a rate of approximately 0.5% per year (Rigby et al., 2008). Some studies suggest that the recent resumption of increasing atmospheric CH_4 is a result of an increase in emissions from northern wetlands and tropical wetlands. The increase in emissions from these regions is attributed to anomalously high temperatures and above-average amounts of precipitation. According to studies, biomass burning in the tropics is also thought to contribute to rising atmospheric CH_4 concentrations (Dlugokencky et al., 2009). Hydroxyl radial (OH) chemistry has also been suggested to be a key influence on the recent change in atmospheric CH_4 levels (Rigby et al., 2008).

Sources and sinks of CH_4 and the processes controlling their variability must be accurately identified and understood in order to predict the influence of climate change on global CH_4 budgets and to develop mitigation strategies. Derived from process studies termed “bottom-up”, estimations of CH_4 levels estimated from natural sources are 238–484 Tg CH_4 yr^{-1} (Kirschke et al., 2013). The breakdown of the natural sources are 177–284 Tg CH_4 yr^{-1} from natural wetlands, 8–73 Tg CH_4 yr^{-1} from fresh water

(lakes and rivers), 15–15 Tg CH_4 yr^{-1} from wild animals, 1–5 Tg CH_4 yr^{-1} from wildfires, 2–22 Tg CH_4 yr^{-1} from termites, 33–75 Tg CH_4 yr^{-1} from geological (including ocean), 2–9 Tg CH_4 yr^{-1} from hydrates, and 0–1 Tg CH_4 yr^{-1} from permafrost (Kirschke et al., 2013). The breakdown CH_4 emissions from anthropogenic sources are 187–224 Tg CH_4 yr^{-1} from agriculture and waste (waste decomposition, rice cultivation, and domestic ruminants), 32–39 Tg CH_4 yr^{-1} from biomass burning (including biofuels), and 85–105 Tg CH_4 yr^{-1} from fossil fuels (Kirschke et al., 2013).

While natural and anthropogenic sources contributing greatly to atmospheric CH_4 levels, the primary sink for atmospheric CH_4 is developed from a chemical reaction with OH, mostly occurring in the troposphere (Lelieveld and Crutzen, 1992). Bottom-up estimates of total CH_4 sinks are 592–785 Tg CH_4 yr^{-1} (Kirschke et al., 2013). The breakdowns of the sinks are 483–738 Tg CH_4 yr^{-1} by chemical loss and 9–47 Tg CH_4 yr^{-1} by soils (Kirschke et al., 2013). Each article has large variability, and global estimates derived from bottom-up approaches are generally much larger than those derived from "top-down" estimate (Kirschke et al., 2013). Top-down approach is based on atmospheric inversion models. These models determine optimal surface sources and sinks that best fit atmospheric CH_4 observations given an atmospheric transport model that includes chemistry, prior estimates of the source and sink magnitudes, and their uncertainties. Much more accumulation of data about CH_4 exchanges at each ecosystem-scale is necessary to close the gap.

1.1.2 Complex CH_4 dynamics in forest ecosystems under Asian monsoon climate

Soils play important roles as CH_4 sources and sinks. CH_4 is produced in anoxic environments, including submerged soils, by methanogenic bacteria during the anaerobic digestion of organic matter. On the contrary, CH_4 is oxidized by methanotorophic bacteria in upland soils. Above all, forest soils are recognized as the most efficient sinks for atmospheric CH_4, because of their CH_4 oxidation capacity in water-unsaturated soil (Le Mer and Roger, 2001).

However, I hypothesized that forest ecosystems, especially in wet warm climates such as Asian monsoon climate, are not always CH_4 sinks. Although such forests mainly consist of water-unsaturated

forest soils, they commonly have wetlands in the riparian zones within the watershed. When evaluating CH_4 budget as a whole forest watershed, CH_4 emission from sparsely distributed wetlands are hardly taken into account because they often cover a small fraction of the watershed. However, chamber studies in a temperate Asian monsoon forest revealed CH_4 flux (emission or absorption rates) ranging from approximately 0 to 720 nmol m^{-2} s^{-1} in wetlands and from -1.7 to 1.4 nmol m^{-2} s^{-1} in water-unsaturated forest floors. Thus, the emissions from wetlands were suggested to be large enough to turn the entire watershed into a net CH_4 source during high-temperature season, even though the source area was very limited (Itoh et al., 2005, 2007, 2009).

In addition, both CH_4 absorption in water-unsaturated forest soils and CH_4 emission from wetlands would be greatly influenced by intensive summer rainfall under Asian monsoon climate. There is a possibility that water-unsaturated soil switches from CH_4 sink to CH_4 source by rainfall. Some upland soils could be CH_4 source when soils become water-saturated following precipitation events (Silver et al., 1999; Savage et al., 1997; Van den Pol-van et al., 1998). Moreover, Wang and Bettany (1997) also reported that upland soils that were incubated anaerobically began producing CH_4 within days or weeks. The CH_4 dynamics in forest ecosystems under Asian monsoon climate would have spatially and temporally heterogeneous variability in each compartment.

1.1.3 Techniques of CH_4 flux measurements: chamber and micrometeorological methods

The main CH_4 flux measurement techniques are the chamber method and the micrometeorological method. The former is a more traditional method to measure CH_4 flux of the two methods. The chamber method is useful for understanding the process controlling CH_4 fluxes on small spatial scales (usually less than 1 m^2). The most traditional chamber method is the static closed chamber method, which involves manual collection of gas from the headspace of a chamber over a time course (typically < 1 hour) by use of a syringe and vials that are subsequently analyzed by gas chromatography in a laboratory. The advantage of this method is that the low cost chamber allows multi-point measurements that increase the chance to find CH_4 emission and absorption hot spots. Because the work can be labor-

intensive and time-consuming, the disadvantage of this method is the low-time resolution. Recently, the availability of fast-response laser-based CH_4 analyzers enabled in-situ methods for continuously measuring soil CH_4 flux with chambers that open and close automatically (Savage et al., 2014; Lai et al., 2014). The high-time resolution measurements allow for detection of responses of CH_4 fluxes to rapidly changing environments such as increase of soil water contents after rainfall. The disadvantages of this method are the relatively high cost of the chamber and the difficulties in making multi-point measurements with it. Moreover, chamber methods (including manually operated and automated chambers) are often criticized because of the changes in environmental factors (generally referred to as "chamber effects") such as influence of wind, increase in air temperature, or decrease in light intensity during the chamber closure (Denmead, 1994). More importantly, the chamber measurements have a problem of poor spatial representation when estimating ecosystem-scale fluxes in heterogeneous terrain such as CH_4 dynamics in forest.

Micrometeorological methods such as eddy covariance method (EC method) measures net vertical turbulent CH_4 fluxes between the atmosphere and surface (vegetation and soil). These fluxes represent the integrated net fluxes from the landscape upwind from the measurement point. The EC method has advantages over the chamber method in that it does not disturb the soil surface microenvironment, and it is ideally suited for continuous ecosystem-scale flux measurements integrated over a larger area without artificial disturbance (Baldocchi et al., 2001). Global networks of micrometeorological flux measurement sites, such as FLUXNET, that measure the exchange of CO_2, H_2O, energy, and sometimes CH_4 between the biosphere and atmosphere now consist of over 650 sites operating on a long-term and continuous basis. Japan participates as Japan Flux, and 30 sites are registered.

The EC method has not been used for CH_4 measurements until recently because it requires a fast-response and high-precision gas analyzer. Recent technological advances in CH_4 analyzers opened the possibility of long-term EC measurement of CH_4 in a variety of ecosystems. Previously, a limited number of CH_4 EC measurements have been obtained in peatlands (Hendriks et al., 2008; Schrier-Uijl et al., 2009), rice paddy fields (Simpson et al., 1994), and prairies (Kim et al., 1998a, b). Most research

on CH_4 fluxes from natural ecosystems has focused on wetlands or rice paddy fields, which are thought to be large CH_4 sources and thus important components of the global CH_4 budget. The lack of long-term CH_4 flux observations in forest ecosystems restricts our understanding of ecosystem-scale CH_4 dynamics. Measuring CH_4 exchange over forest ecosystems is still challenging in comparison to measuring the exchange in wetlands and rice paddy fields because of the small fluxes in forests (Smeets et al., 2009). Even with the state-of-the-art CH_4 analyzer, precisions are still insufficient to measure small CH_4 fluxes in forest ecosystems if the CH_4 fluxes are measured by chamber techniques (Itoh et al., 2005, 2007, 2009) assumed to be representative to the ecosystem-scale exchange. There inherent limitations of CH_4 analyzers have made it difficult to evaluate CH_4 dynamics in whole forest ecosystems. Although the state-of-of-the-art CH_4 analyzers are insufficient for the EC measurements, those analyzers are useful in CH_4 flux measurements by use of a micrometeorological relaxed eddy accumulation (REA) method (Businger and Oncley 1990; Hamotani et al., 1996, 2001). The flux, calculated by the REA method, is equal to the difference in the mean concentrations of the trace gas of interest associated with updraft and downdraft, multiplied by the standard deviation of the vertical wind velocity and an empirical coefficient *b*. CH_4 concentration measurement with the REA method can take more time, so a laser signal can be averaged to optimize the instrumental sensitivity and higher precision of a laser-based CH_4 analyzer can be achieved. Averaging the laser signals reduces random noise, while inadequately long averaging causes drift effect. Therefore, there is an optimal averaging time at which maximum precision is reached. Furthermore, the REA method can choose optimal integration time, which maximizes the precision of CH_4 analyzer. However, both the EC and REA methods have limitations in that they are most applicable over horizontally homogeneous areas in flat terrain and in atmospheric steady-state conditions. It has been suggested that the measurement of total fluxes can be underestimated during nighttime, low turbulence conditions due to the large concentration buildup in the nocturnal boundary layer (Goulden et al., 1996; Gu et al., 2005). Moreover, instead of the acquirement of spatially integrated flux, the method is not suitable for determining the relationship between CH_4 flux and environmental factors for each compartment.

1.2. Objectives

CH_4 fluxes in forest ecosystems under Asian monsoon climate could have wide-ranging spatiotemporal variability in emission and absorption due to wide spatiotemporal ranges in soil water status. In order to assess CH_4 dynamics at ecosystem-scale, the application of micrometeorological method is necessary. On the other hand, in order to understand the processes of variability, application of plot-scale measurements at key compartments in forests, such as wetland and water-unsaturated forest floor, are also necessary. In this study, I conducted three approaches to measuring the CH_4 fluxes in a temperate forest under Asian monsoon climate located in Shiga Prefecture, central Japan (Kiryu Experimental Watershed: KEW). At KEW, amount of precipitation and discharge have been measured since 1967. Ecosystem-scale CO_2 flux has been measured since 2001. Soil CH_4 flux has also measured in wetland and water-unsaturated forest floor by manual static chamber with GC analyzer (Itoh et al., 2005, 2007, 2009). This site is one of the few sites that long-term micrometeorological CO_2 flux data and soil CH_4 flux data are available. Plot-scale soil CH_4 fluxes were measured using the manual and continuous automated chamber methods, and ecosystem-scale CH_4 fluxes were measured using the REA method. All measurements were conducted with laser-based CH_4 analyzers.

In chapter 2, I investigated general spatial and seasonal variability in soil CH_4 fluxes in wetland and water-unsaturated forest floors. A total of 120 multi-point measurements and 18 points biweekly regular measurements of soil CH_4 and CO_2 fluxes for two years were conducted by manual chamber method. I also aimed to identify the location and time of hotspot of CH_4 emission and absorption fluxes appeared. In chapter 3, I investigated continuous variations of soil CH_4 and CO_2 fluxes at 3 plots of water-unsaturated forest floor throughout a year with high temporal resolution by using an automatically opening and closing chamber. I assessed how responses of CH_4 and CO_2 fluxes to rapidly changing environments, such as rainfall, were different according to soil water condition and organic matter content. The aim of this chapter was to elucidate (1) the ranges of CH_4 fluxes, (2) the seasonal variations of CH_4 fluxes and environmental factors (soil temperature and soil water content), which influenced their seasonality at each plot, (3) the detailed temporal responses of CH_4 fluxes to rainfall and how they differed depending on the local topography at each

plot, and (4) the annual budgets of CH_4 fluxes that took into consideration the rainfall responses. In chapter 4, I demonstrate the uncertainty in the experimental coefficient *b* in calculation of REA flux by comparing observational *b* among three sites and comparing it with simulated *b*. This chapter, attempts to clarify conditions of which *b* may not be constant and when the variations in *b* need to be taken into account during REA flux calculation. In order to accomplish this, I employs data from three forest sites that cover different forest types and measurement heights at seasonal timescales under various stability conditions. The simulated *b* was derived from another calculation that uses the Monin–Obukhov similarity theory for the integral turbulence characteristics (Kaimal and Finnigann 1994). In chapter 5, I determined continuous ecosystem-scale CH_4 flux throughout a year by using the REA method. I assessed the validity of the REA method by comparing CH_4 flux with CO_2 flux and examining detection limit. The objective of this chapter is to (1) examine whether the REA method is applicable to measurement of CH_4 fluxes over the forest canopy, (2) reveal the amplitude and seasonal variations in ecosystem-scale CH_4 fluxes, and (3) examine the response of ecosystem-scale CH_4 fluxes to rainfall. Finally, I discuss CH_4 dynamics in a typical temperate forest by integrating chamber results in Chapters 2 and 3, and ecosystem-scale CH_4 fluxes in Chapter 5.

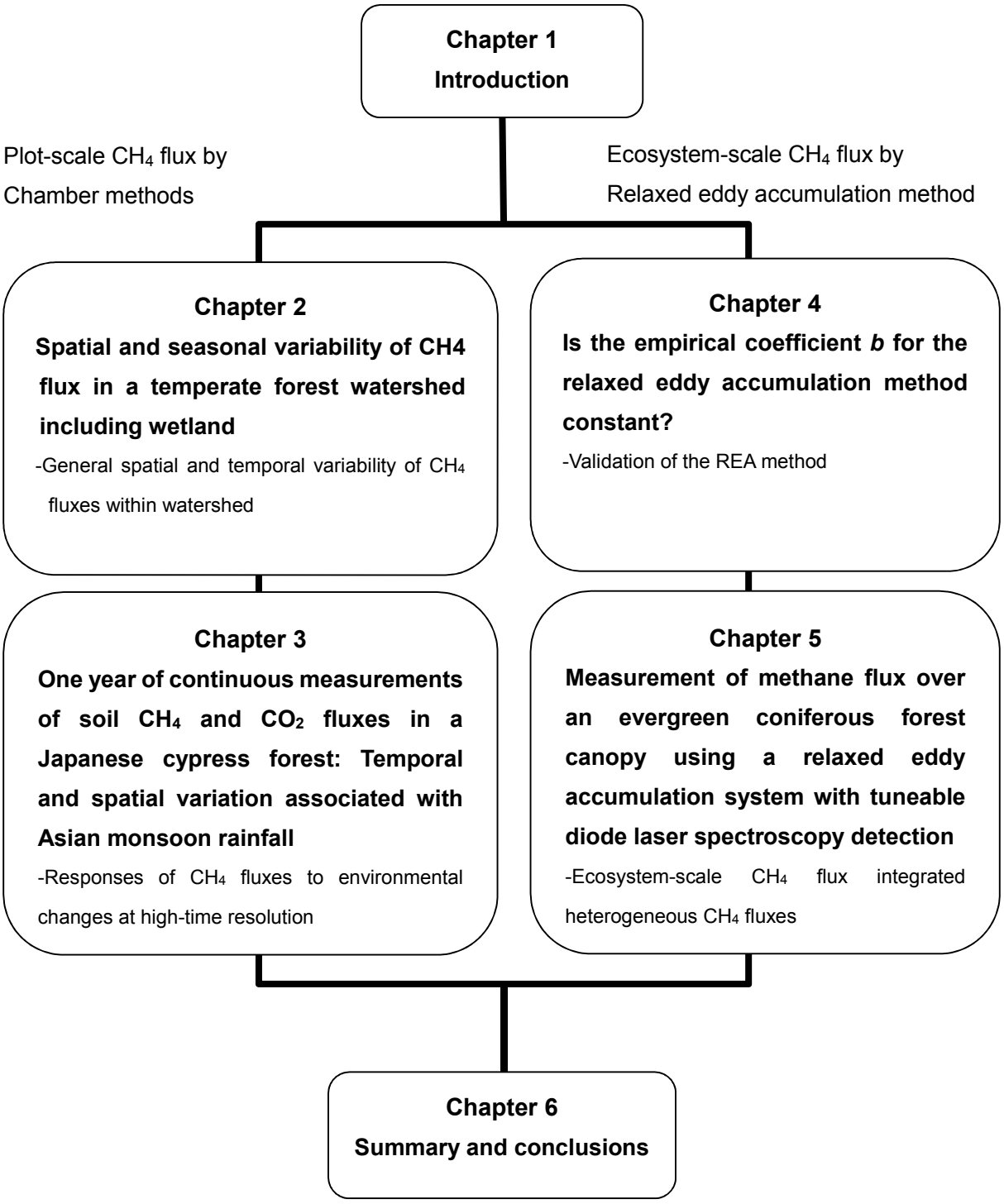

Figure 1.1 Structure of the thesis.

References

Baldocci, D., Falge, E., Gu, L., Olson, R., Hollinger, D., Running, S., Anthoni, P., Bernhofer, C., Davis, K., Evans, R., Fuentes, J., Goldstein, A., Katul, G., Law, B., Lee, X., Malhi, Y., Meyers, T., Munger, W., Oechel, W., Paw U, K.T., Pilegaard, K., Schmid, H.P., Valentini, R., Verma, S., Vesala, T., Wilson, K., and Wofsy, S. (2001) FLUXNET: A new tool to study the temporal and spatial variability of ecosystem-scale carbon dioxide, water vapor, and energy flux densities, Bulletin of the American Meteorological Society, 82, 2415–2434.

Businger, J.A., Oncley, S.P. (1990) Flux measurement with conditional sampling. J. Atmos. Oceanic Technol. 7, 349–352.

Denmead, O.T. (1994) Measuring fluxes of CH_4 and N_2O between agricultural systems and the atmosphere. In: Peng S, Ingram KT, Neue H-U, Ziska LH (eds) Climate change and rice. International Rice Research Institute, Manila, Philippines.

Dlugokencky, E.J., Nisbet, E.G., Fisher, R., and Lowry, D. (2011) Global atmospheric methane: budget, changes and dangers. Phil. Trans. R. Soc. A, 369, 2058–2072, doi: 10.1098/rsta.2010.0341.

Dlugokencky, E.J., Bruhwiler, L., White, J.W.C., Emmons, L.K., Novelli, P.C., Montzka, S.A., Masarie, K.A., Lang, P.M., Crotwell, A.M., and Miller, J.B (2009) Observational constraints on recent increases in the atmospheric CH_4 burden. Geophysical Research Letters, 36, doi: 10.1029/2009GL039780.

Goulden, M.L., Munger, J.W., Fan, S., Daube, B.C., and Wofsy, S.C. (1996) Measurements of carbon sequestration by long-term eddy covariance: methods and a critical evaluation of accuracy. Global Change Biology, 2, 169–182.

Gu, L., Falge, E.M., Boden, T., Baldocchi, D.D., Black, T.A., Saleska, S.R., Suni, T., Verma, S.B., Vesala, T., Wofsy, S.C., and Xu, L. (2005) Objective threshold determination for nighttime eddy flux filtering. Agricultural and Forest Meteorology, 128, 179–197.

Hamotani, K., Monji, N., Yamaguchi, K. (2001) Development of a long-term CO_2 flux measurement system using REA method with density correction. J. Agric. Meteorol. 57, 93–99.

Hamotani, K., Uchida, Y., Monji, N., Miyata, A. (1996) A system of the relaxed eddy accumulation method to evaluate CO_2 flux over plant canopies. J. Agric. Meteorol. 52, 135–139.

Hendriks, D.M.D., Dolman, A.J., van der Molen, M.K., van Huissteden, J. (2008) A compact and stable eddy covariance set-up for methane measurements using off-axis integrated cavity output spectroscopy. Atmos. Chem. Phys. 8, 431–443.

Itoh, M., Ohte, N., and Koba, K. (2009) Methane flux characteristics in forest soils under an East Asian monsoon climate, Soil Biol. Biochem., 41, 388–395, doi: 10.1016/j.soilbio.2008.12.003.

Itoh, M., Ohte, N., Koba, K., Katsuyama, M., Hayamizu, K., and Tani, M. (2007) Hydrologic effects on methane dynamics in riparian wetlands in a temperate forest catchment, J. Geophys. Res., 112, G01019, doi: 10.1029/2006JG000240.

Itoh, M., Ohte, N., Katsuyama, M., Koba, K., Kawasaki, M., and Tani, M. (2009) Temporal and spatial variability of methane flux in a temperate forest watershed, J. Japan Soc. Hydrol. Water Resor., 18, 244–256.

Kaimal, J.C., Finnigan, J.J. (1994) Atmospheric boundary layer flows, their structure and measurement. Oxford University Press, New York 289 pp.

Kim, J., Verma, S.B., Billesbach, D.P. (1998a) Seasonal variation in methane emission from a temperate Phragmites-dominated marsh: effect of growth stage and plant-mediated transport. Global Change Biol. 5, 433–440.

Kim, J., Verma, S.B., Billesbach, D.P., Clement, R.J. (1998b) Diel variation in methane emission from a midlatitude prairie wetland: significance of convective throughflow in Phragmites australis. J. Geophys. Res. 103:28,029–28,039.

Kirschke, S., Bousquet, P., Ciais, P., Saunois, M., Canadell, J.G., Dlugokencky, E.J., Bergamaschi, P., Bergmann, D., Blake, D.R., Bruhwiler, L., Cameron-Smith, P., Castaldi, S., Chevallier, F., Feng, L., Fraser, A., Heimann, M., Hodson, E.L., Houweling, S., Josse, B., Fraser, P., Krummel, P.B., Lamarque, J., Langenfelds, R.L., Le Quéré, C., Nail, V., O'Doherty, S., Palmer, P.I., Pison, I., Plummer, D., Poulter, B., Prinn, R.G., Rigby, M., Ringeval, B., Santini, M.,

Schmidt, M., Shindell, D.T., Simpson, I.J., Spahni, R., Steele, L.P., Strode, S.A., Sudo, K., Szopa, S., van der Werf, G.R., Voulgarakis, A., van Weele, M., Weiss, R.F., Williams, J.E., and Zeng, G. (2013) Three decades of global methane sources and sinks, Nature Geosci., 6, 813–823, doi: 10.1038/NGEO1955.

Lai, D.Y.F., Moore, T.R., and Roulet, N.T. (2014) Spatial and temporal variations of methane flux measured by autochambers in a temperate ombrotrophic peatland, J. Geophys. Res. Biogeosci., 119, doi: 10.1002/2013JG002410.

Le Mer, J., and Roger, P. (2001) Production, oxidation, emission and consumption of methane by soils: A review, Eur. J. Soil Biol., 37, 25–50.

Lelieveld, J., and Crutzen, P. J. (1992) Indirect chemical effects of methane on climate warning, Nature, 335, 339–342.

Rigby, M., Prinn, R.G., Fraser, P.J., Simmonds, P.G., Langenfelds, R.L., Huang, J., Cunnold, D.M., Steele, L.P., Krummel, P.B., Weiss, R.F., O'Doherty, S., Salameh, P.K., Wang, H.J., Harth, C.M., Mühle, J., and Porter, L.W. (2008) Renewed growth of atmospheric methane. Geophysical Research Letters, 35, doi: 10.1029/2008GL036037.

Savage, K., Phillips, R., and Davidson, E. (2014) High temporal frequency measurements of greenhouse gas emissions from soils, Biogeosciences, 11, 2709–2720, doi: 10.5194/bg-11-2709-2014.

Savage, K., Moore, T.R., Crill, P.M. (1997) Methane and carbon dioxide exchanges between the atmosphere and northern boreal forest soils. J. Geophys. Res. 102:29279–29288.

Schrier-Uijl, A.P., Veenendaal, E.M., Leffelaar, P.A., van Huissteden, J.C., Berendse, F. (2009) Methane emissions in two drained peat agro-ecosystems with high and low agricultural intensity. Plant Soil. doi:10.1007/s11104-009-0180-1.

Silver, W.L., Lugo, A.E., Keller, M. (1999) Soil oxygen availability and biogeochemistry along rainfall and topographic gradients in upland wet tropical forests soil. Biogeochemistry. 44, 301–328.

Simpson, I.J., Thurtell, G.W., Kidd, G.E., Lin, M., Demetriades-Shah, T.H., Flitcroft, I.D., Kanemasu, E.T., Nie, D., Bronson, K.F., Neue, H.U. (1994) Tunable diode laser measurements of

methane fluxes from an irrigated rice paddy field in the Philippines. J. Geophys. Res. 100, 7283–7290.

Smeets, C.J.P.P., Holzinger, R., Vigano, I., Goldstein, A.H., Röckmann, T. (2009) Eddy covariance methane measurements at a Ponderosa pine plantation in California. Atmos. Chem. Phys. 9, 8365–8375.

Stocker, T.F., Qin, D., Plattner, G.-K., Alexander, L.V., Allen, S.K., Bindoff, N.L., Brëon, F.–M., Church, J.A., Cubasch, U., Emori, S., Forster, P., Friedlingstein, P., Gillett, N., Gregory, J.M., Hartmann, D.L., Jansen, E., Kirtman, B., Knutti, R., Krishna Kumar, K., Lemke, P., Marotzke, J., Masson-Delmotte, V., Meehl, G.A., Mokhov, I.I., Piao, S., Ramaswamy, V., Randall, D., Rhein, M., Rojas, M., Sabine, C., Shindell, D., Talley, L.D., Vaughan, D.G., and Xie, S.–P. (2013) Technical Summary. In: Climate Change 2013: The Physical Science Basis. Contribution of Working Group I to the Fifth Assessment Report of the Intergovernmental Panel on Climate Change, edited by Stocker, T. F., Qin, D., Plattner, G. –K., Tignor, M., Allen, S. K., Boschung, J., Nauels, A., Xia, Y., Bex, V., and Midgley, P. M., Cambridge University Press, Cambridge, United Kingdom and New York, NY, USA.

van den Pol-van Dasselaar, A., van Beusichem, M.L., Oenema, O. (1998) Effects of soil moisture content and temperature on methane uptake by grasslands on sandy soils. Plant Soil. 204, 213-222.

Wang, F.L., Bettany, J.R. (1997) Methane emission from Canadian prairie and forest soils under short term flooding conditions. Nutr. Cycling Agroecosyst. 49, 197–202.

CHAPTER 2

Spatial and seasonal variability in methane fluxes in a temperate Asian monsoon forest

1. Introduction

In this chapter, I focused on CH_4 dynamics in forest regions with humid summers, such as the region of Monsoon Asian. Although such forests mainly consist of water-unsaturated soils, they commonly have riparian areas within a watershed. When evaluating CH_4 dynamics in a whole forest watershed, emission rates from sparsely distributed wetlands usually are not taken into account, because they cover a small fraction of the watershed; however, chamber studies in temperate Asian monsoon forest revealed that CH_4 flux ranged from 0 to 720 nmol m^{-2} s^{-1} in wetland and from -1.7 to 1.4 nmol m^{-2} s^{-1} in water-unsaturated forest floor. Therefore, CH_4 emission rates from wetlands are large enough to turn the entire watershed into a net CH_4 source, even though the source areas are very limited (Itoh et al., 2005, 2007, 2009). Another chamber study in Scottish peatland revealed that riparian area was a significant CH_4 hotspot contributing approximately ~12% of the total catchment emissions, whilst covering only ~0.5% of the catchment area (Dinsmore et al., 2009). Therefore, it is important to investigate the range and variation patterns of CH_4 fluxes in wetlands, in order to understand the regulating factors of ecosystem-scale CH_4 fluxes.

Traditionally, the static closed chamber method has been used for measuring CH_4 fluxes. This method involves manual collection of gas samples from the chamber headspace at regular intervals over a time course (typically < 1 hour) and analysis by gas chromatography (GC) in laboratory. The advantage of this method is that the low-cost chamber allows multi-point measurements and increases the chance to find CH_4-emission and absorption hotspots.

In forest ecosystems, CH_4 fluxes might have large spatial and seasonal variation. Previous studies that investigated the spatial and seasonal variation in CH_4 fluxes and conducted in wetland, using the closed chamber method, showed that spatial variability of CH_4 flux was due to the differences in particle

size, which affected gas diffusivity (Dorr et al., 1993) or bacterial phase (Wagner et al., 1999). In water-unsaturated forest floor, CH_4 absorption was reported to increase as soil water content decreased (Steudler et al., 1989; Whalen, 1990; Adamsen and King, 1993; Dobbie and Smith, 1996) or as organic matter content at the surface increased (Wang et al., 1993; Whiting and Chantason, 1993; Schimel, 1995; Grosso et al., 2000).

The objective here was to: (1) reveal spatial and seasonal variation in CH_4 fluxes in a temperate Asian monsoon forest by conducting 120 multi-point CH_4 flux measurements and biweekly regular measurements over a 2-year period using a laser based CH_4 analyzer and (2) identify the location and time at which CH_4 emission and absorption hotspot occur.

2.2 Methods

2.2.1 Site description

All observations were made in a temperate coniferous forest at the Kiryu Experimental Watershed (KEW; 35°N, 136°E; 190-255 m above sea level; 5.99 ha), located in Shiga Prefecture, central Japan. The entire watershed was underlain by weathered granite with abundant amounts of albite. The soil type was typical brown forest soil and predominantly Cambisols. The physical and chemical properties of the soil in the watershed were as descried by Ohte et al. (1997). The forest comprised 55-year-old Japanese cypress (*Chamaecyparis obtuse* Sieb. et Zucc.) trees, which were planted in 1959. In 2014, the mean tree height was approximately 17.3 m, and the mean diameter at breast height was 0.19 m. The forest also included sparsely distributed Japanese red pine (*Pinus densiflora*) trees and various broadleaf trees. Some wetlands were located in riparian zones along streams within the watershed, which were either permanently or periodically submerged. The study wetland area was 100–10^2 m^2 and located upstream of check dams that constructed across the main stream approximately 100 years ago to prevent soil erosion (Figure 2.1a). The size of this area could be slightly increased after rainfall. Soils and sediment at KEW were composed predominantly of coarse sand, while some sediments consisted of fine-grained organic mud. Although several tree species (*Alnus japonica*, *Clethra barvinervis*, *Evodiopanax innovans*, and *Rhus trichocarpa*) and sphagnum grew in and around the wetland,

vegetation in the wetland was sparse, probably because of occasional sediment transport with surface flow. The study site had a warm-temperate monsoon climate. Between 2000 and 2010, the mean annual air temperature was 13.4°C and precipitation 1578 mm yr^{-1}. Rainfall occurred throughout the year with two peaks during summer: the early summer 'Baiu' front season and the late summer typhoon season. CH_4 fluxes from wetland and water-unsaturated forest floor were investigated using a static closed chamber method with a GC analyzer (Itoh et al., 2005, 2007, 2009).

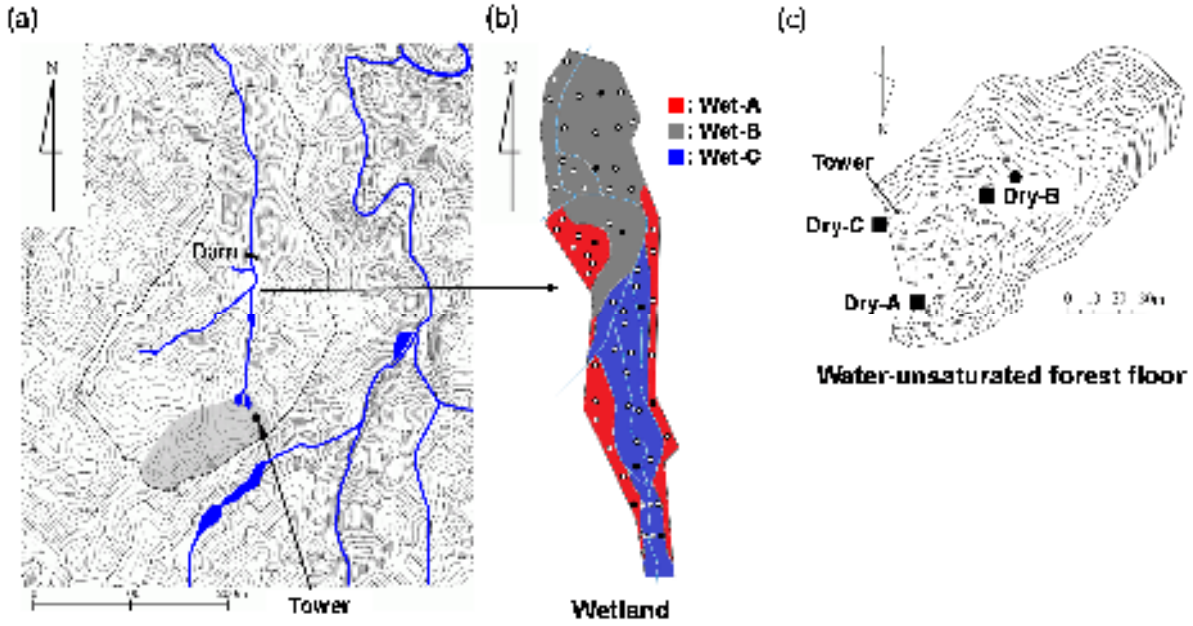

Figure 2.1 Site-description of the Kiryu Experimental Watershed forest in Japan. (a) Topographic large-scale map; the streams are shown as blue lines, and riparian zones are located along the streams. Main wetland areas are shown in blue. (b) Topographic small-scale map of the main wetland. Red zone was identified as Wet-A, gray zone was identified as Wet-B, and blue zone was identified as Wet-C. White dots represent measurement points of multi-point chamber measurements, and black dots represent points of regular chamber measurements. (c) Topographic small-scale map of water-unsaturated forest floor shown in gray in Figure 2.1 (a). The square denotes the location of three measurement plots. Twenty chambers in each plot were placed on a coordinate grid 5 × 4 m at 1-m intervals, and 3 points diagonally to the grid.

2.2.2 Sampling plots

Three plots were established in wetlands according to the particle size: (1) a plot with small particle size composed of mud over litter (Wet-A), (2) a plot with medium particle size composed of mud over gravel (Wet-B), and (3) a plot with large particle size composed of gravel over sparsely litter (Wet-C). Twenty points in each plot were equally spaced as shown in Figure 2.1b.

Similarly, three plots were established in water-unsaturated forest floor according to slope position and organic matter content (Figure 2.1c): (1) a plot located in the lower part of the slope along the stream with a subsurface aquifer all year round an a top layer, consisting of fresh and partially decomposed leaves (0.02-0.03 m depth) below which there was a 0.05-m deep A horizon termed the litter layer and humus layer (Dry-A), respectively, (2) a plot located in the middle part of the slope with subsurface aquifer, except for the driest period and a top layer consisted of a 0-0.02-m deep litter layer, below which there was a 0.07-m deep humus layer (Dry-B), and (3) a plot located in the upper part of the slope and occasionally had a subsurface aquifer with a shallow litter layer (0-0.01 m depth) and no humus layer (Dry-C). Twenty points on each plot were placed on a 5 × 4 m coordinate grid at 1-m intervals.

2.2.3 Soil CH_4 and CO_2 flux measurements

Soil CH_4 and CO_2 fluxes were measured by the dynamic closed chamber method. Chambers consisted of a commercially available 195-mm high PVC bucket (188 mm diameter) with the bottom removed and inserted 5-10 mm into the soil for more than one day before the measurement. Chambers remained in-situ throughout the experiment period. A vented PVC chamber top was fit securely over the collars to create a closed chamber during the measurement. The top of the PVC chamber in wetland was connected to a laser-based $CH_4/CO_2/H_2O$ analyzer (FGGA907-0010, Los Gatos Research, CA, USA) through a polyethylene tube (4 mm inner diameter), while in water-unsaturated forest floor it was connected to a laser-based CH_4 analyzer (FMA-100, Los Gatos Research, CA, USA) and a CO_2/H_2O analyzer (LI-840; Li-Cor Inc., Lincoln, NE, USA). The instrumental performance of both CH_4 analyzers was comparatively examined using the Allan variance analysis before deploying the analyzers in the field. The assessment showed that Allan deviations of both analyzers were similar (approximately 0.7

ppb) for 1-sec signal integration at atmospheric concentration levels and these results were in agreement with a previously reported study (Eugster and Plüss, 2011). A 2-sec moving average filtered the high frequency noises for CO_2/H_2O data, and 1-sec moving average was used for CH_4 data. The chamber remained closed for 3-5 min, and air from the sample chamber was circulated through the analyzer by a diaphragm pump within the analyzer. Sampled air was pre-dried using a gas dryer (PD-50T-48, Perma Pure Inc., Toms River, NJ, USA) before flowing into the analyzer. Dilution by water vapor, which could not be completely removed from the drying system, was corrected using the H_2O concentration measurement by FGGA907-0010 or LI-840 analyzers. Data were recorded at 1 Hz by the CR1000 data logger (CR1000, Campbell Scientific) and stored on a compact flash card using a compact flash module (CFM100, Campbell Scientific).

Soil CH_4 and CO_2 fluxes were deduced from the rate of change in gas concentrations with time, as determined using the following linear regression (Eq. 2.1).

$$Flux = \frac{dc}{dt} \times \frac{V}{S} \times \rho_{amol} \quad (Eq.\ 2.1)$$

where $\frac{dc}{dt}$ is the rate of increase or decrease in the gas concentration c (ppm) with time t (s); $\frac{dc}{dt}$ is determined from the slope of the change in gas concentration between 60 and 120 sec from the start of measurement using the linear least-squares method; V is the volume of the chamber and tube (0.002-0.004 m^3); S is the surface area of the chamber (0.028 m^2); and ρ_{amol} is the air mole density (mol m^{-3}). Positive values represent emission rates, and negative values represent absorption rates. In wetland, boardwalks were constructed to avoid release of gases due to disturbance during measurement. The case of extraordinary abrupt increase in CH_4 concentration was excluded, because it was considered as an artificial flux caused by tread power. Every measurement was conducted between 10:00 and 17:00 JST. Multi-point measurements were conducted on October 27 and 28, 2011, and September 19, 20, and 21, 2012 when CH_4 production was assumed to be the highest throughout a year in temperate Asian

monsoon forest. Regular measurements were conducted biweekly from September 26, 2011 to July 31, 2013.

2.2.4 Environmental monitoring

In the wetland, water levels in each flux-measurement chambers were measured using wells installed at each flux measurement points (Itoh et al., 2007). Dissolved oxygen concentration (DO) at a depth of 0.01 m was measured with a portable DO meter (HQ30d, HACH Company, Colorado, USA). Oxidation-reduction potential (ORP) at a depth of 0.02 m was measured with a portable ORP meter (RM20P, TOA-DKK, Tokyo, Japan). Soil temperature at a depth of 0.02 m was measured with an infrared thermometer (AD-5612A, A & D, Tokyo, Japan). In addition, ORP at a depth of 0.05 m was estimated from the voltage difference between a copper wire soldered to a platinum wire and comparison electrode (KCl-AgCl 3.33 mol L^{-1}) since September 20, 2012.

In water-unsaturated forest floor, soil temperature at a depth of 0.02 m was measured with an infrared thermometer (AD-5612A, A & D). Volumetric soil water content (VWC) at a depth of 0-0.12 m was measured with a CS-620 water content reflectometer (Campbell Scientific) at 4 points around each chamber and average VWC was used for each chamber. VWC was divided by the total pore volume to be converted into water-filled pore space (WFPS). Total pore volume was measured in the laboratory with ten 100-mL undisturbed soil samples taken from a mineral soil layer in each plot.

2.5 Statistical analysis

Data are presented as the mean ± standard deviation (SD) throughout this paper. One-way analysis of variance in conjunction with post-hoc Games-Howell test ($p < 0.05$) was used to compare mean values of CH_4 fluxes, CO_2 fluxes, and environmental factors among plots. Analysis was performed with SPSS Statistics 21 (IBM SPSS Statistics, IBM Corp., Armonk, NY, USA).

2.3 Results

2.3.1 Spatial variability

Spatial variability of CH_4 fluxes obtained from multi-point measurements in wetland and water-unsaturated forest floor is shown in Figure 2.2a. The mean air temperature during the measurement days

was 12.1°C in 2011 and 22°C in 2012. CH_4 emission was observed in wetland, whereas CH_4 absorption was observed in water-unsaturated forest floor. In wetland, CH_4 fluxes were on average 41.2 ± 74.4 nmol m^{-2} s^{-1} with a range between -2.24 and 383.3 nmol m^{-2} s^{-1} in 2011, while in 2012 were on average 78.2 ± 224.2 nmol m^{-2} s^{-1} with a range between 0.04 and 1380.63 nmol m^{-2} s^{-1}. In water-unsaturated forest floor, CH_4 fluxes were on average -1.34 ± 1.84 nmol m^{-2} s^{-1} with a range between -7.08 and 7.22 nmol m^{-2} s^{-1} in 2011, while in 2012 were on average -1.04 ± 0.85 nmol m^{-2} s^{-1} with a range between -3.47 and 1.35 nmol m^{-2} s^{-1}. The coefficient of variation (CV%) of CH_4 fluxes in wetland and water-unsaturated forest floor was used as an indicator of spatial variability. Wetland had a greater spatial variability of CH_4 fluxes (CV=181% in 2011, and 287% in 2012) than water-unsaturated forest floor (CV=137% in 2011, and 81% in 2012). On the other hand, CO_2 emission rates were generally higher in water-unsaturated forest floor than those in wetland (Figure 2.2b). In wetland, CO_2 fluxes were on average 0.51 ± 0.9 μmol m^{-2} s^{-1} with a range between 0.01 and 5.21 μmol m^{-2} s^{-1} in 2011, while in 2012 were on average 0.72 ± 0.91 μmol m^{-2} s^{-1} with a range between 0.01 and 4.81 μmol m^{-2} s^{-1}. In water-unsaturated forest floor, CO_2 fluxes were on average 2.28 ± 1.29 μmol m^{-2} s^{-1} with a range between 0.6 and 7.57 μmol m^{-2} s^{-1} in 2011, while in 2012 were on average 3.34 ± 1.31 μmol m^{-2} s^{-1} with a range between 1.19 and 7.01 μmol m^{-2} s^{-1}.

CH_4 fluxes, CO_2 fluxes, and environmental factors were compared among plots in wetland and water-unsaturated forest floor (Table 2.1). Although, mean CH_4 fluxes were not significantly different among plots in wetland, CH_4 emission rates were the highest in Wet-A, which was characterized by small particle size and composed of mud over litter, in both 2011 and 2012. In Wet-A, a hotspot of CH_4 emission with a rate as high as 1,380.63 nmol m^{-2} s^{-1} was observed in 2012. In Wet-A, water level was the highest, while DO and ORP (-0.02 m) were the lowest among plots (all $p < 0.05$) in both 2011 and 2012. In Wet-A, water level was higher in 2012 than that in 2011. In most chambers of Wet-A, water level was nearly zero in 2011, while water could be seen at the surface in 2012. DO and ORP were lower in 2012 than those in 2011. CH_4 emission rates were the lowest in Wet-B, which was characterized by medium particle size and composed of mud over gravel, in both 2011 and 2012. In Wet-B, water level

was the lowest in both 2011 and 2012, and ORP (-0.02 m) was the highest in 2011. In Wet-C, which was characterized by large particle size and composition of gravel over sparsely litter, CH_4 emission rates were of medium level, but CV of CH_4 fluxes was the highest among plots. DO and ORP (-0.02 m) in Wet-B and Wet-C were comparative and higher than those in Wet-A, while CO_2 fluxes were highly significant different among plots. CO_2 fluxes in Wet-B were the highest among wetland plots in both 2011 and 2012 ($p < 0.05$ in 2011). On the other hand, CO_2 fluxes in Wet-C were the lowest among wetland plots in both 2011 and 2012.

In water-unsaturated forest floor, the mean CH_4 absorption rate was the lowest in Dry-A, which was characterized by the existence of subsurface aquifer all year round and a thick organic layer. Dry-A had the highest WFPS among plots in both 2011 and 2012 ($p < 0.05$). CH_4 emission rates were measured at 3 out of 20 chambers in 2011, and 4 out of 20 chambers in 2012. In 2011, a CH_4 emission rate as high as 7.22 nmol m^{-2} s^{-1} was observed. CH_4 absorption rates were the highest in Dry-B ($p < 0.05$), which was characterized by low WFPS and a thick organic layer, in both 2011 and 2012. The highest CH_4 absorption rate of -7.08 nmol m^{-2} s^{-1} was observed in Dry-B in 2011. CO_2 emission rates were also the highest in Dry-B ($p < 0.05$) in both 2011 and 2012. In Dry-C, which was characterized by the lowest WFPS among plots and a thin organic layer, CH_4 absorption rates were of medium level and CO_2 emission rates were comparable to Dry-A in both 2011 and 2012. CH_4 emission was not observed in Dry-B and Dry-C, except for one chamber in Dry-B in 2011.

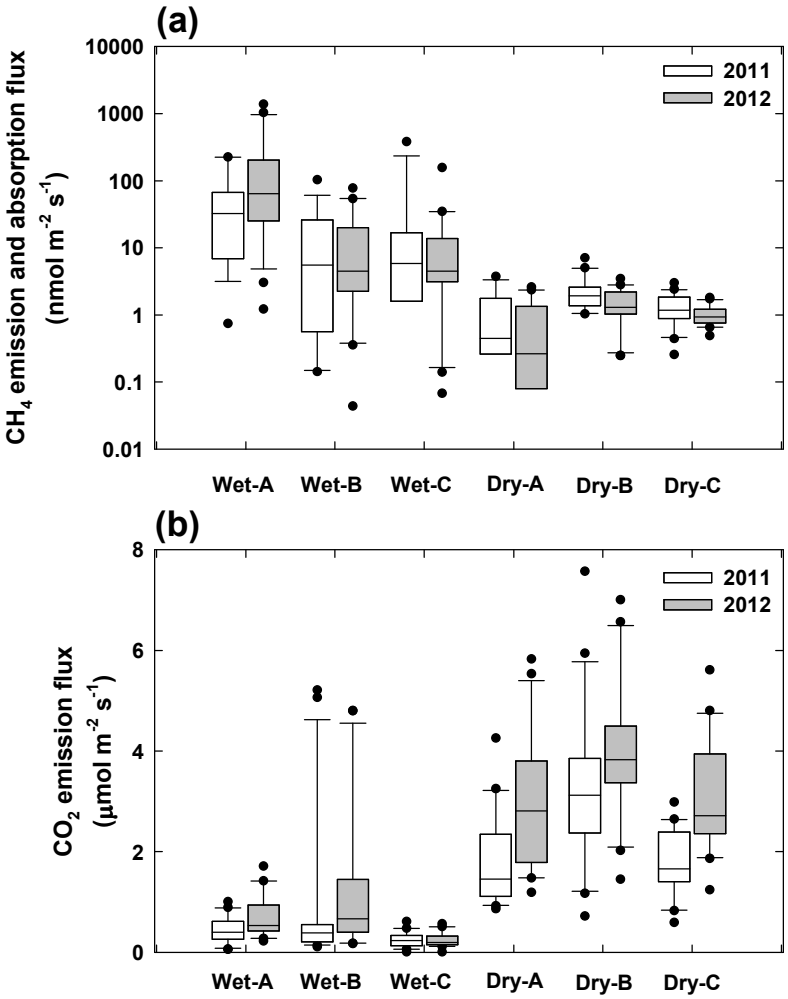

Figure 2.2 Distribution of (a) CH_4 and (b) CO_2 fluxes in each plot obtained from multi-point measurements conducted on October 27 and 28, 2011 (white bars), and on September 19, 20, and 21, 2012 (gray bars). Box plots represent the 25th and 75th percentiles, and the internal horizontal line shows the median. Bars represent the 10th and 90th percentiles and dots represent the outliers. CH_4 fluxes in water-unsaturated forest floor are shown as absorption rates by turning negative fluxes to positive fluxes.

Table 2.1 Mean and standard deviation of CH_4 fluxes, CO_2 fluxes, soil temperature, water level, water filled pore space (WFPS), dissolved oxygen (DO) at a depth of 0.02 m, and oxidation-reduction potential (ORP) at a depth of 0.02 m and 0.05 m obtained from multi-point measurements in wetland and in water-unsaturated forest floor conducted on (a) October 27 and 28, 2011 and (b) on September 19, 20, and 21, 2012. Different letters in each column represent significant differences at $p < 0.05$.

(a)

	Wetland			**Water-unsaturated forest floor**		
	Wet-A	Wet-B	Wet-C	Dry-A	Dry-B	Dry-C
CH_4 flux (nmol m^{-2} s^{-1})	64.1 ± 75.5^{a}	18.9 ± 27.9^{ab}	40.6 ± 98.3^{abc}	-0.45 ± 2.42^{bc}	-2.19 ± 1.68^{c}	-1.34 ± 0.68^{bc}
CO_2 flux (μmol m^{-2} s^{-1})	0.44 ± 0.25^{c}	0.84 ± 1.48^{b}	0.25 ± 0.16^{c}	1.82 ± 0.9^{b}	3.26 ± 1.54^{a}	1.75 ± 0.64^{b}
Soil temperature (°C)	13.9 ± 0.6^{ab}	13.8 ± 0.6^{bc}	14.3 ± 0.3^{a}	13.4 ± 0.2^{cd}	13.2 ± 0.4^{d}	12.6 ± 0.4^{e}
Water level (m)	-0.008 ± 0.023^{a}	-0.056 ± 0.08^{b}	-0.018 ± 0.02^{ab}	-	-	-
WFPS (%)	-	-	-	47.9 ± 16.3^{a}	22.2 ± 5.3^{b}	18.8 ± 3.9^{b}
DO (ml L^{-1})	1.17 ± 2.43^{b}	3.28 ± 3.36^{ab}	3.74 ± 3.39^{a}	-	-	-
ORP (-0.02 m) (mv)	234 ± 90^{b}	338 ± 52^{a}	272 ± 75^{b}	-	-	-

(b)

	Wetland			**Water-unsaturated forest floor**		
	Wet-A	Wet-B	Wet-C	Dry-A	Dry-B	Dry-C
CH_4 flux (nmol m^{-2} s^{-1})	203 ± 360.4^{abc}	15.3 ± 22.2^{a}	16.4 ± 34.9^{abc}	-0.61 ± 0.99^{b}	-1.52 ± 0.84^{c}	-1 ± 0.34^{bc}
CO_2 flux (μmol m^{-2} s^{-1})	0.7 ± 0.42^{b}	1.22 ± 1.37^{bc}	0.25 ± 0.14^{c}	2.94 ± 1.29^{a}	3.99 ± 1.35^{a}	3.08 ± 1.08^{a}
Soil temperature (°C)	21.9 ± 0.3^{c}	21.5 ± 0.5^{de}	21.4 ± 0.5^{e}	21.9 ± 0.4^{cd}	23.2 ± 0.3^{a}	22.7 ± 0.2^{b}
Water level (m)	0.003 ± 0.015^{a}	-0.062 ± 0.078^{b}	-0.001 ± 0.011^{a}	-	-	-
WFPS (%)	-	-	-	47 ± 15.7^{a}	19.6 ± 6.8^{b}	14.3 ± 4^{c}
DO (ml L^{-1})	0.8 ± 1.35^{b}	4.87 ± 3.05^{a}	2.76 ± 2.44^{a}	-	-	-
ORP (-0.02 m) (mv)	207 ± 107^{b}	295 ± 103^{a}	292 ± 89^{a}	-	-	-
ORP (-0.05 m) (mv)	-252 ± 51^{a}	-247 ± 47^{a}	-205 ± 77^{a}	-	-	-

2.3.2 Seasonal variability

As expected, rainfall in KEW occurred during the summer (June -August) and the fall months (September -November) as show in Figure 3. Summer precipitation was the highest in 2012 (794.4 mm), and fall precipitation was the highest in 2013 (761.3 mm). In 2011, summer and fall precipitations was 522.7 mm and 539.8 mm, respectively, while high precipitation (707.5 mm) occurred in spring from March to May. Minimum precipitation occurred in the winter months (December -February) of every year. Among the three years, annual precipitation was the highest in 2011.

In wetland, significantly higher CH_4 emission rates were observed during summer and fall just after heavy rainfall in every plot (Figure 2.3d–f). The highest CH_4 emission rates throughout the measurement period were observed on September 20, 2012 in Wet-A (872.2 nmol m^{-2} s^{-1}), on October 13, 2011 in Wet-B (767.0 nmol m^{-2} s^{-1}), and on July 16, 2012 in Wet-C (376.6 nmol m^{-2} s^{-1}) (Figure 2.3d–f). Seasonal variation in CH_4 fluxes was not smoothly continuous, but occasionally high emission rates were observed during high temperature seasons. The frequency of occasional events was the highest in Wet-A, especially during summer. On the other hand, in Wet-B and Wet-C, high CH_4 emission rates were limited in number from July to October and were less frequent compared to Wet-A during the same period. CO_2 emission showed seasonal variation correlated with temperature change and increased gradually as temperature increased in every plot (Figure 2.3g–i). Among plots, the CO_2 emission rates in Wet-C were the lowest and did not show any significant enhancement during summer (Figure 2.3i). No significant seasonal variation in water level was observed in any plot (Figure 2.3j–l). In Dry-B, the water level at one chamber was significantly lower throughout the measurement period in one of the chambers (Figure 2.3k). Also, DO, ORP (-0.02 m), and ORP (-0.05 m) were remarkably higher than those in other chambers. No significant seasonal variations in DO was observed in Wet-B and Wet-C (Figure 2.3n and o). In Wet-A, DO was nearly zero from spring to fall and increased in winter (Figure 2.3m). ORP (-0.02 m) decreased in spring and summer in Wet-A and Wet-C (Figure 2.3p and r), but no such seasonal variation was observed in Wet-B (Figure 2.3q). No seasonal variation in ORP (-0.05 m) was observed in any plot (Figure 2.3s–u).

In water-unsaturated forest floor, seasonal variation in CH_4 absorption was not correlated with temperature variation in any plot (Figure 2.4d–f). In Dry-A, WFPS differed clearly among chambers, and WFPS were significantly correlated with CH_4 absorption. High CH_4 absorption rates were observed in one of the chambers with the lowest WFPS, while low CH_4 absorption rates were observed in chambers with high WFPS. In the chamber with the lowest WFPS in Dry-A, CH_4 absorption increased from mid-winter to early summer as soil temperature increased and then decreased by intensive rainfall (Figure 2.4d). During the fall and winter months, CH_4 absorption increased again in mid-summer and decreased gradually as soil temperature decreased. In the chamber with the highest WFPS in Dry-A, CH_4 emission was observed occasionally (Figure 2.4d). No significant seasonal variation was observed in the chambers with high WFPS. On the other hand, CO_2 emission rates in Dry-A did not differ significantly among chambers. In Dry-B, the highest CH_4 absorption rates were observed in spring 2012 in all chambers, just before intensive summer rainfall, and they decreased during intensive rainfall period from summer to fall in 2012. After intensive rainfall period, CH_4 absorption increased again in winter 2012, but then decreased and remained low during winter. In spring 2013, CH_4 absorption increased as soil temperature increased and WFPS decreased (Figure 2.4e). In Dry-C, WFPS was variable, while CH_4 absorption rates and seasonal variation were relatively low in the chamber with the lowest WFPS. In other chambers in Dry-C, CH_4 absorption increased in spring 2012 as temperature increased and then decreased by summer intensive rainfall in all chambers. In August 2012, CH_4 absorption rates were remarkably higher in two chambers. No clear seasonal variation was observed in any chamber in Dry-C. CO_2 emission showed seasonal variation correlated with soil temperature, and its mean value was the highest during summer in all plots (Figure 2.4g–i).

In the wetland, CH_4 and CO_2 fluxes were positively correlated with soil temperature in all plots (all $p < 0.05$, Table 2.2). CH_4 emission increased significantly when water level approached to surpasses the surface. In Wet-A, CH_4 and CO_2 emissions were negatively correlated with DO and ORP (-0.02 m) ($p < 0.05$). No significant relationships between DO or ORP and CH_4 or CO_2 fluxes (-0.02 m) were observed in any plot (Table 2.2). Also, no significant relationship between CH_4 or CO_2 fluxes and ORP (-0.05 m)

was observed in any plot.

In water-unsaturated forest floor, CH_4 fluxes were positively correlated with WFPS ($p < 0.05$, Table 2.3) in all plots, but with soil temperature only in Dry-B and Dry-C ($p < 0.05$). On the other hand, CO_2 fluxes were positively correlated with soil temperature ($p < 0.05$) in all plots, but with WFPS only in Dry-A. Correlation coefficient between soil temperature and CO_2 fluxes was higher than that between soil temperature and CH_4 fluxes in both wetland and water-unsaturated forest floor (Table 2.2 and 2.3).

The CV of CH_4 fluxes in all chambers was calculated from the regular measurements obtained biweekly. Generally, the CV of CH_4 fluxes was higher in wetland than that in water-unsaturated forest floor, although it was relatively high in Dry-A due to low CH_4 fluxes. The CV of CH_4 fluxes in wetland ranged from 126% to 439%, while in water-unsaturated forest floor ranged from 38% to 877% (or from 50% to 191% in all plots, excluding Dry-A). Seasonal variation in CH_4 fluxes was higher in wetland than in water-unsaturated forest floor (Figure 2.5a). On the other hand, seasonal variation in CO_2 fluxes was higher in water-unsaturated forest floor than in wetland (Figure 2.5b).

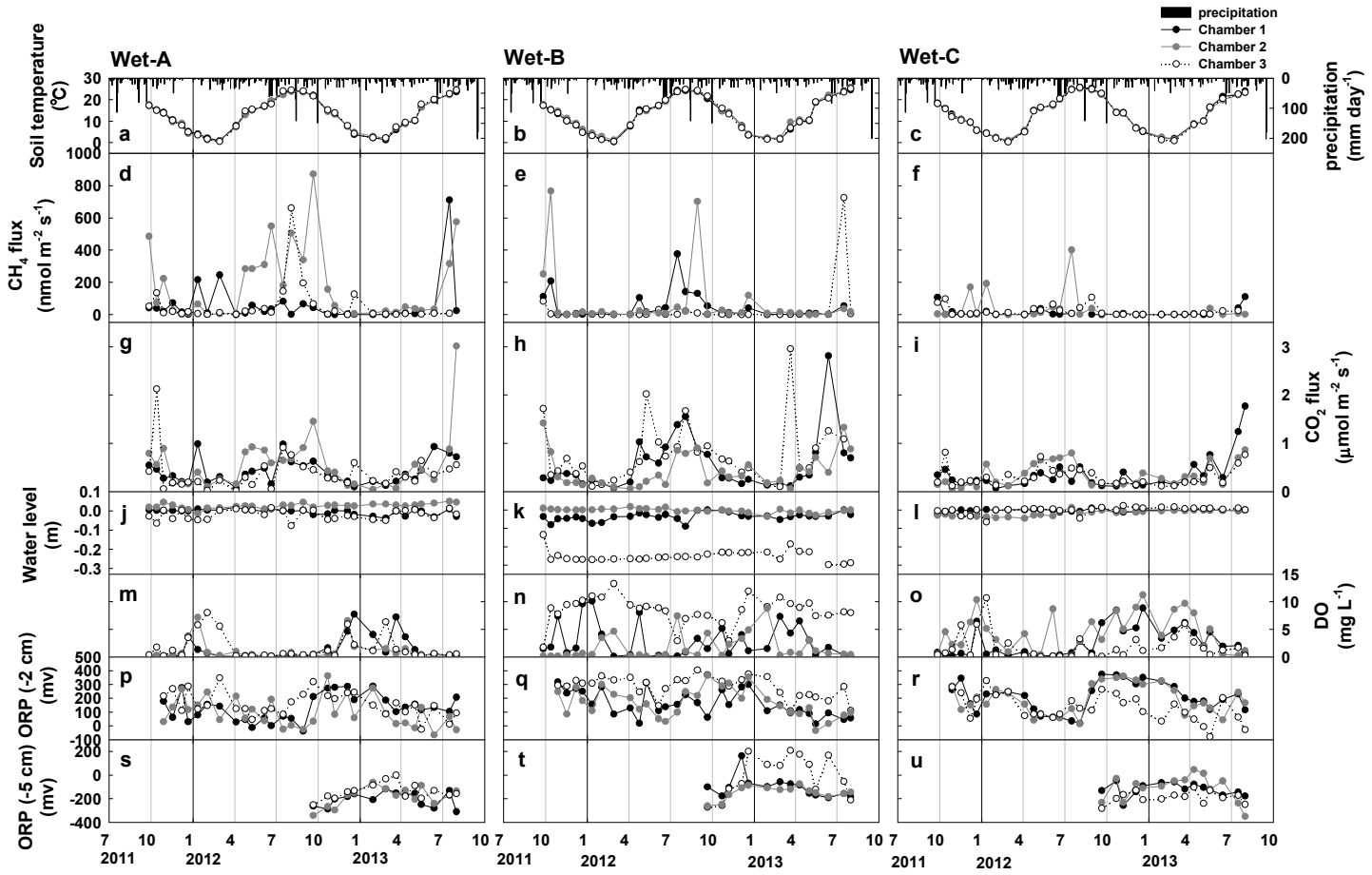

Figure 2.3 Seasonal variation in soil temperature, precipitation (a-c), CH_4 flux (d-f), CO_2 flux (g-i), water level (j-l), dissolved oxygen (DO) at a depth of 0.02 m (m-o), and oxidation-reduction potential (ORP) at a depth of 0.02 m (p-r) and 0.05 (s-u) m in each plot. Data were obtained biweekly over two years.

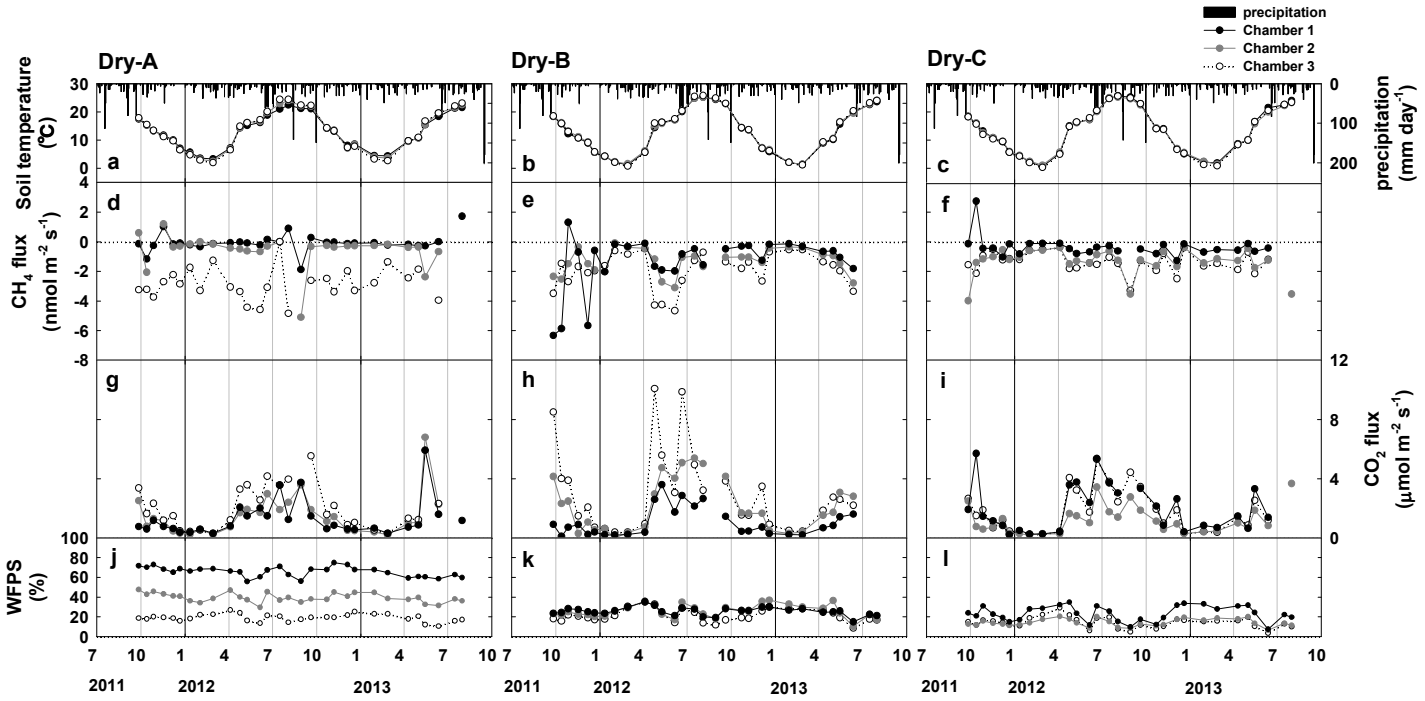

Figure 2.4 Seasonal variation in soil temperature, precipitation (a-c), CH_4 flux (d-f), CO_2 flux (g-i), and water-filled pore space (WFPS) (j-l) in each plot. Data were obtained biweekly over two years.

Table 2.2 The Pearson correlation coefficients (*r*) are shown for each plot between CH_4 or CO_2 fluxes and soil temperature, water-filled pore space (WFPS), dissolved oxygen (DO) at a depth of 0.02 m, and oxidation-reduction potential (ORP) at a depth of 0.02 m and 0.05 m. Data obtained biweekly over two years. (Asterisk (*), $p = 0.05$; double asterisk (**) $p = 0.01$).

	CH_4 flux			**CO_2 flux**		
	Wet-A	Wet-B	Wet-C	Wet-A	Wet-B	Wet-C
Soil temperature	0.46**	0.3**	0.23*	0.53**	0.53**	0.45**
Water level	0.2	0.08	-0.02	0.09	-0.2	0.03
DO	-0.25*	-0.17	-0.11	-0.25*	0.03	-0.2
ORP (-0.02 m)	-0.23*	0.01	-0.16	-0.34**	-0.1	-0.35**
ORP (-0.05 m)	-0.2	0.01	-0.13	-0.21	0.1	-0.24

Table 2.3 The Pearson correlation coefficient (*r*) are shown for each plot between CH_4 or CO_2 fluxes and soil temperature, and water-filled pore space (WFPS). Data obtained biweekly over two years were analyzed. (Asterisk (*), $p = 0.05$; double asterisk (**) $p = 0.01$).

	CH_4 flux			**CO_2 flux**		
	Dry-A	Dry-B	Dry-C	Dry-A	Dry-B	Dry-C
Soil temperature	-0.11	-0.33**	-0.26*	0.67**	0.63**	0.7**
WFPS	0.73**	0.4**	0.49**	-0.26*	-0.11	0.03

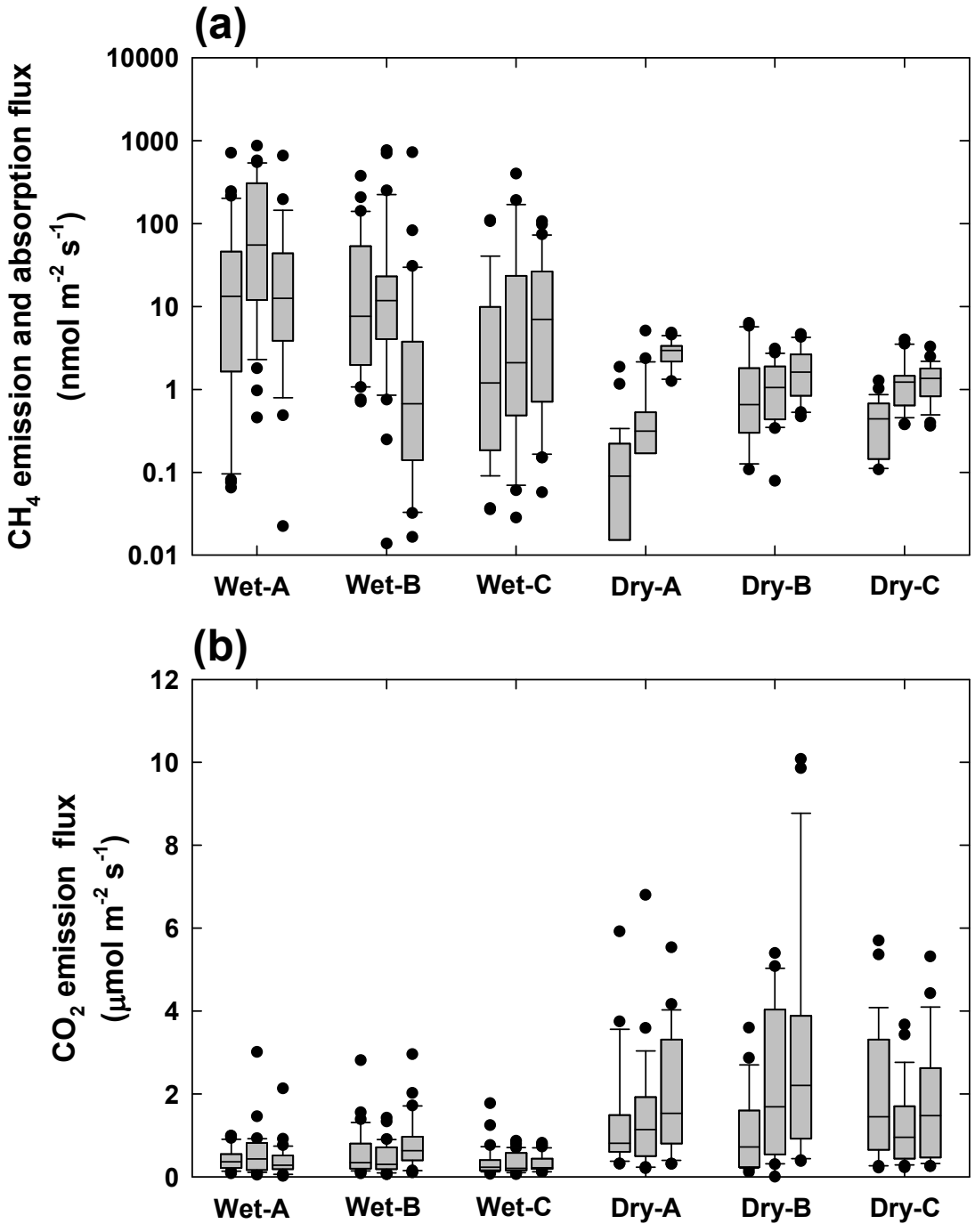

Figure 2.5 Distribution of (a) CH_4 and (b) CO_2 fluxes obtained from biweekly regular measurements conducted from September 26, 2011 to July 31, 2013. Box plots represent the 25th and 75th percentiles, and the internal horizontal line shows the median. Bars represent the 10th and 90th percentiles, and the dots represent the outliers. CH_4 fluxes in water-unsaturated forest floor are shown as absorption rates by turning negative fluxes to positive fluxes.

Discussion

2.4.1 Spatial variability in CH_4 and CO_2 fluxes

In both 2011 and 2012, CH_4 emission rates were high in Wet-A, where water levels were also high, but DO and ORP (-0.02 m) were relatively low. However, the lowest CH_4 emission rates were observed in Wet-B, where water level was low, but DO and ORP (-0.02 m) were high. CH_4 emission rates were also low in Wet-C, where DO and ORP (-0.02 m) were high.

Wet-A had low DO and ORP; therefore, it was considered an anaerobic environment favorable for methanogens. On the other hand, Wet-B and Wet-C were considered relatively aerobic environments. Wet-A was composed of mud that creates an anaerobic environment, because it has less pore space than gravel and restricts gas diffusivity, especially oxygen from the atmosphere. Fine-textured soils with high moisture retention capacity remain substantially wetter throughout the year than coarse-textured soils (Potter et al., 1996). Soil texture, which showed substantial infiltration, and drainage, are negatively correlated with WFPS. In Australian subtropical rainforests, fine-textured soil remained waterlogged for longer periods of time and potentially created anaerobic microsites (Rowlings et al., 2012).

The particle size has an effect on CH_4 emission, because it influences the probability of microbial existence including methanogens. Wagner et al. (1999) compared CH_4 production rates of different textured soils inoculated with methanogenic bacteria under aerobic and anaerobic conditions and reported that CH_4 production is higher in sand than in gravel or clayey silt. They also showed that indigenous microflora in combination with the sorptive quality of soil particles (clay, silt, and organic matter) enables methanogenic activity in the presence of oxygen, promoting microscale anoxia within the slurries. Mineral composition is also an important factor, because it determines the cation exchange capacity and thus the attachment ability of microorganisms. The cation exchange capacity increased in the following sequence: sand, gravel, clayey silt marshland soil, and bentonite. In Wet-A, anaerobic conditions and the high capacity of attached microbes, including methanogens might lead to high CH_4 emission. Indeed, higher CH_4 emission rates were observed more frequently in 2012, when DO and ORP (-0.02 m) were lower than in 2011. On the other hand, in Wet-B and Wet-C where particle size was large,

anaerobic conditions occurred less frequently, and therefore the attachment ability of microorganisms was low. In Wet-C, not only CH_4 emission, but also CO_2 emission was the lowest. Soil CO_2 fluxes have been used as an indicator of labile C availability, microbial activity, and plant root respiration (Mummey et al., 1997). In Wet-C, low organic-matter levels and consequently low CO_2 fluxes might lead to low CH_4 emission.

In water-unsaturated forest floor, the lowest CH_4 absorption was observed in Dry-A, where WFPS was high and organic layer was thick. One of the possible reasons is that CH_4 production in wet reductive microsites obscures CH_4 oxidation. Even if the surface of water-unsaturated forest floor is not saturated with water, CH_4 production occurs deeper in the ground, because this area always has a subsurface aquifer. Itoh et al. (2009) reported that CH_4 emission occurred during rainy summers from the water-unsaturated forest floor, adjacent to the riparian zone, and they suggested that it was due to CH_4 production in wet reductive microsites in the lower part of the slopes close to water pathways. Additionally, an increase in CH_4 concentration below the soil surface was observed with increasing soil temperature. It is known that CH_4 oxidation and production determines CH_4 absorption; thus, net CH_4 oxidation can be reduced by an increase in CH_4 production in a plot where WFPS. CH_4 emission observed at some points in Dry-A suggesting an active CH_4 production in the plot.

When WFPS was low, CH_4 absorption flux was significantly higher in Dry-B, which had a thick organic layer, than in Dry-C, which had a thin organic layer. Plots with thick organic layers and high CO_2 emission rates supply nutrients to microbes and leads to high CH_4 absorption (Del Grosso et al., 2000). Plots with thin organic layers and low CO_2 emission rates have low microbial activity, including that of methanotrophs. (Temporally detailed responses of CH_4 flux to environmental factors such as soil temperature and WFPS at each plot are shown in Chapter 3.)

Mean CH_4 fluxes of each plots obtained in wetland and water-unsaturated forest floor were compared to those obtained from sites all over the world. Turetsky et al. (2014) reported the mean CH_4 emission rate in temperate wetlands (16 sites mainly in Europe and North America) was 78.8 ± 3.3 nmol m^{-2} s^{-1}. CH_4 flux measurements were obtained using the static closed chamber method with GC weekly,

or monthly during the growing season. Mean CH_4 emission rates in Wet-A (64.1 ± 75.5, and 203 ± 360.4 nmol m^{-2} s^{-1}) were higher than those in Wet-B (18.9 ± 27.9, and 15.3 ± 22.2 nmol m^{-2} s^{-1}) and Wet-C (40.6 ± 98.3, and 16.4 ± 34.9 nmol m^{-2} s^{-1}). Smith et al. (2000) reported that CH_4 absorption rate was on average -0.95 nmol m^{-2} s^{-1} in temperate forest (6 sites in Europe and North America). CH_4 flux measurements were obtained using the static closed chamber method with GC. In KEW, mean CH_4 absorption rates in Dry-B (-2.19 ± 1.68, and -1.52 ± 0.84 nmol m^{-2} s^{-1}) and Dry-C (-1.34 ± 0.68, and -1 ± 0.34 nmol m^{-2} s^{-1}) were higher than those in Dry-A (-0.45 ± 2.42, and -0.61 ± 0.99 nmol m^{-2} s^{-1}). Both CH_4 emission and absorption exhibited high spatial variability. Spatial variability in CH_4 fluxes was higher in wetland than in water-unsaturated forest floor, because a hotspot of CH_4 emission was identified in wetland.

2.4.2 Seasonal variation in CH_4 and CO_2 fluxes

Seasonal variation in CH_4 flux was not associated with temperature variations, but occasionally high CH_4 emission rates were observed during high temperature seasons with intense rainfall (Figure 2.3d–f). In Wet-A, high CH_4 emission rates were observed when DO and ORP (-0.02 m) were low (Table 2) and temperature was high; hence, the formation of an anaerobic environment during high temperature season led to high CH_4 emission rates. Wet-B was the plot where water levels were relatively low throughout the measurement period, which led to high DO values. An aerobic environment might inhibit methanogenic CH_4 production. In Wet-C, high CH_4 emission was rarely observed even in summer, probably because less organic matter content led to a lesser amount of substitutes for microbes including methanogens. In Wet-C, CO_2 emission was also low. Purvaja and Ramesh (2001) suggested that increasing soil temperatures and degradation of soil organic matter contributed to strong summer and pre-monsoon peaks in CH_4 emission in mangrove sediments, whilst monsoonal floodwaters possibly restricted CH_4 emissions. In KEW, gas diffusivity was not a limiting factor for CH_4 production by methanogens, which gradually increased with continuous and intensive rainfall from summer to fall.

Seasonal variations in CH_4 absorption was not associated with temperature variations and patterns were unique in each chamber (Figure 2.4d–f). On the other hand, CO_2 fluxes showed seasonal variation

that was correlated with soil temperature variation in all chambers. Correlation analysis showed that CH_4 absorption was more strongly influenced by soil water than by soil temperature (Table 2.2). Compared to CH_4 absorption, CO_2 fluxes had a stronger correlation with soil temperature than with WFPS (Table 2.2). Usually, CO_2 fluxes have usually unidirectional responses to soil temperature and emission increases with increasing soil temperature. On the other hand, CH_4 absorption may have a bidirectional responses to soil temperature, because most methanogens and methanotrophs are mesophiles; thus, it is assumed that both CH_4 consumption and production increase with the temperature. In two chambers in Wet-A with high WFPS did not show clear seasonal variations.

No significant correlation between CH_4 absorption and soil temperature was observed in Dry-A, probably due to the competition between methanogens and methanotrophs. This competition resulted in increase of CH_4 absorption with temperature, which decreased with CH_4 emission. In Dry-B, the highest CH_4 absorption was observed in spring, and low in fall, in spite of the similar temperature conditions. This was probably due to the soil being drier in spring than it was in fall after continuous rainfall during the summer and fall months. Although CH_4 absorption increased with temperature, the correlation of CH_4 flux with WFPS was stronger and could mask any changes with temperature. For instance, CH_4 absorption in Dry-A and Dry-C in August could be reduced during a rainless period that last for several days.

Seasonal variation in CH_4 fluxes was higher in wetland than in water-unsaturated forest floor (Figure 2.5a), thus it was suggested that seasonal variation in wetlands was strongly correlated with seasonal variation in ecosystem-scale CH_4 flux. CH_4 flux in wetland ranged from 0 to 872.2 nmol m^{-2} s^{-1}, while in water-unsaturated forest floor ranged from -6.32 to 2.74 nmol m^{-2} s^{-1}. Wetland area was about 3% of the total watershed, thus it was expected that high CH_4 emission in wetlands would influence watershed-scale CH_4 flux, especially in summer. Generally, CH_4 emission is expected to be very high, if wetlands include plots that have high water levels and are composed of mud as Wet-A in KEW. Moreover, CH_4 emission through bubble was not measured in this chapter, which would increase the total CH_4 rate. These results suggest that the investigation of CH_4 dynamics in anaerobic environments

such as wetlands is important to understand ecosystem-scale CH_4 fluxes, even though they are spatially limited within a watershed.

2.5 Conclusion

Spatial variability of CH_4 fluxes ranged from -2.24 to 1,380.63 nmol m^{-2} s^{-1} in wetland and from -7.08 to 7.22 nmol m^{-2} s^{-1} in water-unsaturated forest floor. Spatial variability in CH_4 fluxes was increased wetland and showed that it is a necessary evaluation factor of CH_4 budgets in forests. Biweekly measurements over two years helped identify a hotspot of CH_4 emission in a plot that composed of mud during summer and fall when precipitation is intense in temperate Asian monsoon forest. In water-unsaturated forest floor, CH_4 absorption did not show any seasonal variation. However, some measurement points with low WFPS showed an increase in CH_4 absorption in spring before intense summer rainfall. CH_4 emission in wetland showed higher seasonal variation than CH_4 absorption in water-unsaturated forest floor. Therefore, it was suggested that CH_4 emission in wetland had a stronger effect on seasonal variation in ecosystem-scale CH_4 flux than CH_4 absorption in water-unsaturated forest floor. In Japanese forests, complex terrain and Asian monsoon rainfall often cause spatially and temporally heterogeneous distribution of soil water conditions, which strongly influence the balance between CH_4 production and oxidation. My findings suggest that the investigation of CH_4 dynamics in a water-unsaturated forest floor as well as anaerobic environments such as wetlands is important to delineate ecosystem-scale CH_4 fluxes, though they are spatially limited within a whole forest watershed.

References

Adamsen, A. P. S., and King, G. M. (1993) Methane consumption in temperate and subarctic forest soils: rates, vertical zonation, and responses to water and nitrogen, Appl. Environ. Microbiol., 59, 485–490.

Baldocci, D., Falge, E., Gu, L., Olson, R., Hollinger, D., Running, S., Anthoni, P., Bernhofer, C., Davis, K., Evans, R., Fuentes, J., Goldstein, A., Katul, G., Law, B., Lee, X., Malhi, Y., Meyers,

T., Munger, W., Oechel, W., Paw U, K.T., Pilegaard, K., Schmid, H.P., Valentini, R., Verma, S., Vesala, T., Wilson, K., and Wofsy, S. (2001) FLUXNET: A new tool to study the temporal and spatial variability of ecosystem-scale carbon dioxide, water vapor, and energy flux densities, Bulletin of the American Meteorological Society, 82, 2415–2434.

Del Grosso, S.J., Parton, W.J., Mosier, A.R., Ojima, D.S., Potter, C.S., Broken, W., Brumme, R., Butterbach-Bahl, K., Crill, P.M., Dobbie, K., and Smith, K.A. (2000) General CH_4 oxidation model and comparisons of CH_4 oxidation in natural and managed systems, Global Biochem. Cy., 14, 999–1019.

Dinsmore, K.J., Skiba, U.M., Billett, M.F., Rees, R.M., and Drewer, J. (2009) Spatial and temporal variability in CH4 and N2O fluxes from a Scottish ombrotrophic peatland: Implications for modelling and up-scaling, Soil Biol. Biochem., 41, 1315–1323.

Dobbie, K.E., and Smith, K.A. (1996) Comparison of CH_4 oxidation rates in woodland, arable and set aside soils, Soil Biol. Biochem., 28, 1357–1365.

Dörr, H., Katruff, L., and Levin, I. (1993) Soil texture parameterization of the methane uptake in aerated soils, Chemosphere, 26, 697–713.

Eugster, W., and Plüss, P. (2010) A fault-tolerant eddy covariance system for measuring CH_4 fluxes, Agric. For. Meteorol., 150, 841–851.

Itoh, M., Ohte, N., and Koba, K. (2009) Methane flux characteristics in forest soils under an East Asian monsoon climate, Soil Biol. Biochem., 41, 388–395, doi: 10.1016/j.soilbio.2008.12.003.

Itoh, M., Ohte, N., Koba, K., Katsuyama, M., Hayamizu, K., and Tani, M. (2007) Hydrologic effects on methane dynamics in riparian wetlands in a temperate forest catchment, J. Geophys. Res., 112, G01019, doi: 10.1029/2006JG000240.

Itoh, M., Ohte, N., Katsuyama, M., Koba, K., Kawasaki, M., and Tani, M. (2009) Temporal and spatial variability of methane flux in a temperate forest watershed, J. Japan Soc. Hydrol. Water Resor., 18, 244–256.

Kirschke, S., Bousquet, P., Ciais, P., Saunois, M., Canadell, J.G., Dlugokencky, E.J., Bergamaschi, P.,

Bergmann, D., Blake, D.R., Bruhwiler, L., Cameron-Smith, P., Castaldi, S., Chevallier, F., Feng, L., Fraser, A., Heimann, M., Hodson, E.L., Houweling, S., Josse, B., Fraser, P., Krummel, P.B., Lamarque, J., Langenfelds, R.L., Le Quéré, C., Nail, V., O'Doherty, S., Palmer, P.I., Pison, I., Plummer, D., Poulter, B., Prinn, R.G., Rigby, M., Ringeval, B., Santini, M., Schmidt, M., Shindell, D.T., Simpson, I.J., Spahni, R., Steele, L.P., Strode, S.A., Sudo, K., Szopa, S., van der Werf, G.R., Voulgarakis, A., van Weele, M., Weiss, R.F., Williams, J.E., and Zeng, G. (2013) Three decades of global methane sources and sinks, Nature Geosci., 6, 813–823, doi: 10.1038/NGEO1955.

Lai, D.Y.F., Moore, T.R., and Roulet, N.T. (2014) Spatial and temporal variations of methane flux measured by autochambers in a temperate ombrotrophic peatland, J. Geophys. Res. Biogeosci., 119, doi: 10.1002/2013JG002410.

Le Mer, J., and Roger, P. (2001) Production, oxidation, emission and consumption of methane by soils: A review, Eur. J. Soil Biol., 37, 25–50.

McDermitt, D., Burba, G., Xu, L., Anderson, T., Komissarov, A., Riensche, B., Schedlbauer, J., Starr, G., Zona, D., Oechel, W., Oberbauer, S., Hastings, S. (2011) A new low-power, open-path instrument for measuring methane flux by eddy covariance. Appl Phys. B102:391-405.

Mummey, D.L., Smith, J.L., and Bolton Jr., H. (1997) Small-scale spatial and temporal variability of N_2O flux from a shrub-steppe ecosystem, Soil. Biol. Biochem, 29, 1699–1706.

Ohte, N., Tokuchi, N., and Suzuki, M. (1997) An in situ lysimeter experiment on soil moisture influence on inorganic nitrogen discharge from forest soil, J. Hydrol., 195, 78–98.

Potter, C.S., Davidson, E.A., and Verchot, L.V. (1996) Estimation of global biogeochemical controls and seasonality in soil methane consumption, Chemosphere, 32, 2219–2246.

Purvaja, R. and Ramesh, R. (2001) Natural and Anthropogenic methane emission from coastal wetlands of south India, Environmental Management, 27, 547–557.

Rowlings, D.W., Grace, P.R., Kiese, R., and Weiler, K.L. (2012) Environmental factors controlling temporal and spatial variability in the soil-atmosphere exchange of CO_2, CH_4 and N_2O

from an Australian subtropical rainforest, Global Change Biology, 18, 726–738, doi: 10.1111/j.1365-2486.2011.02563.x.

Sakabe, A., Hamotani, K., Kosugi, Y., Ueyama, M., Takahashi, K., kanazawa, A., and itoh, M. (2012) Measurement of methane flux over an evergreen coniferous forest canopy using a relaxed eddy accumulation system with tunable diode laser spectroscopy detection, Theor. Appl. Climatol., 109, 39–49, doi: 10.1007/s00704-011-0564-z.

Savage, K., Phillips, R., and Davidson, E. (2014) High temporal frequency measurements of greenhouse gas emissions from soils, Biogeosciences, 11, 2709–2720, doi: 10.5194/bg-11-2709-2014.

Schimel, J.P. (1995) Plant transport and methane production as controls on methane flux from arctic wet meadow tundra, Biogeochemistry, 28, 183–200.

Schrier-Uijl, A.P., Veenendaal, E.M., Leffelaar, P.A., van Huissteden, J.C., Berendse, F. (2009) Methane emissions in two drained peat agro-ecosystems with high and low agricultural intensity. Plant Soil. doi:10.1007/s11104-009-0180-1.

Smith, K.A., Dobbie, K.E., Ball, B.C., Bakken, L.R., Siaura, B.K., Hansen, S., Brumme, R., Brokn, W., Christensen, S., Prieme, A., Fowler, D., Macdonald, J.A., Skiba, U., Klemedtsson, L., Kasimir-Klemedtsson, A., Degórska, A., and Orlanski, P. (2000) Oxidation of atmospheric methane in Northern European soils, comparison with other ecosystems, and uncertainties in the global terrestrial sink, 6, 791–803.

Steudler, P.A., Bowden, R.D., Melillo, J.M., and Aber, J.D. (1989) Influence of nitrogen fertilization on methane uptake in temperate forest soils, Nature, 341, 314–316.

Stocker, T.F., Qin, D., Plattner, G.-K., Alexander, L.V., Allen, S.K., Bindoff, N.L., Brëon, F.–M., Church, J.A., Cubasch, U., Emori, S., Forster, P., Friedlingstein, P., Gillett, N., Gregory, J.M., Hartmann, D.L., Jansen, E., Kirtman, B., Knutti, R., Krishna Kumar, K., Lemke, P., Marotzke, J., Masson-Delmotte, V., Meehl, G.A., Mokhov, I.I., Piao, S., Ramaswamy, V., Randall, D., Rhein, M., Rojas, M., Sabine, C., Shindell, D., Talley, L.D., Vaughan, D.G., and Xie, S.–P. (2013) Technical Summary. In: Climate Change 2013: The Physical Science Basis. Contribution of

Working Group I to the Fifth Assessment Report of the Intergovernmental Panel on Climate Change, edited by Stocker, T.F., Qin, D., Plattner, G.–K., Tignor, M., Allen, S.K., Boschung, J., Nauels, A., Xia, Y., Bex, V., and Midgley, P.M., Cambridge University Press, Cambridge, United Kingdom and New York, NY, USA.

Turetsky, M.R., Kotowska, A., Bubier, J., Dise, N.B., Crill, P., Hornibrook, E.C., Minkkinen, K., Moore, T.R., Myers-Smith, I.H., Nykänen, H., Olefeldt, D., Rinne, J., Saarnio, S., Shurpali, N., Tuittila, E., Waddington, J.M., White, J.R., Wickland, K.P., and Wilmking, M. (2014) A synthesis of methane emissions from 71 northern, temperate, and subtropical wetlands, 20, 2183–2197, doi: 10.1111/gcb.12580.

Wagner, D., Pfeiffer, E.-M., and Bock, E. (1999) Methane production on aerated marshland and model soils: effects of microflora and soil texture, Soil Biol. Biochem., 31, 999–1006.

Wang, Z.P., Lindau, C.W., Delaune, R.D., and Patrick, Jr., W.H. (1993) Methane emission and entrapment in flooded rice soils as affected by soil properties, Biol. and Fertlity of Soils, 16, 163–168.

Whalen, S.C., Reeburgh, W.S., and Sandbeck, K.A. (1990) Rapid methane oxidation in a landfill cover soil, Appl. Envi. Microb., 56, 3405–3411.

Whiting, G.J., and Chanton, J.P. (1993) Primary production control of methane emission from wetlands, 364, 794–795.

CHAPTER 3

One year of continuous measurements of soil CH_4 and CO_2 fluxes in a Japanese cypress forest: Temporal and spatial variations associated with Asian monsoon rainfall

3.1. Introduction

CH_4 consumption in soils due to microbial oxidation by methanotrophs is the only significant biological sink, representing about 1.4–7.4% of the total global sink (Kirschke et al., 2013). Above all, forest soils are recognized as the most efficient sinks for atmospheric CH_4 (Le Mer and Roger, 2001). The average and standard deviation (SD) of CH_4 fluxes in forest soils around the world were reviewed by Dutaur and Verchot (2007), and the highest CH_4 absorption flux and largest variability were observed in temperate forests: 1.13 ± 1.11 nmol m^{-2} s^{-1} in temperate forests (number of sites, n = 92), 0.52 ± 0.56 nmol m^{-2} s^{-1} in boreal forests (n = 51), and 0.66±0.43 nmol m^{-2} s^{-1} in tropical forests (n = 62). Thus, CH_4 fluxes in temperate forests are thought to have larger spatial variability than those in other types of forests. However, the mechanisms mediating these characteristics are not sufficiently clear.

In terms of environmental factors, CH_4 absorption increases as soil water content decreases and as temperature increased (Steudler et al., 1989; Whalen, 1990; Adamsen and King, 1993; Dobbie and Smith, 1996). Most of these studies have been performed in North America and Europe, where high CH_4 absorption flux is observed in the summer due to high temperatures and low precipitation (Dobbie and Smith, 1996; Broken and Brumme, 2000; Steinkamp et al., 2001). In contrast, CH_4 absorption under climates with humid summers, such as the Asian monsoon climate, is likely to be greatly influenced by intensive summer rainfall. Morishita et al. (2007) measured soil CH_4 fluxes at 26 forest sites in Japan and reported that there are no clear seasonal changes in CH_4 fluxes at most sites. Moreover, they suggested that the efficient promotion of CH_4 absorption by increased temperature may be impeded by the simultaneous increase in soil moisture associated with intensive summer precipitation. Additionally,

Itoh et al. (2009) measured soil CH_4 fluxes from the upper to lower hill slope areas within Japanese cypress forests. The CH_4 absorption flux significantly differs depending on the sampling location on the hill slope, and changes in soil water content following precipitation were shown to affect CH_4 fluxes in all plots. In particular, summer soil water content affects the estimated annual CH_4 fluxes. In wetter areas, the soil can switch from a CH_4 sink in a dry year to a CH_4 source in a wet year (Itoh et al., 2009). These previous works revealed the comprehensive ranges of CH_4 fluxes throughout Japan and the considerable influence of the Asian monsoon summer rainfall on CH_4 absorption ability.

Most soil CH_4 fluxes have been measured by manually operated chamber methods, with a weekly or monthly time resolution (Morishita et al., 2007; Itoh et al., 2009). While manual measurement has its merits, i.e., that multiple measurement points are possible as shown in Chapter 2, this method suffers from limited information on relatively short-term variations in fluxes. As for CO_2, several studies using continuous measurements of soil respiration have revealed that CO_2 emission increases immediately (within less than 1 h) after rain events (Lee et al., 2004; Xu et al., 2004). These studies demonstrated that continuous measurement is imperative for accurate estimation of soil respiration and net ecosystem production. The same is true of CH_4 fluxes. Moreover, the CH_4 flux is determined by the balance between two conflicting responses: CH_4 production by methanogens and CH_4 oxidation by methanotrophs, which are dependent on soil moisture status (redox conditions) and may therefore change rapidly with rainfall. In the Asian monsoon climate in particular, high precipitation occurs in the summer when CH_4 production increases (Itoh et al., 2009). Considering the substantial effects of rainfall on the variations in CH_4 fluxes, continuous measurement with high time resolution is necessary for making measurements immediately before, during, and after rainfall. CH_4 flux in forest soils is known to show large spatial variation according to topographic conditions (Ishizuka et al., 2000; Morishita et al., 2007); however, few studies have investigated how the seasonal variations or responses to rainfall differ according to topographic conditions.

Recently, the development of a laser-based CH_4 analyzer has made it possible to perform in-situ continuous measurements of CH_4 concentrations. In this chapter, I employed this laser-based CH_4

analyzer to measure soil CH_4 and CO_2 fluxes continuously in a Japanese temperate cypress forest by using automated chambers. I examined three characteristic plots in order to investigate how these CH_4 fluxes changed temporally at each plot. Therefore, the aim of this chapter was to elucidate (i) the ranges of CH_4 fluxes; (ii) the seasonal variations in CH_4 fluxes and environmental factors (soil temperature and soil water content), which influenced their seasonality at each plot; (iii) the detailed temporal responses of CH_4 fluxes to rainfall and how they differed depending on the local topography at each plot; and (iv) the annual budgets of CH_4 fluxes that took into consideration the rainfall responses. While I primarily focused on variations in CH_4 flux, simultaneous measurements in CO_2 flux provided information on the mechanisms controlling the CH_4 flux in the context of microbial activity and gas diffusivity. Moreover, comparing the environmental response of CH_4 fluxes to that of CO_2 fluxes helped me to understand the characteristics of CH_4 fluxes. The findings are expected to contribute to our understanding of the mechanisms determining soil CH_4 flux in forests under the Asian monsoon climate.

3.2. Materials and Methods

3.2.1. Site description

The observations were made in a temperate coniferous forest in the Kiryu Experimental Watershed (KEW; 35°N, 136°E; 190–255 m above sea level; 5.99 ha), located in Shiga Prefecture, central Japan (Figure 3.1a). The entire watershed was underlain by weathered granite, with abundant amounts of albite. The soil type was typical brown forest soil and predominantly cambisols. Ohte et al. (1997) detailed the physical and chemical properties of the soil in the watershed. The forest consisted of 55-year-old Japanese cypress (*Chamaecyparis obtusa* Sieb. et Zucc.), which was planted in 1959. The trees at this site were not disturbed or diseased. The mean tree height was approximately 17.3 m, and the mean diameter at breast height was 0.19 m in 2014. The forest also contained sparsely distributed Japanese red pine (*Pinus densiflora*) and broadleaf trees. The study site had a warm temperate monsoon climate. The annual mean air temperature and precipitation measured at KEW from 2000 to 2010 were 13.4°C and 1578 mm yr^{-1}, respectively. Rainfall occurred throughout the year with two peaks in the summer due to the Asian monsoon: the early summer ‘Baiu’ front season and the late summer typhoon seasons.

At the study site, canopy fluxes of heat, water, and CO_2 have been measured by the eddy covariance method (Takanashi et al., 2005; Kosugi and Katsuyama, 2007; Kosugi et al., 2007; Ohkubo et al., 2007). Soil CH_4 fluxes from wetlands located in riparian zones along streams within KEW and water-unsaturated forest floors were investigated using manually operated chambers with a gas chromatograph analyzer as mentioned above (Itoh et al., 2005, 2007, 2009). Neither CH_4 emission nor absorption from the leaves and trunk were detected by continuous measurement using the automated chamber system (Takahashi et al., 2012).

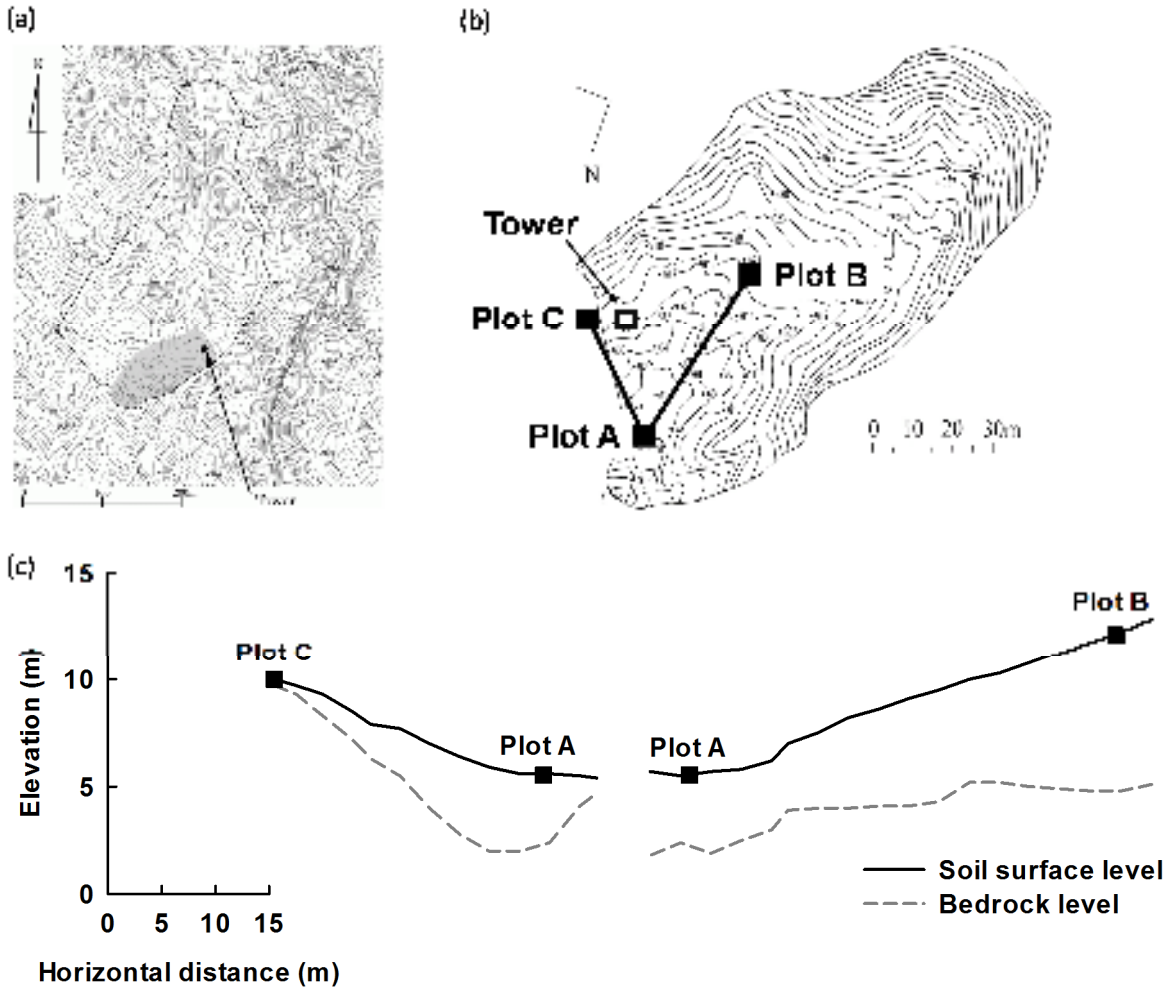

Figure 3.1 Site description of the Kiryu Experimental Watershed forest in Japan. (a) Topographic large-scale map; gray shading indicates the location of the study site. (b) Topographic small-scale map of the study site. The squares denote the location of three measurement plots and the micrometeorological tower. (c) Longitudinal and cross sections along the lines indicated in Figure 3.1 (b). The squares denote the location of measurement plots.

3.2.2. Sampling plot

I established three sampling plots within the small catchment (gray shaded zone in Figure 3.1a and b). The catchment had a sloped topography, and the water content in the soils differed depending on the location of the slope. The plots were located in 1) the lower part of the slope adjacent to the stream, with a subsurface aquifer year round (plot A); 2) the middle part of the slope, with a subsurface aquifer except during the driest period (plot B); and 3) the upper part of the slope, generally lacking a subsurface aquifer (plot C), as shown in Figure 3.1b and c (Ohte et al., 1995). The maximum distance between plots was approximately 40 m (between plots A and B). In plot A, the top layer of the forest floor consisted of fractional fresh and partly decomposed leaves (0.02–0.03 m depth), below which there was a 0.05-m deep A horizon, these layers were termed the litter layer and humus layer, respectively. The depth from soil surface to the bedrock level was 3.2 m. In plot B, the top layer also consisted of a litter layer (0–0.02 m depth), below which there was a 0.07-m deep humus layer. The depth from the soil surface to the bedrock level was 7.5 m. In plot C, there was a shallow litter layer (0–0.01 m depth) and no humus layer. The depth from the soil surface to the bedrock level was 0.3 m (Table 3.1).

Mineral and organic soil samples were obtained in bulk at each of the three plots, representing vertical profiles, on May 1, 2013. Topsoil samples (0–0.05, 0.05–0.10, and 0.10–0.20 m) were obtained (n = 3 at each depth). Soils were sieved through a 2-mm mesh sieve to remove coarse fragments and then homogenized. Soil pH was determined in a 1:5 w/v air-dried soil/distilled water mixture using a glass electrode pH meter (S40, Mettler Toledo, Switzerland). Electric conductivity (EC) was determined for the same slurry using a conductivity meter (CM-30V, TOA, Japan). The soil total carbon (C) and nitrogen (N) were measured with a CN analyzer (Sumigraph NC-900, Sumigraph Co., Japan)

Table 3.1 Soil properties in each plot at three vertical profiles.

	Soil depth (cm)								
	Plot A			Plot B			Plot C		
Parameter	0-0.05 m	0.05-0.1 m	0.1-0.2 m	0-0.05 m	0.05-0.1 m	0.1-0.2 m	0-0.05 m	0.05-0.1 m	0.1-0.2 m
Porosity (%) n=10	64.4±6.2			63.8±4.3			57.4±4.5		
Bulk density (g cm^{-3}) n=10	0.89±0.19			0.87±0.13			1.03±0.14		
EC (mS m^{-1}) n=3	8.7±6.1	3.6±0.2	3.1±0.5	6±1.5	3.6±0.6	3±0.6	2.9±0.6	2.5±1	1.9±0.7
pH (H_2O) n=3	4.5±0.6	4.8±0.3	4.9±0.1	4.9±0.5	4.9±0.3	5.2±0.6	5.2±0.2	5.3±0.6	5.8±0.6
Total C (mg g^{-1}) n=3	167.5±96.5	20.2±1.4	17.1±6.5	88.4±14.8	20.2±2.6	12.8±3.7	18.4±3.9	15.7±11	5.5±2.1
Total N (mg g^{-1}) n=3	6.9±3.4	1.6±0.1	1.3±0.4	4.4±0.8	1.6±0.2	1.1±0.2	1.4±0.1	1.2±0.5	0.6±0.2
C/N ratio n=3	23.4±3.1	13±0.7	13±0.7	20.1±2.3	12.8±1.1	11.4±1	13.5±2.1	12.3±3.1	8.5±1.6

3.2.3. CH_4 and CO_2 production in forest soils during anaerobic incubation

I conducted anaerobic incubation of the soils (0–0.03 m depth) for the three sampling plots to investigate CH_4 production potential at each plot. Soil samples were collected on August 26, 2014 under hot and humid conditions, when CH_4 production was supposed to be the most active at any point during the year. Soils were sieved through a 2-mm mesh sieve, and wet-soil samples (10 g) were submerged in distilled water to a volume of 10 mL in 65-mL glass vials, which were sealed with butyl rubber stoppers and capped with plastic caps within 6 h after sampling (n = 10 at each plot). The soil solutions were purged, and headspace gas was replaced completely with pure N_2 gas using needles that reached the solution. Vials were incubated under static conditions in the dark at 30°C. CH_4 and CO_2 concentrations in the vial headspace were sampled and injected into the gas chromatographs equipped with flame ionization detectors and a thermal-conductivity detector (GC-2014, Shimadzu, Japan) using a gas-tight syringe (injection volume of 0.3 mL for each measurement). Vials were shaken gently before gas concentration measurements. Measurements were carried out 1, 2, 3, 9, and 21 days after starting incubation. I calculated the CH_4 and CO_2 production rates under anaerobic conditions by dividing the amount of produced gases by the incubation period. Potential CH_4 and CO_2 production rates are expressed on a dry-soil basis (oven dried at 105°C for 48 h).

3.2.4. CH_4 absorption and CO_2 emission measurements

Soil surface CH_4 absorption and CO_2 emission were measured using dynamic closed chambers with automatically opening and closing lids (30 cm × 30 cm × 20 cm = L × W × H). A chamber was installed at each plot. The same system was used to measure CH_4 fluxes from the leaves and trunk (Takahashi et al., 2012). The collars were inserted tightly into the ground up to 5 cm in depth prior to the start of the sampling period. A small fan (3 cm × 3 cm × 1cm) was installed in the chamber to homogenize the inside air. Air from the sample chamber was circulated to a CO_2/H_2O analyzer (LI-840; Li-Cor Inc., Lincoln, NE, USA) and a laser-based spectrometer CH_4 analyzer (FMA-200; Los Gatos Research, Mountain View, CA, USA) through polyethylene tubes (inner tube: 4 mm in diameter) by a diaphragm pump (APN-085, IWAKI PUMPS, Tokyo, Japan; DM-403ST-25, MFG. CO., LTD., Kyoto, Japan)

controlled using a mass flow controller (MPC0005, Yamatake, Tokyo, Japan) at a flow rate of 1.8 L min^{-1}. After measuring, the sampled air was returned to the chamber. Opening and closing of the chamber lid were controlled by pressurized air supplied by an air-compressor (FH-02, MEIJI, Osaka, Japan). The switching among the chambers was regulated by the solenoid valves (CKD USB3-6-3-E, CKD Corp., Aichi, Japan) and a 16-channel AC/DC controller (SDM-CD16AC, Campbell Scientific, UT, USA). Three filters were inserted in the gas sample line to protect the CH_4 analyzer from dust and insects. Before entering the CO_2/H_2O and CH_4 analyzers, the sampled air was dried using a gas dryer (PD-50T-48, Perma Pure Inc., Toms River, NJ, USA). Dilution by water vapor, which could not be completely removed by the drying system, was corrected using the H_2O concentration measured with the CO_2/H_2O analyzer.

Chamber measurements were repeated every 30 min. Data were recorded at 1 Hz using a CR1000 data logger (CR1000, Campbell Scientific) and stored on a compact flash card using a compact flash module (CFM100, Campbell Scientific). A 2-s moving average filtered the high frequency noises for the CO_2/H_2O analyzer, and a 1-s moving average was used for the CH_4 analyzer. The data analyzed in this chapter were recorded from August 1, 2009 to August 31, 2010. Data were missing from September 19 to 24, 2009 in plot B, from September 9 to 24, 2009 in plot C due to chamber instrumental malfunctions, and from June 29 to August 6, 2010 in all plots due to CH_4 analyzer malfunctions.

CH_4 and CO_2 fluxes were deduced from the rate of change of gas concentrations with time, as determined using linear regression as follows (Eq. 3.1).

$$flux = \frac{dc}{dt} \times \frac{V}{S} \times \rho_{amol} \qquad \text{(Eq. 3.1)}$$

where $\frac{dc}{dt}$ is the rate of increase in the gas concentration c (ppm) with time t (s); $\frac{dc}{dt}$ is determined from the slope of the change in gas concentration from 90 to 170 s from the start of measurement using the linear least-squares method; V is the volume of the chamber (0.018 m^3); S is the surface area of the

chamber (0.09 m^2); and ρ_{amol} is the air mole density (mol m^{-3}). Generally, negative flux means net CH_4 absorption, whereas positive flux does net CH_4 emission. In this paper, however, we present positive flux values as CH_4 absorption in order to simplify the comparison between CH_4 and CO_2 flux variations. The zero offset of the CO_2/H_2O and CH_4 analyzers was checked against nitrogen gas every day at 12:15 h. The CO_2/H_2O analyzer was calibrated every few months using a standard CO_2 gas cylinder and a humidity calibrator (HG-1, Michell Instruments, Tokyo, Japan). To examine the accuracy and precision of the CH_4 analyzer, calibration experiments were performed on site using a standard CH_4 gas cylinder (Takachiho, Tokyo, Japan; 1,773 ppb CH_4 in synthetic air) during the course of this measurement. The performance of the CH_4 analyzer was tested using the Allan variance method (e.g., Eugster and Plüss, 2010). This assessment suggested that the Allan deviation of our analyzer was 0.7 ppb, with a 1-s integration time at atmospheric levels of CH_4 (Takahashi et al., 2012). The possible error in CH_4 flux, estimated from the overall precision of our system at atmospheric levels of CH_4, was 0.5 nmol m^{-2} s^{-1}.

3.2.5. Environmental monitoring

Volumetric soil water content (VWC) at a depth of 0–30 cm was measured with a CS616 water content reflectometer (Campbell Scientific) at each plot. Soil moisture was converted into water-filled pore space (WFPS) as follows: WFPS = VWC/total pore volume. Total pore volume was measured in the laboratory with ten 100-mL undisturbed soil samples taken from a mineral soil layer at each plot. Soil temperatures were measured with copper-constantan thermocouples at depths of 2 cm just adjacent to each of the three chambers. Precipitation was measured with a tipping bucket rain gauge at an open screen site near the tower.

3.2.6. Gap filling

To evaluate the annual budgets of CH_4 absorption and CO_2 emission fluxes, I applied the linear interpolation method for gaps within 6 h and the mean diurnal variation (MDV) method (Falge et al., 2001) for gaps longer than 6 h. The MDV was created for each day with a 15-day moving window. CH_4 and CO_2 fluxes were filled 19.2% and 18.8% in plot A, 19.2% and 18.7% in plot B, and 20.1% and 19.6% in plot C.

3.2.7. Statistical analysis

The mean and SD of CH_4 absorption and CO_2 emission over the entire measurement period in each plot were calculated using half-hourly fluxes. Mean fluxes are presented as the mean ± SD. The ranges of CH_4 absorption and CO_2 emission fluxes were calculated from half-hourly fluxes. One-way analysis of variance (ANOVA) with post hoc Games-Howell test at the 0.05 significance level was used to compare the means of topsoil C and N concentrations and potential CH_4 and CO_2 production rates at each plot. This analysis was performed with SPSS Statistics 21 (IBM SPSS Statistics, IBM Corp., Armonk, NY, USA).

3.3. Results

3.3.1. Soil properties

There were no significant differences in the topsoil (0–0.05 m) pH and EC among plots (Table 3.1). The topsoil N concentration ranged from 6.9 mg g^{-1} (plot A) to 1.4 mg g^{-1} (plot C). The topsoil C concentration ranged from 167.5 mg g^{-1} (plot A) to 13.4 mg g^{-1} (plot C). The topsoil N and C concentrations in plot C were significantly lower than those in plot A ($p < 0.05$ and $p = 0.041$, respectively). This is probably because sandy soil with larger particle sizes was more common in plot C. Plot B had moderate N and C concentrations among the three plots, i.e., lower than plot A and higher than plot C; however, these differences were not significant. The topsoil C/N ratio ranged from 23.4 (plot A) to 13.5 (plot C). The C/N ratio in plot C was significantly lower than those of plots A and B ($p < 0.01$ and $p < 0.05$, respectively). There were no significant differences in topsoil C/N ratios between plots A and B.

3.3.2. CH_4 and CO_2 production in forest soils during anaerobic incubation

In terms of the potential to produce CH_4, no CH_4 production was observed the next day after incubation at all plots, except for one soil in plot A (Figure 3.2a). Two days after incubation, CH_4 production was observed at all plots. Nine days after incubation, a sharp increase in CH_4 production was observed in plot A, and this distinguished plot A from the other two plots. In plot C, both potential CH_4 and CO_2 production rates were significantly lower than those in the other plot throughout the

experimental period ($p < 0.01$; Figure 3.2a and b).

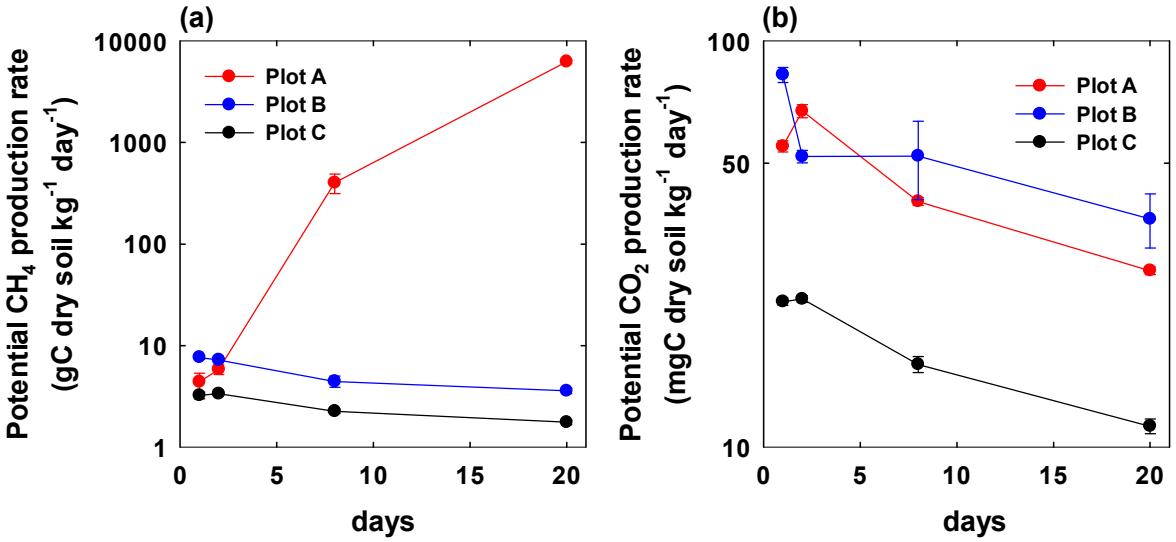

Figure 3.2 The potential production rates of (a) CH_4 and (b) CO_2 of sampled soils in each plot 1, 2, 8, and 20 days after the first measurement day. The samples were incubated at 30°C. Means and standard deviations (error bars) are shown (n = 10).

3.3.3. Time course analysis of soil environment, CH_4 absorption, and CO_2 emission

Figure 3.3 illustrates annual variations in daily average soil temperature, precipitation, and WFPS, and 30-min CH_4 absorption and CO_2 emission fluxes in each plot. Higher soil temperature and more precipitation were observed in summer than in winter (Figure 3.3a). Among plots, plot A had higher WFPS than plots B and C throughout the experimental period (Figure 3.3b). Although plot C also had higher WFPS than plot B, the WFPSs in plots B and C were smaller than those of plot A for all seasons. The CH_4 absorption fluxes ranged from -0.45 to 1.25 nmol m^{-2} s^{-1} (annual average, 0.38 ± 0.16 nmol m^{-2} s^{-1}) in plot A, from 0.13 to 3.70 nmol m^{-2} s^{-1} (annual average, 2.16 ± 0.49 nmol m^{-2} s^{-1}) in plot B, and from -1.20 to 2.02 nmol m^{-2} s^{-1} (annual average, 0.44 ± 0.34 nmol m^{-2} s^{-1}) in plot C (Figure 3.3c). The CO_2 emission fluxes ranged from 0.22 to 6.17 μmol m^{-2} s^{-1} (annual average, 2.44 ± 1.46 μmol m^{-2} s^{-1}) in plot A, from 0.26 to 7.55 μmol m^{-2} s^{-1} (annual average, 2.57 ± 1.73 μmol m^{-2} s^{-1}) in plot B, and from -0.94 to 7.13 μmol m^{-2} s^{-1} (annual average, 1.81 ± 1.54 μmol m^{-2} s^{-1}) in plot C (Figure 3.3d).

Annual budgets of CH_4 absorption from September 1, 2009 to August 31, 2010 were 142 mg C m^{-2} yr^{-1} in plot A, 825 mg C m^{-2} yr^{-1} in plot B, and 162 mg C m^{-2} yr^{-1} in plot C (Table 2). Those of CO_2 emission were 871 mg C m^{-2} yr^{-1} in plot A, 912 mg C m^{-2} yr^{-1} in plot B, and 608 mg C m^{-2} yr^{-1} in plot C. In plot A, which was characterized by thick organic layers and a high WFPS, the annual budget of CH_4 absorption was the smallest among plots; however, the annual budget of CO_2 emission was the second largest after plot B. In plot B, which was characterized by a thick humus layer and a low WFPS, the annual budget of CH_4 absorption and CO_2 emission were the highest among plots. In plot C, which was characterized by a thin humus layer and a low WFPS, the annual budget of CH_4 absorption and CO_2 emission were significantly smaller than those in plot B. The coefficients of variation for both CH_4 and CO_2 fluxes in plot C were the highest among plots.

Table 3.2 Annual budgets of CH_4 absorption and CO_2 emission at each plot from September 1, 2009 to August 31, 2010.

	Plot A	Plot B	Plot C
Annual budget of CH_4 absorption flux (mg C m^{-2} yr^{-1})	142	825	162
Annual budget of CO_2 emission flux (mg C m^{-2} yr^{-1})	871	912	608

3.3.4. Effects of soil temperature and moisture on seasonal variations in CH_4 absorption

CH_4 absorption showed seasonal variations in every plot (Figure 3.3c), and the largest variation was observed in plot B. Although the ranges of CH_4 absorption fluxes in plots A and C were smaller than that in plot B, a similar seasonal pattern of CH_4 absorption was observed in every plot. The rainy season 'Baiu' occurred in June 2009, and the Baiu front became active in late July 2009. In addition, the typhoon 'Etau' brought much rain from August 8 to August 11, 2009 (32.8 mm within 96 h). After heavy

rainfall, the CH_4 absorption became small in early August 2009 and gradually increased as WFPS decreased from late August 2009. The highest absorption among plots in 2009 was observed on September 29 in plot B. In early October 2009, the typhoon 'Melor' brought much rain (136.2 mm within 48 h), and CH_4 absorption decreased. A gradual decrease was observed as the temperature decreased. The WFPS was maintained at relatively high levels during the winter, and there was no remarkable decline in CH_4 absorption. In plot B, the CH_4 absorption increased again as the temperature increased in spring 2010. However, CH_4 absorption was decreased by the summer intensive rainfall, and 'Baiu' began on June 13, 2010 (shown as the first arrow in Figure 3.3c). From July 17, after the 'Baiu', CH_4 absorption increased again as WFPS decreased and temperature increased (shown as the second arrow in Figure 3.3c). The highest absorption in 2010 was observed on August 26 in plot B when the soil temperature was high and the soil was dried (shown as the third arrow in Figure 3.3c). The seasonal variation in soil CH_4 absorption was strongly influenced by intensive summer rainfall resulting from the Asian monsoon climate and typhoon at my site. In contrast, the seasonality in CO_2 emission was strongly correlated with soil temperature in every plot (Figure 3.3d). High CO_2 emission was observed during summer, but decreased as the temperature decreased heading into winter. The WFPS also affected the seasonality of CO_2 emission. CO_2 emission decreased when the soil was dried, even at high temperatures, in the middle of September 2009, in late June 2010, and in early August 2010.

I focused on soil temperature and WFPS as major factors controlling the seasonal variations in CH_4 absorption and CO_2 emission. The relationships between soil temperature and CH_4 absorption or CO_2 emission are shown in Figure 3.4. Linear regression equations for CH_4 fluxes (Potter et al., 1996; Ridgwell et al., 1999; Del Grosso et al., 2000) and the first-order exponential equations for CO_2 fluxes (Lloyd and Taylor, 1994) were used to determine the coefficient R^2, which measures the goodness of the fit of the regression model. All regression models were significant ($p < 0.01$). Both CH_4 absorption and CO_2 emission generally increased as the soil temperature increased in every plot, but CH_4 absorption exhibited larger variation than CO_2 emission. The R^2 of CH_4 fluxes was lower than that of CO_2 fluxes. In particular, the R^2 of the CH_4 flux in plot A was the lowest among plots (Figure 3.4a). The relationships

between soil temperature and CH_4 absorption or CO_2 emission were affected by the WFPS; high WFPS inhibited CH_4 absorption and CO_2 emission in every plot (Figure 3.4a–f). CO_2 emissions showed similar temperature dependence among plots, while CH_4 absorption showed unique temperature dependences among plots and was not universal across plots. In plot A, CH_4 absorption increased slightly as soil temperature increased (Figure 3.4a). In plot B, CH_4 absorption clearly increased from 10°C to 20°C, and the maximum absorption was observed when the soil temperature was 20.3°C and the WFPS was 11.6% (Figure 3.4b). On the other hand, CH_4 absorption flux did not increase simply according to the increase in temperature, and a greater variation was observed above 20°C, where CH_4 absorption with high WFPS was low. In plot C, CH_4 absorption increased with increasing temperature above 10°C and had a larger variation at higher temperatures (Figure 3.4c). The maximum absorption was observed when the soil temperature was 26.2°C and the WFPS was 21.3%.

Figure 3.5 shows the relationships between WFPS and CH_4 absorption or CO_2 emission flux. Comparing the relationship between WFPS and CH_4 absorption or CO_2 emission, CH_4 absorption was decreased as the WFPS increased at every plot (Figure 3.5a), while CO_2 emission exhibited varying behaviors upon changes in the WFPS (Figure 3.5e). CH_4 absorption increased as the WFPS decreased over the whole temperature range studied in this work (Figure 3.5b–d), while CO_2 emission depended moderately on the WFPS only at high soil temperatures above about 20°C in plots B and C (Figure 3.5g and h). It should also be noted that the relationship between CH_4 absorption and WFPS was not universal, but rather unique to each plot (Figure 3.5a). Additionally, this relationship seemed to be mitigated at the driest conditions. CH_4 absorption seemed to be decreased in plots B and C when the WFPS was relatively low (< 20%; Figure 3.5a). Corresponding CO_2 emission also seemed to be decreased when the WFPS was relatively low in plots B and C (Figure 3.5e).

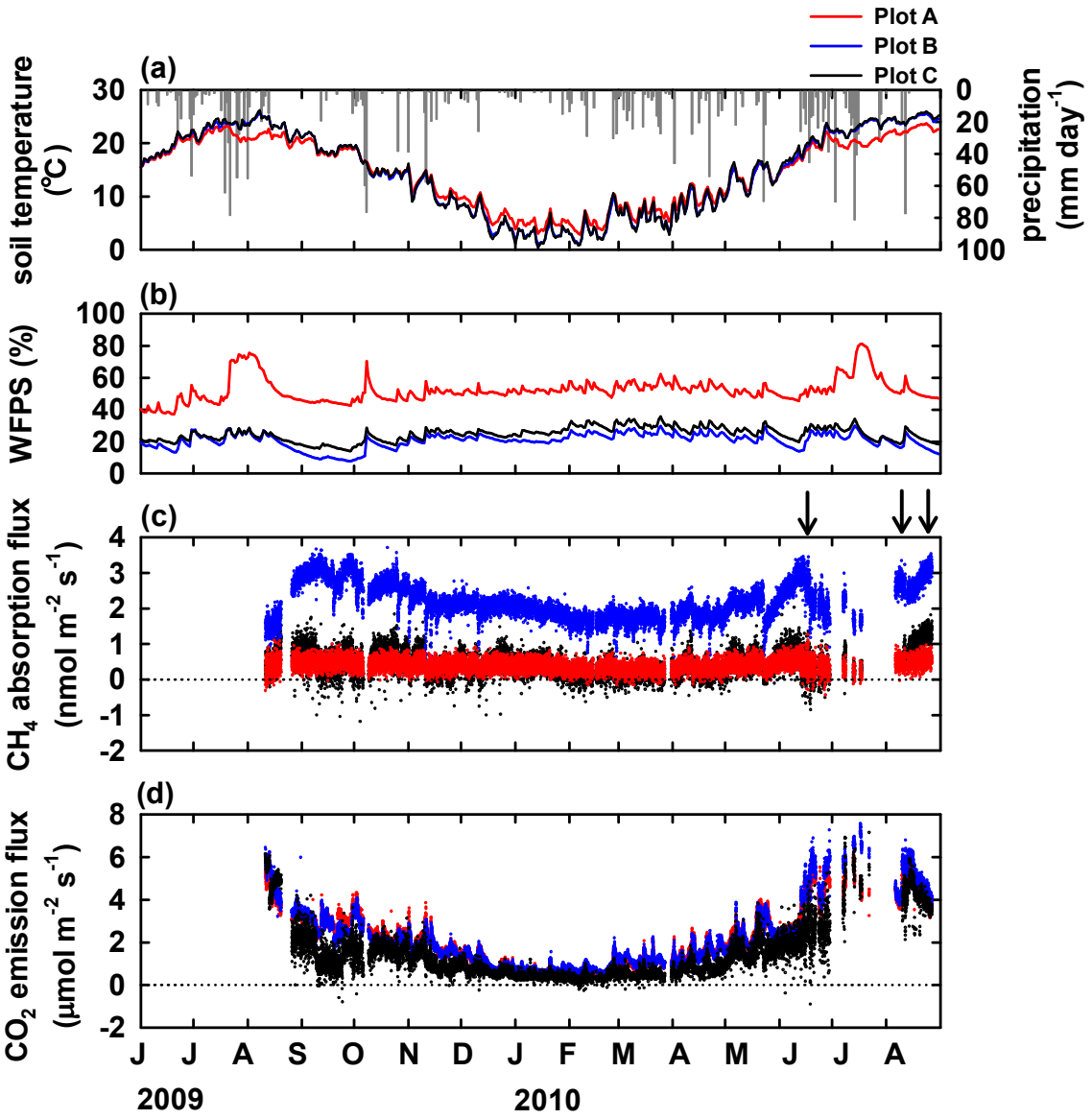

Figure 3.3 Annual variations in daily averaged (a) soil temperature and precipitation, (b) WFPS, (c) 30-min CH_4 absorption, and (d) 30-min CO_2 emission in each plot from August 1, 2009 to August 31, 2010.

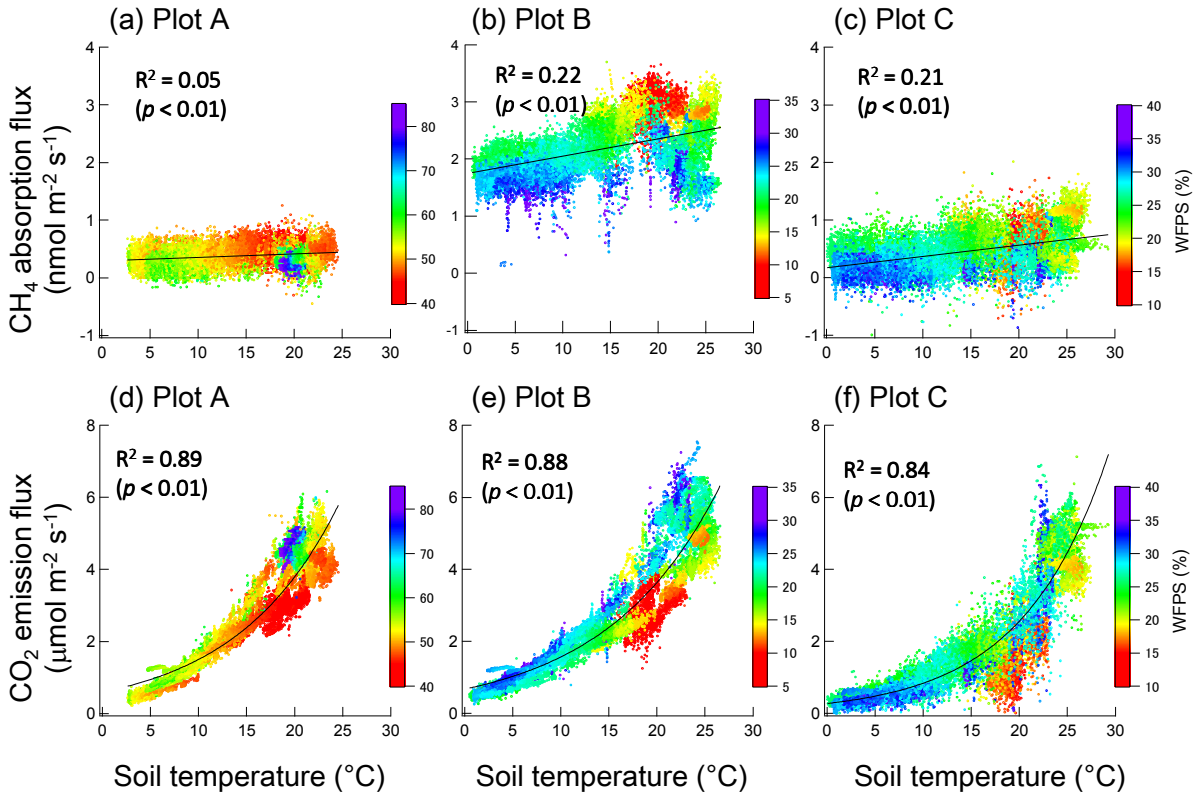

Figure 3.4 Relationships between soil temperature and CH_4 absorption in (a) plot A, (b) plot B, and (c) plot C. The plots are color-coded according to WFPS. Relationships between soil temperature and CO_2 emission in (d) plot A, (e) plot B (e), and plot C (f). The black line shows the linear equation for CH_4 flux and the first-order exponential equation for CO_2 flux. The determination coefficient R^2 represents the goodness of the fit of the regression model. The probability values of each regression model are shown.

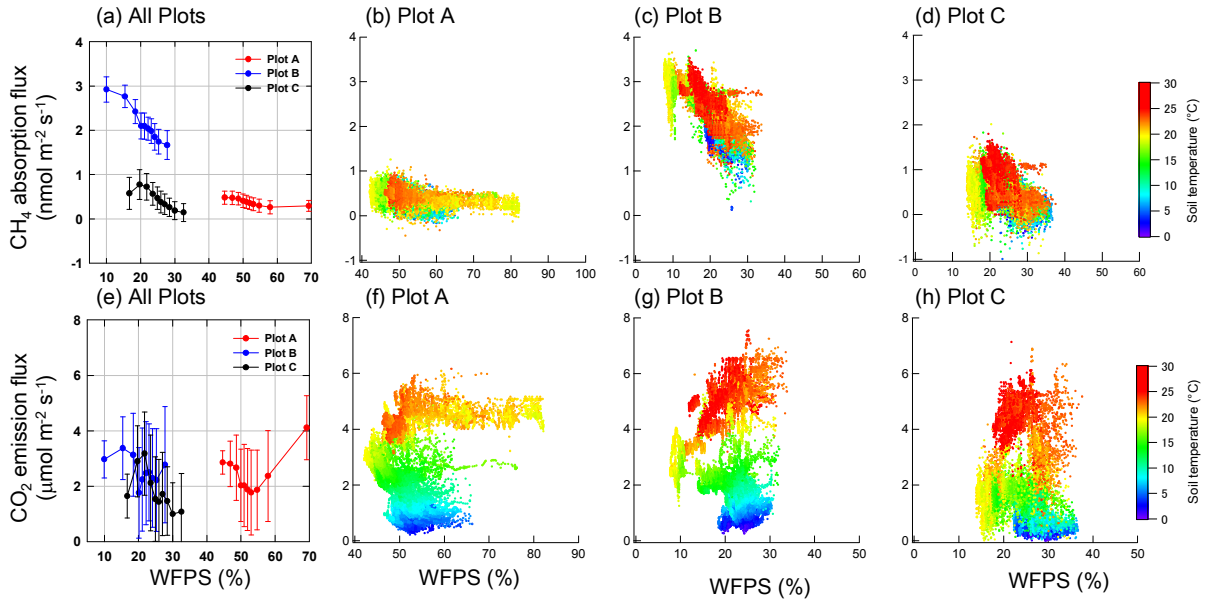

Figure 3.5 Relationship between WFPS and CH_4 absorption or CO_2 emission in each plot. Half-hourly CH_4 absorption fluxes were binned into 10 classes according to WFPS (a). Circles and error bars represent the average and standard deviation of CH_4 absorption. The relationships between WFPS and CH_4 absorption are color-coded according to soil temperatures in plot A (b), plot B (c), and plot C (d). The relationships between WFPS and CO_2 emission were binned into 10 classes according to WFPS (e), and the relationships were color-coded according to soil temperature in plot A (f), plot B (g), and plot C (h).

3.3.5. Responses of CH_4 absorption and CO_2 emission to rainfall

Next, I examined data describing dramatic temporal changes in CH_4 absorption and CO_2 emission fluxes due to rainfall. I focused on the responses of CH_4 absorption and CO_2 emission to different total amounts of precipitation at 30-min intervals. Figure 3.6 shows two representative examples of the plot-dependent responses in CH_4 absorption and CO_2 emission to different rainfall patterns: total rainfall of 38.7 mm with a maximum intensity of 18.1 mm h^{-1} (Figure 3.6a–d), and total rainfall of 71.2 mm with a maximum intensity of 10.2 mm h^{-1} (Figure 3.6e–h). In both rainfall events, the characteristics of the responses of CH_4 and CO_2 fluxes to rainfall events were similar, but their patterns were different for each plot. These data can be summarized as follows: 1) the most prominent responses among the plots

were observed in plot B for CH_4 fluxes; 2) in plot A, remarkable changes in CO_2 flux were observed, while changes in CH_4 flux were not significant; and 3) in plot C, both CH_4 and CO_2 fluxes showed decreases during and after rainfall events.

When I took a closer look at the characteristics of each plot, in plot B, which had a thick humus layer and a normally low WFPS, CO_2 emission increased at the beginning of rainfall in both rainfall events and then decreased abruptly with minima at the peaks of rainfall intensity (Figure 3.6c and g). CH_4 absorption also showed minima at the same time. The reduction in CH_4 absorption and CO_2 emission at the peaks of the rainfall intensity were greater in the case of the 71.2-mm rainfall event than the 38.7-mm rainfall event. After rainfall, however, the responses of CH_4 and CO_2 fluxes were different: CO_2 emission showed abrupt increases followed by long decreases, while CH_4 absorption showed only increases. In plot A, which had a thick humus layer and constantly high WFPS, CO_2 fluxes increased at the beginning in both rainfall events (Figure 3.6b and f), similar to those in plot B, but showed maxima at the peak of rainfall intensity. After rainfall, CO_2 fluxes showed long decreases, similar to those in plot B. On the other hand, CH_4 fluxes in plot A did not exhibit dramatic changes with respect to the rainfall events. In plot C, which exhibited a thin humus layer and a low WFPS, both CO_2 and CH_4 fluxes decreased clearly during rainfall events (Figure 3.6d and h). However, in the case of the 71.2-mm rainfall event, CO_2 flux showed a distinct minimum at the peak of the rainfall intensity (Figure 3.6h). After rainfall, CH_4 fluxes increased quite slowly compared to those in plot B.

Interestingly, in plots A and C, where CH_4 absorption was originally low compared to that in plot B, water-unsaturated forest soil switched from acting as a sink to neutral following rainfall (Figure 3.6b, d, f, and h). Soil in plot C returned to its role as a CH_4 sink after rainfall, concurrent with the decrease in WFPS.

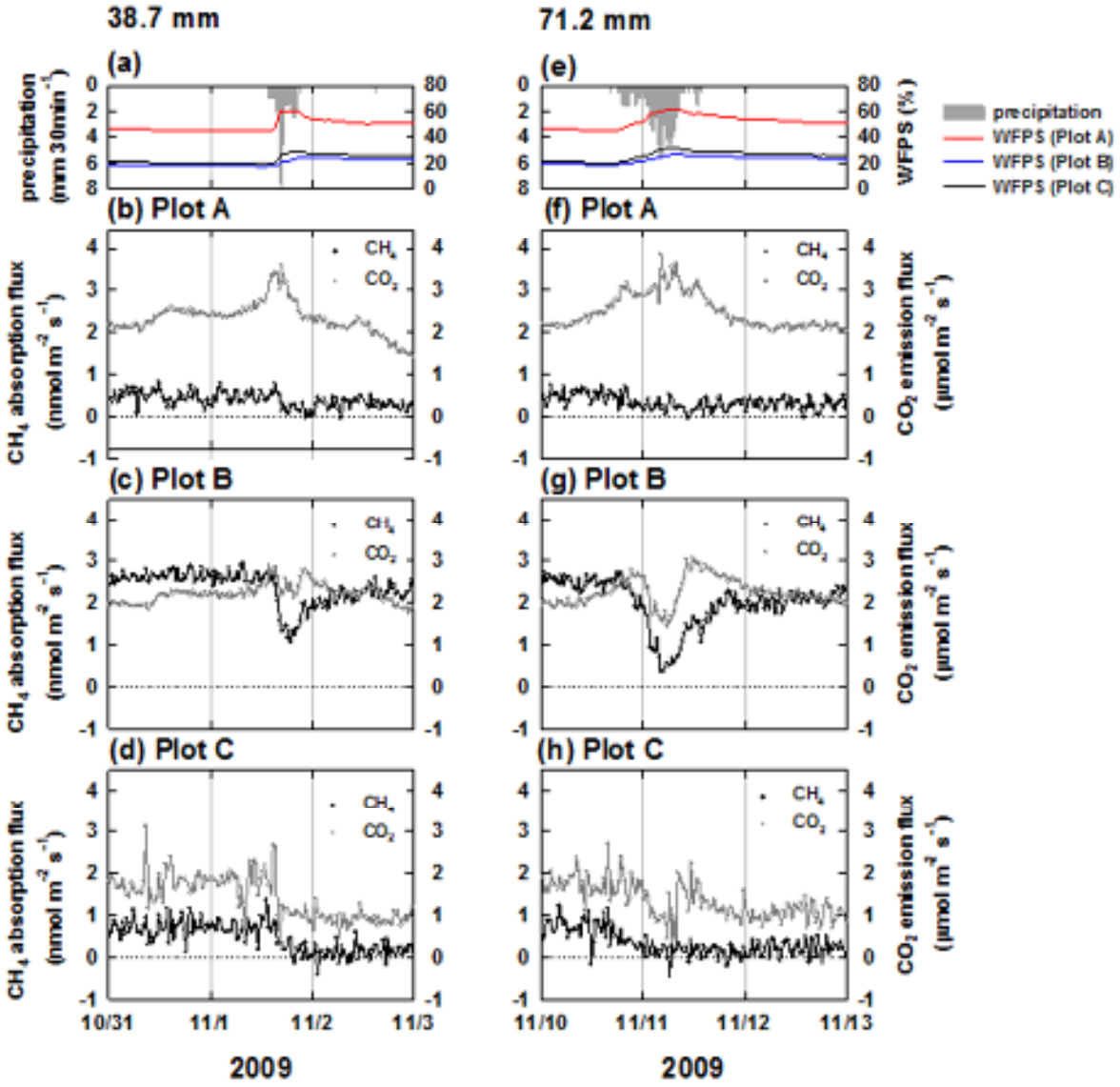

Figure 3.6 Variations in half-hourly precipitation, WFPS, CH_4 absorption, and CO_2 emission during and after rainfall. Responses in CH_4 absorption and CO_2 emission to 38.7 mm precipitation from November 1, 2009 (a) in plot A (b), plot B (c), and plot C (d), and response to 71.2 mm precipitation from November 10, 2009 (e) in plot A (f), plot B (g), and plot C (h) are shown.

3.4. Discussion

3.4.1. Variations in CH_4 absorption

In this chapter, I compared CH_4 absorption among soils with different characteristics in a Japanese temperate Cypress forest. There are three possible reasons for the low CH_4 absorption in the plot with a

thick organic layer and a high WFPS (plot A). First, CH_4 production in wet reductive microsites would have obscured CH_4 oxidation. Even if the surface of the forest floor was usually not saturated with water, CH_4 production could occur deeper within the ground, because the area always had a subsurface aquifer. From the incubation experiment, I found that the potential to produce CH_4 was markedly higher in plot A than in the other two plots (Figure 3.2a). Itoh et al. (2009) reported that CH_4 emission occurred during rainy summers from the water-unsaturated forest floor, adjacent to the riparian zone. Moreover, they suggested that their results were due to CH_4 production in wet reductive microsites on the lower hillslope and near water pathways (Itoh et al., 2005, 2009). To support this, an increase in the CH_4 gas concentration below the soil surface was observed with increasing soil temperature (Itoh et al., 2009). The balance of CH_4 oxidation and production determines the CH_4 absorption flux; thus, net CH_4 oxidation could be reduced by an increase in CH_4 production in a plot with a high WFPS. I assumed that the surface soil water content and the presence of a subsurface aquifer could affect CH_4 fluxes. Second, higher WFPSs lead to smaller pore space, which may restrict the variation range of the WFPS, causing the variation range of CH_4 absorption in plot A to be smaller than that in the other plots (Figure 3.3b and c). Finally, in addition to the anaerobic environment, rich organic matter would contribute to the low CH_4 absorption. Plot A had high C and N concentrations and a high C/N ratio. The high C/N ratio in plot A, which may have resulted from the lower decomposition rate in anaerobic soil than that in aerobic soil, may indicate a reductive environment. A positive correlation between CH_4 production and organic matter content was observed only in the reductive environment, consistent with the observation that organic C is first used by the other reducers before being used by methanogenic bacteria in soils containing significant quantities of oxidants (Wang et al., 1993). Therefore, in plot A, rich organic matter content might activate CH_4 production under a reductive environment. Additionally, CH_4 production is generally thought to be influenced by both the quality and quantity of organic matter present; Whiting and Chanton (1993) suggested that recent plant residues or fresh plant materials are the main substrates for methanogens. If the high C and N concentrations in plot A are indicative of increased input from fresh litters, these contents may be usable for methanogens. Although the CH_4 absorption in plot C was

also low, the low WFPS would contribute to more pore space and larger variations in the WFPS, which would lead to greater variability in CH_4 absorption than that in plot A.

Interestingly, under low WFPS conditions, the CH_4 absorption flux was significantly higher in plot B, which had a thick humus layer, than in plot C, which had a thin humus layer. In the plot with a thick humus layer and high CO_2 emission (plot B), the rich organic content would supply nutrients for microbes, leading to high CH_4 absorption flux. Del Grosso et al. (2000) showed clear contrasts between deciduous forests and other types of ecosystems: the CH_4 oxidation rate in the deciduous forest soils showed a more variable response to soil water content, and this response was generally higher than those observed in other soils. This was thought to be because the high gas diffusivity would promote availability to CH_4 and O_2 for methanotrophs in the porous rich organic layer. In plot C, which had a thin humus layer, and lower CO_2 emission than plot B, the low C and N concentrations may lead to low microbial activity, including that of methanotrophs. I found that the potential to produce CH_4 and CO_2 was the lowest in plot C among the plots examined in my study, although this result was found the incubation experiment under anoxic conditions. These data suggested that the microbial activity under oxic conditions in plot C was also lower than those in the other two plots.

3.4.2. Seasonal variations in soil CH_4 absorption, CO_2 emission, and environmental factor

Intensive summer rainfall due to the Asian monsoon climate controlled seasonal variations in soil CH_4 absorption at my study site (Figure 3.3c). Similarly, Morishita et al. (2007) reported that VWC is an important factor mediating seasonal variations in CH_4 fluxes in Japanese forests, and increased CH_4 absorption resulting from increasing temperature is suppressed by intensive summer rainfall. In addition to this earlier study, I found that CH_4 absorption was decreased after an intensive summer rainfall to the level observed in winter and subsequently recovered along with the recovery of the WFPS from continuous measurements. In winter, high CH_4 absorption was not observed because the temperature was low and the WFPS did not decline very much due to low evapotranspiration.

CO_2 emission flux usually has a unidirectional response to temperature: emission increases with

increasing temperature. On the other hand, CH_4 absorption should have bidirectional responses to temperature because most methanogens and methanotrophs are mesophiles; thus, both CH_4 consumption and production increase as the temperature increases. Dunfield et al. (1993) have shown that methane production and consumption in temperate and subarctic peats are optimum around 20–30 °C for both activities, while some researchers have reported that methanotrophy is preferred over methanogenesis at lower temperatures (King and Adamsen, 1992; Castro et al., 1993; Sitaula et al., 2000). Using incubation experiments using soil cores from a mixed hardwood-coniferous forest, King and Adamsen (1992) found that the increases in the CH_4 oxidation rate with increasing temperatures occurred only at the lower temperature variation (near 0°C), whereas temperature increases in the upper range had little effect on CH_4 consumption. Observations in temperate forests showed that methanotrophy was affected between –5 and 10 °C but not between 10 and 20°C (Castro et al., 1993). Significant methanotrophy was still observed in forest soils at average temperatures lower than 1°C (Sitaula et al., 2000). At my study site, CH_4 fluxes showed large variability at higher temperatures (Figure 3.4b and c), probably because temperature-dependent increases in the activity of methanotrophs decreased, while methanogens can be active at high temperatures and therefore conceal the activity of methanotrophs. In addition, the CH_4 absorption showed a clear dependence on the WFPS throughout the entire temperature range (Figure 3.5b–d), while CO_2 flux showed no clear dependence on the WFPS at low temperatures (Figure 3.5f–h). This result strongly suggested that the activity of methanogens and/or methanotrophs occurred even at low temperatures. Thus, abiotic factors, such as gas diffusivity, which is controlled by the WFPS, would be also important for CH_4 absorption and/or emission by affecting the exchange of CH_4 and O_2 (as substrates for methanotrophs or inhibitors for methanogens) between soil and air. Moreover, if the location of the source of CH_4 was deep in the soil, the temperature would not change very much compared to that at the surface. Thus, I can assume that, as a result of these factors, the CH_4 absorption flux would show much more complex dependence on temperature than the CO_2 emission flux (Figure 3.4a–c). The variability observed in the relationship between the CH_4 absorption flux and soil temperature at high temperatures could be ascribed to the large variability in the WFPS. In summer,

the WFPS exhibited greater variability, and the high temperature promoted the activity of methanogens and methanotrophs, resulting in substantial variability in CH_4 flux. In contrast, in winter, the WFPS exhibited smaller variations, and the activity of methanogens and methanotrophs was low due to the low temperature. Therefore, the variability in CH_4 absorption would be small. During the relatively dry period (WFPS < 20%), CH_4 absorption was decreased, even at temperatures as high as 20°C (plots B and C; Figure 3.5c and d). This is because of the decrease in CH_4 absorption resulting from light rainfall (less than 4 mm h^{-1}) during summer with no antecedent rainfall. At this time, the soil water reflectometer (CS616, Campbell) did not respond to light rainfall, but CH_4 absorption was decreased by rainfall in plots B and C. The small variation in soil water content would cause large variations in CH_4 absorption when the soil dried antecedently; thus, such artifact mitigation of CH_4 absorption fluxes in the driest period could be observed (Figure 3.7).

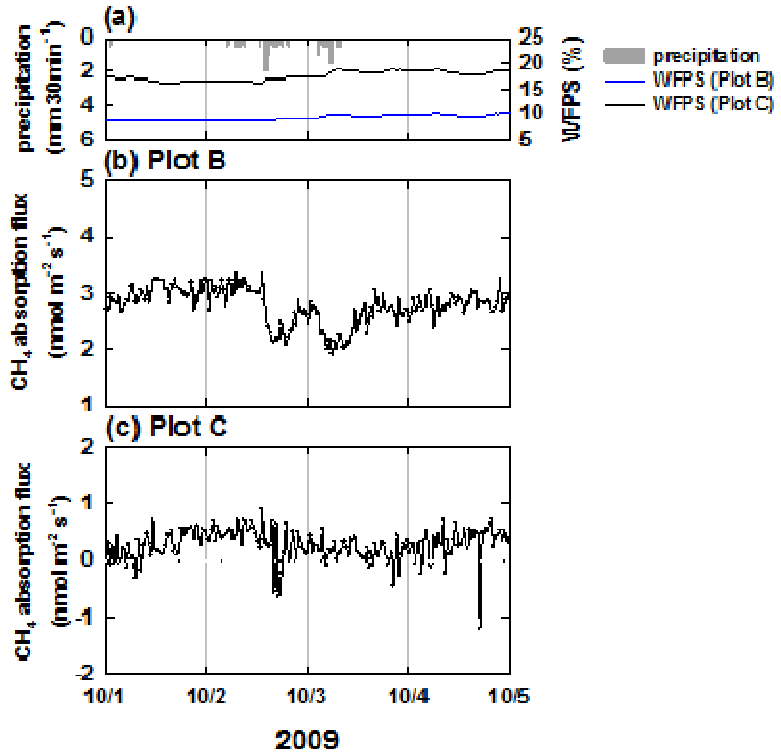

Figure 3.7 Variations in half-hourly precipitation, water filled pore space (WFPS), and CH_4 absorption flux during and after rainfall. (a) 14.8 mm precipitation from October 2, 2010 and response of WFPSs to the precipitation in plots B and C, (b) responses of CH_4 absorption flux to the precipitation in plot B, and (c) plot C are shown.

3.4.3. Responses of CH_4 absorption and CO_2 emission to rainfall

In general, rainfall caused decreases in CH_4 absorption in every plot, though the extent of the depression was plot dependent. In the plot with a normally low WFPS and thick humus layer (plot B), the CH_4 absorption and CO_2 emission showed distinct depressions at the same time at the peak of rainfall intensity (Figure 3.6c and g). The depressions were greater in the case of the 71.2-mm rainfall event than in the case of the 38.7-mm rainfall event. This suggested that the depressions were caused mainly by restricted gas diffusivity at the soil surface by rain water, which would be more restricted as the total amount of rainfall increased. In the plot with a normally high WFPS and thick humus layer (plot A) and the plot with a normally low WFPS and thinner humus layer (plot C), the abrupt depressions in CH_4 fluxes could not be observed clearly, probably because CH_4 absorption was originally low in these plots.

With respect to the differences in responses of CH_4 absorption and CO_2 emission just after rainfall in plot B, CO_2 emission showed abrupt increases followed by long decreases, while CH_4 absorption showed only gradual increases. Such abrupt increases in CO_2 emission could be explained by the observation that accumulated CO_2 in the soil during rainfall would be released immediately after rainfall because of increased gas diffusivity. On the other hand, the restricted gas diffusivity at the soil surface would decrease CH_4 consumption by methanotrophs due to the limited supply of substrate, such as CH_4 and O_2, from the atmosphere (Steudler et al., 1989; Whalen et al., 1990; Adamsen and King, 1993; Castro et al., 1993; MacDonald et al., 1996; MacDonald et al., 1997). Moreover, CH_4 absorption may be obscured in anoxic soil with increased WFPS due to the decreased activity of methanotrophs and increased activity of methanogens long after rainfall. From the incubation experiment, I found that CH_4 production was observed as early as the next day after starting the incubation (Figure 3.2a). Therefore, when rainfall occurs intermittently, it is possible that changes in the activities of methanogens and methanotrophs occur soon after rainfall. Another interesting aspect is that the recovery of CH_4 absorption and CO_2 emission after rainfall in plot B was faster than that in plot C. This is probably because the microbial activities, such as those involved in CH_4 consumption and/or CO_2 production, were lower in plot C than in plot B, as suggested from the incubation experiment.

Moreover, in plots A and C, CH_4 absorption shifted from a sink to neutral state after rainfall. This small, transient shift may be missed under less frequent and less sensitive sampling strategies. Moreover, if the plot exhibiting switching from sink to neutral is large, the effects on ecosystem-scale fluxes may need to be considered during scale-up. Therefore, it is important to understand the process of sink-to-neutral switching (and vice versa) at the plot-scale. I showed that CH_4 absorption was greatly decreased by rainfall and subsequently recovered through the process of sink-to-neutral switching (and vice versa) at the plot-scale. Thus, it is possible that the annual budget of CH_4 absorption flux would be overestimated without considering the rain pulse or underestimated without considering the recovery. Consistent with this hypothesis, simulated annual budgets of CH_4 absorption under the assumption that CH_4 fluxes were measured weekly during fair weather (previously no rain for 24 h) and daytime hours (from 09:00 to 15:00 h) were overestimated from 2.8% to 7.6% in plot A, from 0.9% to 5.6% in plot B, and from 3.1% to 20.1% in plot C. Overestimation was significant in plot C, where CH_4 absorption substantially shifted to neutral after rainfall.

As for CO_2 fluxes, CO_2 emission increased in plots A and B, which both had thick humus layers, at the beginning of rainfall (Figure 3.6b, c, f, and g), while in the plot C, which had a thin humus layer, the CO_2 emission did not increase at the beginning of rainfall (Figure 3.6d and h). This difference may be associated with the high and low microbial activities that produce CO_2 (Orchard and Cook, 1983). The higher CO_2 emission in plots A and B than in plot C were consistent with the incubation experiments, despite being measured under anoxic conditions (Figure 3.2b).

Finally, I note that this type of high time resolution analysis examining the effects of rainfall on CH_4 and CO_2 fluxes was not easily achieved without an automated chamber system coupled to an in-situ trace gas analyzer. In particular, I believe that my approach was a powerful and efficient method to study the short-time dynamics of CH_4 absorption/emission at the soil surface as well as long-term variations in CH_4 flux.

3.4.4. Annual budgets of CH_4 absorption

I obtained annual budgets of CH_4 absorption by taking into consideration the rainfall responses and

compared annual budgets of CH_4 absorption to published data from forest soils around the world, particularly for Japan. The annual budgets of CH_4 absorption in plots A, B, and C were 142, 825, and 162 mg C m^{-2} yr^{-1}, respectively. Detaur and Verchot (2007) reported that the mean annual budgets of CH_4 absorption in boreal, temperate, and tropical forest soils were 198 ± 925 (number of study sites, n = 51), 426 ± 249 (n = 92), and 249 ± 419 (n = 62) mg C m^{-2} yr^{-1}, respectively. Japanese forest soil has been mainly divided into two types: approximately 70% of Japanese forest soils are brown forest soil, mostly cambisols and some andisols, and 13% are black soil (andisols) (Morisada et al., 2004). Based on the synthesis of soil CH_4 absorption measured at 26 sites, the annual budget of CH_4 absorption fluxes is estimated to be 526 mg C m^{-2} yr^{-1} in brown forest soil and 832 mg C m^{-2} yr^{-1} in black forest soil (Morishita et al., 2007). Moreover, CH_4 absorption in black soil has been reported to be significantly higher than that in brown soils because the lower bulk density and higher soil porosity of brown soils lead to increasing supply of CH_4 from the atmosphere through soil pores (Morishita et al., 2007). Within KEW, where the climate is temperate and the soil type is brown forest soil, the annual budget of CH_4 absorption had larger variations than the global average of temperate forests. Moreover, the variation in the annual budget of CH_4 absorption in the plot with a low WFPS and a thick humus layer was comparable to that black forest soil. On the other hand, those in plots with either a high WFPS and thick organic layer or a low WFPS and thin humus layer were smaller than that of brown forest soil, as reported by Morishita et al. (2007). Most modeling to estimate global soil sink for atmospheric CH_4 has focused on the climatic zone, ecosystem type, and soil type. However, the capacity of CH_4 absorption cannot be evaluated by only these factors, and it is necessary to consider spatial variability depending on local soil environments, such as soil water content and the amount of organic matter, temporal variations caused by rainfall, and the observation that the temporal variations greatly differ for the local soil environment.

3.5. Conclusion

In this chapter, I conducted continuous and high time resolution measurements of soil CH_4 absorption and CO_2 emission in a Japanese cypress forest in the Asian monsoon climate with intensive

summer rainfall using an automated chamber system with a TDLS CH_4 analyzer. I found that the highest CH_4 absorption was observed within the summer; however, the CH_4 absorption was greatly decreased by summer intensive rainfall and recovered after rainfall as soil water content decreased. The relationship between CH_4 absorption and soil temperature varied more than that of CO_2 within each plot because CH_4 absorption was strongly affected by soil water content and active over a wide temperature range. Notably, the relationships between CH_4 absorption and soil temperature or soil water content were not universal among plots, with differences in soil physical conditions that controlled the gas exchange between the soil and air. In plots with a high WFPS and thick organic layer, CH_4 absorption was low. When comparing CH_4 absorption in two plots with low WFPSs, I found that CH_4 absorption was significantly higher in the plot with a thick humus layer and lower in the plot with a thin humus layer. Moreover, CH_4 absorption was high in the plot in which decomposition would be active and low in the plots in which decomposition would not be active. Importantly, CH_4 absorption was dramatically inhibited during rainfall and recovered after rainfall, and the responses to rainfall were unique to the specific local environment, which influences gas diffusivity and the balance of activity between methanotrophs and methanogens. The response also changed depending on the amount of rainfall. Therefore, when evaluating the expected CH_4 absorption flux in forests, considering these responses of CH_4 fluxes to rainfall is important, especially in the Asian monsoon climate. Simultaneous measurements of CO_2 fluxes will provide useful information when considering the controlling factors affecting complex CH_4 fluxes.

References

Adamsen, A.P.S., and King, G.M. (1993) Methane consumption in temperate and subarctic forest soils: rates, vertical zonation, and responses to water and nitrogen, Appl. Environ. Microbiol., 59, 485–490.

Broken, W., and Brumme, R. (2000) Effects of prolonged soil drought on CH_4 oxidation in a temperate spruce forest, J. Geophys. Res., 105, 7079–7088.

Castro, M.S., Steudler, P.A., Melillo, J.M., Aber, J.D., and Millham, S. (1993) Exchange of N_2O and CH_4 between the atmosphere and soils in spruce-fir forests in the northeastern United States, Biogeochemistry, 18, 119–135.

Del Grosso, S.J., Parton, W.J., Mosier, A.R., Ojima, D.S., Potter, C.S., Broken, W., Brumme, R., Butterbach-Bahl, K., Crill, P.M., Dobbie, K., and Smith, K.A. (2000) General CH_4 oxidation model and comparisons of CH_4 oxidation in natural and managed systems, Global Biochem. Cy., 14, 999–1019.

Dobbie, K.E., and Smith, K.A. (1996) Comparison of CH_4 oxidation rates in woodland, arable and set aside soils, Soil Biol. Biochem., 28, 1357–1365.

Dunfield, P.F., Topp, E., Archambault, C., and Knowles, R. (1993) Effect of nitrogen fertilizers and moisture content on CH4 and N2O fluxes in a humisol: measurements in the field and intact soil cores, Biogeochemistry, 29, 199–222.

Dutaur, L., and Verchot, L.V. (2007) A global inventory of the soil CH_4 sink, Global Biogeochem. Cy., 21, GB4013, doi: 10.1029/2006GB002734.

Eugster, W., and Plüss, P. (2010) A fault-tolerant eddy covariance system for measuring CH_4 fluxes, Agr. For. Meteorol., 150, 841-851.

Falge, E., Baldocchi, D., Olson, R., Anthoni, P., Aubinet, M., Bernhofer, C., Burba, G., Ceulemans, R., Clement, R., Dolman, H., Granier, A., Gross, P., Grünwald, T., Hollinger, D., Jensen, N., Katul, G., Keronen, P., Kowalski, A., Lai, C.T., Law, B.E., Meyers, T., Moncrieff, J., Moors, E., Munger, J.W., Pilegaard, K., Rannik, Ü, Rebmann, C., Suyker, A., Tenhunen, J., Tu, K., Verma, S., Vesala, T., Wilson, K., and Wofsy, S. (2001) Gap filling strategies for defensible annual sums of net ecosystem exchange, Agr. For. Meteorol., 107, 43–69.

King, G.M., and Adamsen, A.P.S. (1992) Effects of temperature on methane consumption in a forest soil and in pure cultures of the methanotroph methylomonas rubra, Appl. Environ. Microbiol., 58, 2758–2763.

Kirschke, S., Bousquet, P., Ciais, P., Saunois, M., Canadell, J.G., Dlugokencky, E.J., Bergamaschi, P., Bergmann, D., Blake, D.R., Bruhwiler, L., Cameron-Smith, P., Castaldi, S., Chevallier, F., Feng, L.,

Fraser, A., Heimann, M., Hodson, E.L., Houweling, S., Josse, B., Fraser, P., Krummel, P.B., Lamarque, J., Langenfelds, R.L., Le Quéré, C., Nail, V., O'Doherty, S., Palmer, P.I., Pison, I., Plummer, D., Poulter, B., Prinn, R.G., Rigby, M., Ringeval, B., Santini, M., Schmidt, M., Shindell, D.T., Simpson, I.J., Spahni, R., Steele, L.P., Strode, S.A., Sudo, K., Szopa, S., van der Werf, G.R., Voulgarakis, A., van Weele, M., Weiss, R.F., Williams, J.E., and Zeng, G. (2013) Three decades of global methane sources and sinks, Nature Geosci., 6, 813–823, doi: 10.1038/NGEO1955.

Kosugi, Y., Takanashi, S., Tanaka, H., Ohkubo, S., Tani, M., Yano, M., and Katayama, T. (2007) Evapotranspiration over a Japanese cypress forest. I. Eddy covariance fluxes and surface conductance characteristics for 3 years, J. Hydrol., 337, 269–283, doi: 10.1016/j.jhydrol.2007.01.039.

Kosugi, Y., and Katsuyama, M. (2007) Evapotranspiration over a Japanese cypress forest: II. Comparison of the eddy covariance and water budget methods, J. Hydrol., 334, 305–311, doi: 10.1016/j.jhydrol.2006.05.025.

Lelieveld, J., and Crutzen, P. J. (1992) Indirect chemical effects of methane on climate warning, Nature, 335, 339–342.

Le Mer, J., and Roger, P. (2001) Production, oxidation, emission and consumption of methane by soils: A review, Eur. J. Soil Biol., 37, 25–50.

Lee, X., Wu, H., Sigler, J., Oishi, C., and Siccama, T. (2004) Rapid and transient response of soil respiration to rain, Global Change Biol., 10, 1017–1026, doi: 10.1111/j.1365-2486.2004.00787.x.

Ishizuka, S., Sakata, T., and Ishizuka, K. (2000) Methane oxidation in Japanese forest soils, Soil Biol. Biochem., 32, 767–777.

Itoh, M., Ohte, N., and Koba, K. (2009) Methane flux characteristics in forest soils under an East Asian monsoon climate, Soil Biol. Biochem., 41, 388–395, doi: 10.1016/j.soilbio.2008.12.003.

Itoh, M., Ohte, N., Koba, K., Katsuyama, M., Hayamizu, K., and Tani, M. (2007) Hydrologic effects on methane dynamics in riparian wetlands in a temperate forest catchment, J. Geophys. Res., 112, G01019, doi: 10.1029/2006JG000240.

Itoh, M., Ohte, N., Katsuyama, M., Koba, K., Kawasaki, M., and Tani, M. (2009) Temporal and spatial variability of methane flux in a temperate forest watershed, J. Japan Soc. Hydrol. Water Resor., 18, 244–256.

Lloyd, J., and Taylor, J. A. (1994) On the temperature dependence of soil respiration, Functional Ecol., 8, 315–323.

MacDonald, J.A., Skiba, U., Sheppard, L.J., Ball, B., Roberts, J.D., Smith, K.A., and Fowler, D. (1997) The effect of nitrogen deposition and seasonal variability on methane oxidation and nitrous oxide emission rates in an upland spruce plantation and moorland, Atmos. Environ., 31, 3693–3706.

MacDonald, J.A., Skiba, U., Sheppard, L.J., Hargreaves, E.J., Smith, K.A., and Fowler, D. (1996) Soil environmental variables affecting the flux of methane from a range of forest, moorland and agricultural soils, Biogeochemistry, 34, 113–132.

Morisada, K., Ono, K., and Kanomata, H. (2004) Organic carbon stock in forest soils in Japan: Geoderma, 119, 21–32, doi: 10.1016/S0016-7061(03)00220-9.

Morishita, T., Hatano, R., Nagata, O., Sakai, K., Koide, T., and Nakahara, O. (2007) Effect of nitrogen deposition on CH4 uptake in forest soils in Hokkaido, Japan, Soil Sci. Plant Nutrition, 50, 1187–1194.

Ohkubo, S., Kosugi, Y., Takanashi, S., Mitani, T., and Tani, M. (2007) Comparison of the eddy covariance and automated closed chamber methods for evaluating nocturnal CO_2 exchange in a Japanese cypress forest, Agri. For. Meteorol., 142, 50–65, doi: 10.1016/j.agrformet.2006.11.004.

Ohte, N., Tokuchi, N., and Suzuki, M. (1997) An in situ lysimeter experiment on soil moisture influence on inorganic nitrogen discharge from forest soil, J. Hydrol., 195, 78–98.

Ohte, N., Tokuchi, N., and Suzuki, M. (1995) Biogeochemical influences on the determination of water chemistry in a temperate forest basin: factors determining the pH value, Water Resource Res., 31, 2823–2834.

Orchard, V.A., and Cook, F.J. (1983) Relationship between soil respiration and soil moisture, Soil Biol. Biochem., 15, 447–453.

Potter, C.S., Davidson, E.A., and Verchot, L.V. (1996) Estimation of global biogeochemical controls and seasonality in soil methane consumption, Chemosphere, 32, 2219–2246.

Ridgwell, A., Marshall, S.J., and Gregson, K. (1999) Consumption of atmospheric methane by soils: A process-based model, Global Biogeochem. Cy., 13, 59–70.

Sakabe, A., Hamotani, K., Kosugi, Y., Ueyama, M., Takahashi, K., kanazawa, A., and Itoh, M. (2012) Measurement of methane flux over an evergreen coniferous forest canopy using a relaxed eddy accumulation system with tunable diode laser spectroscopy detection, Theor. Appl. Climatol., 109, 39–49, doi: 10.1007/s00704-011-0564-z.

Sitaula, B.K., Hansen, S., Sitaula, J.I.B., and Bakken, L.R. (2000) Methane oxidation potentials and fluxes in agricultural soil: Effects of fertilization and soil compaction, Biogeochemistry, 48, 323–339.

Steinkamp, R., Butterbach-Bahl, K., and Papen, H. (2001) Methane oxidation by soils of an N limited and N fertilized spruce forest in the Black Forest, Germany, Soil Biol. Biochem. 33, 145–153.

Steudler, P.A., Bowden, R.D., Melillo, J.M., and Aber, J.D. (1989) Influence of nitrogen fertilization on methane uptake in temperate forest soils, Nature, 341, 314–316.

Stocker, T.F., Qin, D., Plattner, G.-K., Alexander, L.V., Allen, S.K., Bindoff, N.L., Brëon, F.–M., Church, J.A., Cubasch, U., Emori, S., Forster, P., Friedlingstein, P., Gillett, N., Gregory, J.M., Hartmann, D. L., Jansen, E., Kirtman, B., Knutti, R., Krishna Kumar, K., Lemke, P., Marotzke, J., Masson-Delmotte, V., Meehl, G.A., Mokhov, I.I., Piao, S., Ramaswamy, V., Randall, D., Rhein, M., Rojas, M., Sabine, C., Shindell, D., Talley, L.D., Vaughan, D.G., and Xie, S.–P. (2013) Technical Summary. In: Climate Change 2013: The Physical Science Basis. Contribution of Working Group I to the Fifth Assessment Report of the Intergovernmental Panel on Climate Change, edited by Stocker, T.F., Qin, D., Plattner, G.–K., Tignor, M., Allen, S.K., Boschung, J., Nauels, A., Xia, Y., Bex, V., and Midgley, P.M., Cambridge University Press, Cambridge, United Kingdom and New York, NY, USA.

Takahashi, K., Kosugi, Y., Kanazawa, A., and Sakabe, A. (2012) Automated closed-chamber measurements of methane fluxes from intact leaves and trunk of Japanese cypress, Atmos. Environ., 51, 329–332, doi: 10.1016/j.atmosenv.2012.01.033.

Takanashi, S., Kosugi, Y., Tanaka, Y., Yano, M., Katayama, T., Tanaka, H., and Tani, M. (2005) CO_2 exchange in a temperate Japanese cypress forest compared with that in a cool-temperate deciduous broad-leaved forest, Ecol. Res., 20, 313–324, doi: 10.1017/s11284-005-0047-8.

Wang, Z.P., Lindau, C.W., Delaune, R.D., and Patrick, Jr., W.H. (1993) Methane emission and entrapment in flooded rice soils as affected by soil properties, Biol. and Fertility of Soils, 16, 163–168.

Whalen, S.C., Reeburgh, W.S., and Sandbeck, K.A. (1990) Rapid methane oxidation in a landfill cover soil, Appl. Envi. Microb., 56, 3405–3411.

Whiting, G.J., and Chanton, J.P. (1993) Primary production control of methane emission from wetlands, 364, 794–795.

Xu, L., Baldocchi, D.D., and Tang, J. (2004) How soil moisture, rain pulses, and growth alter the response of ecosystem respiration to temperature, Global Biochem. Cy., 18, GB4002, doi: 10.1029/2004GB00228.

CHAPTER 4

Is the empirical coefficient *b* for the relaxed eddy accumulation method constant?

4.1. Introduction

The eddy covariance method is the most direct approach for continuous ecosystem-scale flux measurements integrated over a large area (~10^4 m^2) without artificial disturbances. However, for some trace gases, fast-response analyzers are not often available to employ direct eddy covariance measurements. The relaxed eddy accumulation (REA) method has been proposed to overcome this limitation (Businger and Oncley, 1990; Hamotani et al., 1996, 2001). The REA method has growing importance in measuring ecosystem-scale trace gas fluxes such as methane fluxes (Sakabe et al., 2012; Ueyama et al., 2013), biogenic volatile organic compounds fluxes (Bowling et al., 1998; Pattey et al., 1998), and isotope fluxes (Bowling et al., 1999; Baldocchi et al., 2003). In the REA method, the flux of a scalar (c) by the eddy covariance method ($\overline{w'c'}$) is approximated as the product of the difference in mean concentrations between the air sampled during updraft and downdraft ($\overline{c^+} - \overline{c^-}$) and the standard deviation of vertical wind velocity (w) (σ_w), multiplied by an empirically determined coefficient b as follows:

$$\overline{w'c'} = b\sigma_w\left(\overline{c^+} - \overline{c^-}\right) \quad (Eq.\ 4.1)$$

where the overbar represents time average (half-hour), and prime represents the fluctuation around the average value.

The principle underlying the REA method is similar to that of the eddy covariance method,

but the former method does not require fast-response gas analyzers. The biggest advantage of the REA method is that optimal precision in gas concentration measurements is achievable by appropriate signal integration over a longer duration (Ueyama et al., 2009). Another advantage of the REA method is that it requires minimal influential corrections such as high-frequency attenuation corrections for closed-path eddy covariance methods (Aubinet et al., 2000), or the Webb, Pearman, and Leuning correction (Webb et al., 1980) for open-path eddy covariance methods. These corrections may cause uncertainties in small true fluxes by an eddy covariance system (Kondo et al., 2008).

On the other hand, one possible limitation of the REA method is the difficulty in developing accurate systems. In particular, the switching speed of the valve system presents a challenge, which may lead to the loss of high-frequency information (Baker et al., 1992). Another possible limitation is that the REA method includes the empirically determined coefficient b (Equation 4.1).

The theoretically expected value for the coefficient b is 0.627 if based on the assumption of an ideal Gaussian joint frequency distribution of turbulent fluctuations and the assumption of a linear relationship between the fluctuations of w and the transported scalar quantities (Baker et al., 1992; Wyngaard and Moeng, 1992; Katul et al., 1996). Observational b (b_{obs}) derived from simultaneous eddy covariance measurements of w and scalars is generally smaller than the expected value of 0.627. The reason for the overestimation of the expected b is that the two assumptions mentioned above are commonly not met (Baker et al., 1992). The reported mean values for b_{obs} range from 0.5 to 0.6 for air temperature (T), carbon dioxide (CO_2), and water vapor (H_2O) (Businger and Oncley, 1990; Baker et al., 1992). Because values for b_{obs} differ from the expected value for b, it is of great practical importance to determine the actual nature of the b_{obs}.

A number of studies have examined the consistency of b_{obs} under various atmospheric stability

conditions. Some have concluded that there is no relationship between b_{obs} and atmospheric stability (Baker et al., 1992; Katul et al., 1996). Others have suggested that b_{obs} is a function of stability (Businger and Oncley, 1990; Andreas et al., 1998; Ammann and Mexiner, 2002; Tsai et al., 2012). It has been suggested that b_{obs} can be considered as a constant of around 0.55 under unstable to neutral conditions, and increases up to 0.63 or higher with stability under stable conditions (Ammann and Mexiner, 2002; Tsai et al., 2012). The dependence of b_{obs} on atmospheric stability may vary with site conditions, data handling such as data quality control, or the limited availability of data on the range of stability conditions.

The value for b_{obs} may also vary with measurement height relative to canopy height, because the values were reported to have wide ranges within and near forest canopy (Gao, 1995). Gao (1995) has found that b_{obs} for air temperature and H_2O decreases as measurement height approaches the canopy top. Ueyama et al. (2009) have reported that the REA method tends to underestimate nighttime CO_2 emission compared with the eddy covariance method. They have suggested nonstationarity under stable conditions as one of the reason of the underestimation.

Most previous REA studies used two different approaches for determining b. Some used mean values of b_{obs} for the entire study period as a constant b_{obs} (Baker et al., 1992; Beverland et al., 1996), and the others recommended the use of variable b_{obs} for each half hour (Oncley et al., 1993; Pattey et al., 1993; Gao, 1995). On the other hand, Katul et al. (1996) concluded that there is no clear advantage in using a variable b_{obs} determined from another scalar versus a constant b_{obs}. Since most previous studies have been based on a short field campaign (Baker et al., 1992; Katul et al., 1996; Ammann and Mexiner, 2002), the consistency of b_{obs} at seasonal timescales remains uncertain.

Investigations of the consistency of b_{obs}, including its dependency on atmospheric stability, measurement height, canopy height, and season are essential in order to minimize the

uncertainties in the REA method. If b_{obs} has site-specific dependency on atmospheric stability, consideration of the effect of atmospheric stability on b_{obs} at each site is necessary. The variability in b_{obs} directly affects the fluxes measured by the REA method. For example, the variation of b_{obs} from 0.5 to 0.6 may result in a difference of about 18% error ($=(0.6-0.5)/0.55$) in the REA fluxes if a constant b_{obs} is used.

This chapter attempts to clarify under what conditions b_{obs} may not be constant and when the variations in b_{obs} need to be taken into account when calculating the REA fluxes. In order to accomplish this, this chapter employs data from three forest sites, covering different forest types and measurement heights at seasonal timescales under various stability conditions. This chapter is focused on the values of b only for air temperature solely because most previous studies have found that the differences of b among scalars were not significant (Gao, 1995 for air temperature and H_2O; Katul et al., 1996 for air temperature, H_2O, O_3 and CO_2; Ammann and Meixner, 2002 for air temperature, H_2O and CO_2).

When estimating fluxes of trace gases for which b_{obs} cannot be obtained directly from simultaneous fast measurements, REA fluxes are calculated using b_{obs} obtained from proxy scalars such as air temperature, by assuming that trace gases are transported by atmospheric turbulence in the same manner (Bowling et al., 1999; Park et al., 2010; Sakabe et al., 2012; Ueyama et al., 2013). In addition, air temperature is less uncertain than H_2O or CO_2 because air temperature does not need corrections for density fluctuations or sensor separation in case all three axes of the sonic anemometer samples the same approximate volume. Furthermore, air temperature fluctuations are generally measured by a sonic anemometer at most sites. In order to interpret b_{obs}, the similarity b ($b_{similarity}$) is derived using the Monin-Obukhov similarity theory for the integral turbulence characteristics (Kaimal and Finnigann, 1994).

4.2. Methods

4.2.1. Site Description and Measurements

The Data were collected for 10 months at a temperate evergreen coniferous forest with complex terrain, for one year at a tropical evergreen broadleaf forest with flat terrain and high canopy height where surface conditions do not change throughout the year, and for one year at a cool-temperate deciduous coniferous forest with flat terrain where surface conditions change throughout the year (Table 4.1).

4.2.1.1. Kiryu Experimental Watershed

The Kiryu Experimental Watershed (KEW) (34°58'N, 136°00'E) is a temperate evergreen coniferous forest in central Japan. The site has a northward slope of approximately 9.2% (Kosugi et al., 2007). The forest consists of 50-year-old Japanese cypress (*Chamaecyparis obtusa*). The mean tree height (h) is approximately 17 m. The total plant area index measured using a plant canopy analyzer (LAI-2000; LI-COR Inc., Lincoln, NE, USA), ranges from 4.5 to 5.5 m^2 m^{-2} with some seasonal fluctuation.

The annual mean air temperature and precipitation from 2002 to 2009 were 13.3°C and 1576 mm yr^{-1}, respectively. Fluctuations in the three-dimensional wind velocity (m s^{-1}) and air temperature (°C) were measured by a sonic anemometer (SAT-550; Kaijo Corp., Tokyo, Japan) at 29 m above ground level. Further details are given by Kosugi et al. (2007) and Takanashi et al. (2005). Data were collected from March 1 to December 31, 2009.

4.2.1.2. Palangkaraya Drained Forest

The Palangkaraya Drained Forest (PDF) (2°20'N, 114°2'E) is a tropical evergreen broadleaf forest in Indonesia drained in the 1990's. The terrain is very flat (Hirano et al., 2007). Dominant tree species are Tumih (*Combretocarpus rotundatus*), Clusiaceae (*Cratoxylum arborescens*), Buchanania (*Buchanania sessifolia*) and Entuyut (*Tetramerista glabra*). Rich shrubs, including

young trees of the dominant species, grow in the understory. The canopy height is approximately 26 m. The plant area index measured using a plant canopy analyzer (LAI2000; Li-Cor Inc.) is 5.6 m^2 m^{-2} at 1.3 m height, measured in June 2006.

The annual mean air temperature and precipitation from 2002 to 2004 were 26.3°C and 2235 mm yr^{-1}, respectively. Fluctuations in the three-dimensional wind velocity (m s^{-1}) and air temperature (°C) were measured by a sonic anemometer (CSAT3; Campbell Scientific Inc.) at 41.3 m above ground level. Further details are given by Hirano et al. (2007). Data were collected from August 1, 2003 to July 31, 2004.

4.2.1.3. Tomakomai Flux Research Site

The Tomakomai Flux Research Site (TMK) (42°44'N, 141°31'E) is a cool-temperate coniferous forest in Japan. The terrain is almost flat (Hirano et al., 2003; Hirata et al., 2007). The forest is a Japanese larch (*Larix kaempferi*) plantation. The forest includes birch (*Betula ermanii*, *Betura platyphylla*) and fern (*Dryopteris crassirhizoma*) plants. The mean tree height is approximately 15 m.

Because the wood area density was determined from the plant area index measured after defoliation using a plant canopy analyzer (LAI-2000; LI-COR Inc.), the leaf area index was estimated as the difference between the plant area index and the wood area index (Hirata et al., 2007). The leaf area index showed strong seasonality. Snow covers the forest floor from early December to early April. After snowmelt, larch trees begin to leaf out in April. The leaf area index increases rapidly in the beginning of May associated with new leaves emerging and reaches a maximum between July and August. The maximum leaf area index is about 5.6 m^2 m^{-2} in summer. The leaf area index value then decreases gradually during August-November (Hirata et al., 2007).

Annual mean air temperature and total precipitation were 7.0◦C and 1030 mm yr^{-1}, respectively. Fluctuations in the three-dimensional wind speed velocity (m s^{-1}) and air temperature (◦C) were

measured with a three dimensional sonic anemometer (DA-600-3TV; Kaijo) at 27 m above ground level. Further details are available in Hirano et al. (2003) and Hirata et al. (2007). Data were collected from January 1 to December 31, 2003.

Table 4.1 Forest type, measurement height, canopy height, and *z*/*h* values at the three study sites.

Site	Forest type	Measurement height (m)	Canopy height (m)	*z*/*h*
KEW	Temperate evergreen conifer	29.0	17.3	1.68
PDF	Tropical evergreen broadleaf	41.3	26.0	1.59
TMK	Temperate deciduous broadleaf	27.0	15.0	1.80

4.2.2. Measurement and Analyses

4.2.1.1. Turbulent Fluctuations

The half-hourly covariance ($\overline{w'T'}$) of *w* and air temperature (*T*) was calculated after several corrections, such as crosswind correction (Kaimal and Gaynor, 1991), humidity correction (Hignett, 1992), and double rotation (McMillen, 1988). Sensible heat flux (***H***) was calculated from $\overline{w'T'}$.

An atmospheric stability index, (*z*-*d*)/*L* was calculated, where *z* is measurement height, *L* is the Obukhov Length, and *d* is a zero-plane displacement calculated as 78% of canopy height (*h*) (Hattori, 1985). The Obukhov Length is determined as follows:

$$L = -\frac{u_*^{3} \times (T + 273.15)}{\kappa \times g \times \overline{w'T'}} \qquad (Eq.\ 4.2)$$

where κ is the von Karman's constant ($\kappa = 0.4$), g is the gravitational constant (g = 9.8 m s^{-2}), and u_* is the friction velocity.

4.2.1.2. Relaxed Eddy Accumulation Method

Fluxes by the REA method are determined from three components: 1) the difference in the mean concentrations between updraft and downdraft; 2) the standard deviation of w (σ_w); and 3) an empirical coefficient b (b_{obs}). The value for b_{obs} was determined for every half-hour period as follows:

$$b_{obs} = \frac{\overline{w'T'}}{\sigma_w\left(\overline{T^+} - \overline{T^-}\right)} \qquad (Eq.\ 4.3)$$

where $\overline{T^+}$ and $\overline{T^-}$ (°C) are the half-hour mean air temperature associated with updraft and downdraft, respectively. The difference $(\overline{T^+} - \overline{T^-})$ is defined as ΔT. $\overline{T^+}$ and $\overline{T^-}$ are calculated after humidity correction (Hignett, 1992).

The b_{obs} values when H was less than 10 W m^{-2} or when ΔT was less than 0.01°C were not included in order to avoid analyzing unreliable data associated with the ratio of two small numbers (Baker, 2000; Bowling et al., 1998: Amman and Meixner, 2002). A stationary test was applied as a data quality control (Foken and Wichura, 1996, Aubinet et al., 2000). Applying the quality controls, datasets reduced to 60.9% in KEW, 34.5% in PDF, and 40.2% in TMK of the original data collected.

Moreover, the b_{obs} values were deleted if the measured integral turbulence characteristics of the $\frac{\sigma_w}{u_*}$ or $\frac{\sigma_T}{|T_*|}$ differed by more than 30% from the function of $(z\text{-}d)/L$ derived from the Kansas experiment (Kaimal and Finnigan, 1994; Equations (6) to (9) in Appendix). Here, T_* denotes

$\frac{\overline{w'T'}}{u_*}$. Foken and Wichura (1996) demonstrated that the data quality is good if the difference between the measured integral turbulence characteristics and the calculated value differs by not more than 20–30%. After the integral turbulence characteristics tests, datasets reduced to 17.3% in KEW, 4.6% in PDF, and 21.5% in TMK of the original data collected. These selected subsets were used for the subsequent analysis. I also showed the results before applying integral turbulence characteristics tests to clarify the effect of the screening.

4.2.1.3. Derivation of Similarity *b*

Based on the integral turbulence characteristics of *w* and air temperature derived from the Kansas experiment (Kaimal and Finnigan 1994) (see Appendix for details), new expressions were derived for similarity *b* ($b_{\text{similarity}}$) and are shown in Equations (4.4) and (4.5), depending on the value of the atmospheric stability index:

$$b_{similarity} = \frac{\sigma_T}{1.25(1-3\frac{(z-d)}{L})^{\frac{1}{3}} 2(1-9.5\frac{(z-d)}{L})^{-\frac{1}{3}} \Delta T} \quad \text{for} \quad (-2 \le \frac{(z-d)}{L}) \le 0) \quad (Eq.\ 4.4)$$

$$b_{similarity} = \frac{\sigma_T}{-1.25(1+0.2\frac{(z-d)}{L}) 2(1+0.5\frac{(z-d)}{L})^{-1} \Delta T} \quad \text{for} \quad (0 \le \frac{(z-d)}{L}) \le 1) \quad (Eq.\ 4.5)$$

The introduced $b_{\text{similarity}}$ is applicable for ideal conditions for flux measurements assuming a homogeneous flat plain, although only the component of $\frac{\sigma_T}{\Delta T}$ was observed value in each site.

4.2.3. Results

Values for b_{obs} were nearly constant among the three sites under a range of unstable conditions (Figure 4.1a-c). The average and standard deviation of the b_{obs} under unstable conditions (-2 < (*z*-

$d)/L < 0$) were 0.54 ± 0.04 in KEW, 0.58 ± 0.04 in PDF and 0.56 ± 0.03 in TMK (Table 4.2). Although both the median and the average of b_{obs} under the unstable conditions were within a narrow range (0.54–0.57), irrespective of different forest types and instrumentation, z and h (z/h values were 1.68 in KEW, 1.59 in PDF and 1.80 in TMK) (Table 4.1), there were statistically significant differences in the average values of b_{obs} among sites by one-way analysis of variance with post hoc Games-Howell test ($p < 0.01$). Under the unstable conditions, b_{obs} in KEW was significantly smaller than both PDF and TMK, as determined by the multiple comparison test ($p < 0.01$). Similarly, b_{obs} under the unstable conditions before applying the integral turbulence characteristics tests (see detailed explanation in section 2.2.2) was within a narrow range (0.54–0.56), and b_{obs} in KEW was significantly smaller than both PDF and TMK ($p < 0.01$).

The b_{obs} increased with increasing $(z-d)/L$ under stable conditions (Figure 1a-c). The values for b_{obs} under stable conditions had larger differences among the sites than those under unstable conditions. The average and standard deviation of the b_{obs} under the stable conditions ($0 < (z-d)/L < 1$) were 0.55 ± 0.05 in KEW, 0.65 ± 0.07 in PDF and 0.60 ± 0.04 in TMK (Table 4.2). The b_{obs} under the stable conditions were significantly larger than those under unstable conditions by 2.5% in KEW ($p < 0.01$), 11.7% in PDF ($p < 0.01$) and 6.9 % in TMK ($p < 0.01$) by t-test.

The values for b_{obs} in KEW changed less with changes in atmospheric stability than those in the other two sites, and the average value was the smallest of the sites under stable conditions. The relations between b_{obs} and atmospheric stability were similar before and after applying the integral turbulence characteristics tests at every site (Figure 4.1a-c). The values for b_{obs} increased with decreasing σ_w under stable conditions (Figures 4.2a-c). The values for b_{obs} under low σ_w conditions (< 0.5 m s^{-1}) were higher than those under high σ_w conditions (> 0.5 m s^{-1}) by 4.6% in KEW ($p < 0.01$), 9.7% in PDF ($p < 0.01$), and 5.4% in TMK ($p < 0.01$). The relations between b_{obs} and σ_w were similar before and after applying the integral turbulence characteristics tests

at every site.

Seasonal variations in b_{obs} ($-2 < (z-d)/L < 0$) are shown in Figure 4.3. Results for unstable and stable conditions are shown separately in order to exclude the effect of the atmospheric stability. No clear seasonal variation in b_{obs} is observed at any of the sites under all conditions of atmospheric stability. The variations in the values of b_{obs} at the PDF site are widely scattered, which could be due to limited availability of qualified data (Table 4.2). Seasonal variations in b_{obs} did not change before and after the integral turbulence characteristics test at every site (Figure 3).

A comparison of the values for $b_{similarity}$ and b_{obs} (Table 4.2 and Figure 4.1) shows that the $b_{similarity}$ under the unstable conditions showed a range similar to that of the b_{obs} at each site, even though the variations in $b_{similarity}$ were significantly larger than those of b_{obs} by F-test ($p < 0.01$). The average and standard deviation of $b_{similarity}$ under unstable conditions ($-2 < (z-d)/L < 0$) were 0.52 ± 0.07 in KEW, 0.61 ± 0.09 in PDF, and 0.60 ± 0.08 in TMK. The average and standard deviation of $b_{similarity}$ under stable conditions ($0 < (z-d)/L < 1$) were 0.59 ± 0.12 in KEW, 0.70 ± 0.13 in PDF, and 0.76 ± 0.11 in TMK. Similar to the observations for b_{obs}, the values for $b_{similarity}$ also increased with increasing $(z-d)/L$ under stable conditions in the three sites. The value for $b_{similarity}$ in KEW were also the smallest among the sites under both unstable and stable conditions. When the integral turbulence characteristics tests were not applied, $b_{similarity}$ largely deviates from b_{obs}, because similarity functions of the integral turbulence characteristics do not perform well (Figure 4.1d-f).

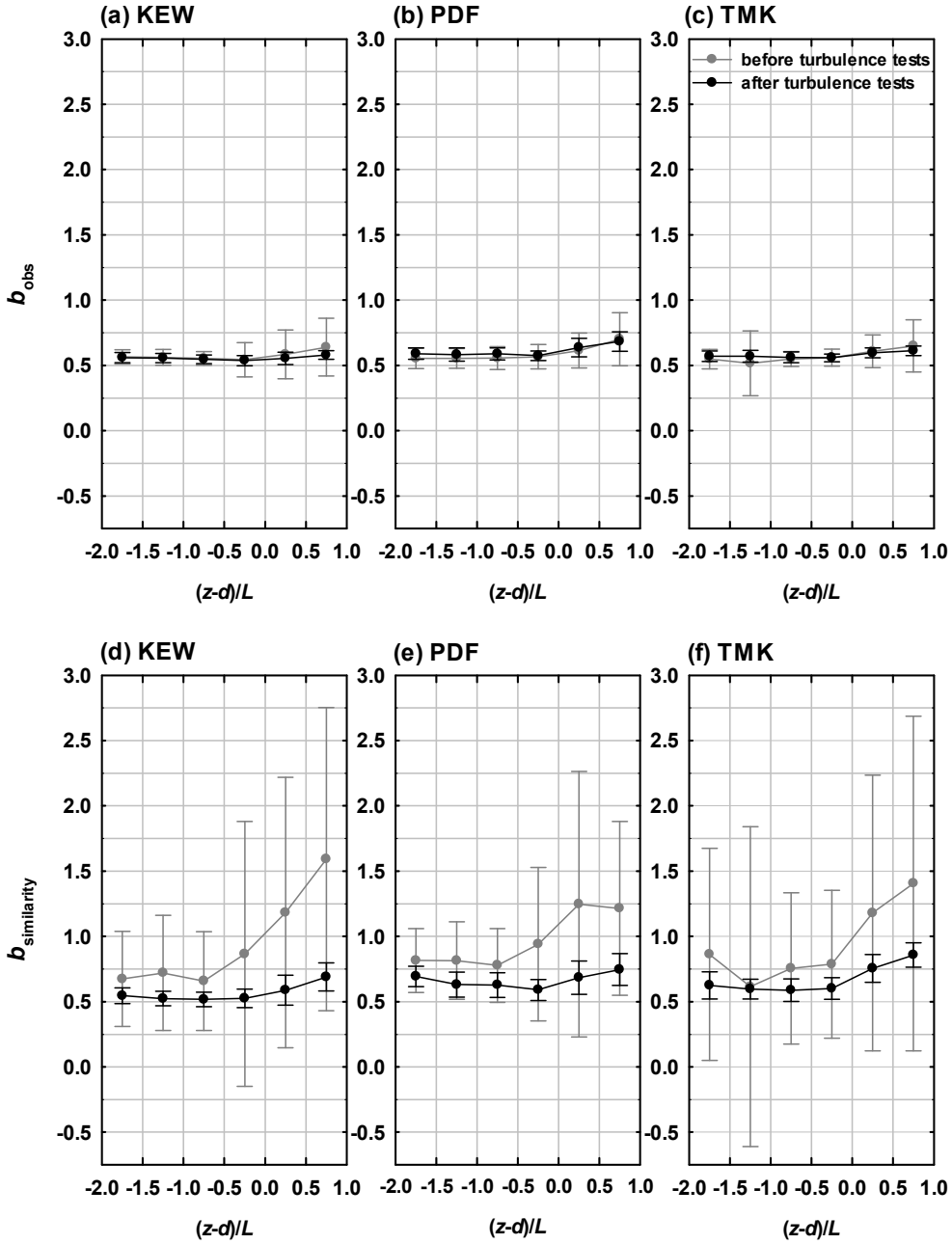

Figure 4.1 Scatterplots of b_{obs} with atmospheric stability $(z\text{-}d)/L$ at KEW (a), PDF (b) and TMK (c), and those of $b_{similarity}$ at KEW (d), PDF (e), and TMK (f). Data were binned into 6 classes according to $(z\text{-}d)/L$ by 0.5 from -2 to 1 and averaged within each class. Gray circles and error bars represent the average and one standard deviation for b before the integral turbulence characteristics tests, respectively, and black circles and error bars represent those for b after the turbulence tests.

Table 4.2 Statistics for b_{obs} and $b_{similarity}$ at the three study sites for unstable and stable conditions. The turbulence tests indicate that *b* was deleted if the measured integral turbulence characteristics of the $\frac{\sigma_w}{u_*}$ or $\frac{\sigma_T}{|T_*|}$ differed by more than 30% from the function of (*z*-*d*)/*L* derived from the Kansas experiment (Kaimal and Finnigan 1994).

		b_{obs}				$b_{similarity}$			
		before turbulence tests		after turbulence tests		before turbulence tests		after turbulence tests	
site		unstable	stable	unstable	Stable	unstable	stable	unstable	stable
KEW	average±SD	0.55±0.12	0.59±0.19	0.54±0.04	0.55±0.05	0.81±0.89	1.24±1.06	0.52±0.07	0.59±0.12
	median	0.54	0.57	0.54	0.55	0.59	0.97	0.52	0.59
	count	4107	4099	1558	779	4107	4099	1558	779
PDF	average±SD	0.56±0.09	0.62±0.15	0.58±0.04	0.65±0.07	0.89±0.52	1.24±0.98	0.61±0.09	0.70±0.13
	median	0.56	0.61	0.57	0.63	0.77	1.08	0.6	0.71
	count	3227	2205	521	201	3227	2205	521	201
TMK	average±SD	0.56±0.07	0.62±0.14	0.56±0.03	0.60±0.04	0.78±0.59	1.22±1.11	0.6±0.08	0.76±0.11
	median	0.56	0.6	0.56	0.59	0.64	0.95	0.59	0.76
	count	4007	2651	2577	988	4007	2651	2577	988

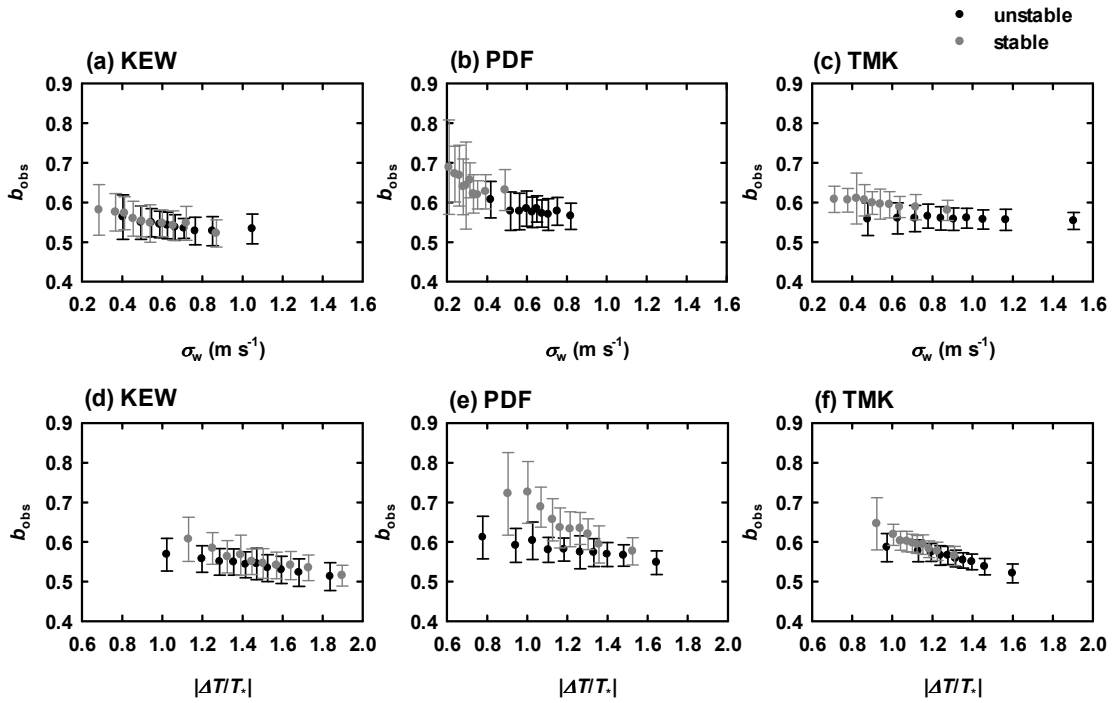

Figure 4.2 Scatterplot of σ_w and b_{obs} at KEW (a), PDF (b) and TMK (c), and scatterplots of $\left|\frac{\Delta T}{T_*}\right|$ and b_{obs} at KEW (d), PDF (e) and TMK (f). Data was binned into 10 classes and averaged within each class. Black circles and error bars represent the average and one standard deviation for b_{obs} under unstable conditions, respectively, and gray circles and error bars represent those under stable conditions, respectively.

4.2.4. Discussion

4.2.4.1. Ranges of Observational *b* under Unstable Conditions

The range of the b_{obs} under unstable conditions at the three sites was similar to previously reported b_{obs} over bare soil (Baker et al., 1992; b_{obs}=0.56 over a soybean field during a period without rain of 1-5 days), over short vegetation fields (Katul et al., 1996; b_{obs}=0.58 over a corn field from mid-June to the end of July and b_{obs}=0.58 over a short grass from early August to mid-

October in 1994) and over tall canopy (Gao, 1995; b_{obs}=0.51-0.61 over a deciduous forest during the Fall of 1986 and the Summer of 1987). In the present study, the values for b_{obs} at all three sites were nearly identical under unstable conditions (0.54–0.57) using an experiment of approximately one year.

No dependency of b_{obs} to relative measurement height (z/h) was found. Gao (1995) has shown that b_{obs} decreases as z approaches to h at a deciduous forest site with mean canopy height of approximately 18 m; values for b_{obs} were 0.51 when z/h=1.0, 0.55 when z/h=1.9 and 0.58 when z/h=2.4. Gao (1995) has suggested that the decrease in the value of b_{obs} may be the result of turbulent transport associated with the canopy structure becoming more organized and transport efficiency improving as z approaches the canopy top within the roughness sublayer.

Considering the limited range of z/h in the present chapter (z/h=1.68 at KEW, 1.58 at PDF, and 1.80 at TMK), the values for b_{obs} are consistent with the results of Gao (1995; b_{obs}=0.55 for z/h=1.9). The present chapter did not detect any dependence of b_{obs} with z/h between the three study sites. The values of z/h in the present chapter (1.58–1.80) are typical for AsiaFlux or EUROFLUX forest sites. At 13 AsiaFlux sites, z/h ranged from 1.3 to 6.7, with a median 1.4 (Hirata et al., 2008). At 6 EUROFLUX sites, z/h ranged from 1.1 to 3.6, with a median of 2.3 (Amiro et al., 2006).

The seasonal variation in plant area index in the deciduous forest did not affect b_{obs}. At the TMK site, seasonal variation in b_{obs} was not observed (Figure 4.3e,f), even though the canopy structure was substantially different in each season (as described in section 2.1.3). These results are consistent with those of Tsai et al. (2012), who observed poor correlations between b_{obs} and canopy height and between b_{obs} and plant area index for a paddy field. Gao (1995) obtained similar result where b_{obs} was independent of leaf area index.

Although there was no seasonal variation in b_{obs} in any of the three forests, some physical factors

might cause variations in b_{obs}. Changes in d associated with changes in the plant area index influence the relative measurement height z-d. When z-d decreases, the contribution of energy-containing large eddy motion decreases, resulting in potential increases in b_{obs} (see detailed explanation in section 4.2). Within the measurement heights of the present chapter, b_{obs} did not increase or decrease with changes in the plant area index, either because the effects of the energy-containing large eddy motion and the roughness sublayer (Gao, 1995) canceled out each other or because both effects did not change with the plant area index.

4.2.4.2. Dependence of b_{obs} on Atmospheric Stability

The dependence of b_{obs} on $(z\text{-}d)/L$ in the present chapter was consistent with findings from previous studies (Businger and Oncley, 1990; Andreas et al., 1998; Ammann and Meixner, 2002; Tsai et al., 2012). Katul et al. (1996) have demonstrated that dominance of energy-containing large eddy motion reduced b_{obs} due to improved transport efficiency and an associated increase in ΔT. The contribution of large eddy motion could be smaller under stable conditions with low σ_w compared to unstable conditions with high σ_w.

Under stable conditions, therefore, the values for b_{obs} are expected to be larger than under unstable conditions, owing to a smaller ΔT relative to σ_w than expected under unstable conditions. In the present chapter observed ΔT was standardized with T_* to investigate the relation between b_{obs} and ΔT. Clear increases in b_{obs} were associated with a decrease in $\left|\frac{\Delta T}{T_*}\right|$ (Figures 4.2d-f). Increases in b_{obs} under stable conditions were largest at the PDF site, because the magnitude of σ_w was substantially different between unstable and stable conditions (Figure 4.2b). The differences in σ_w between daytime and nighttime are caused by the significant difference in σ_w for unstable and stable stratification. Since b_{obs} increases with decreasing σ_w

and $\left|\frac{\Delta T}{T_*}\right|$ (Figures 4.2), values for b_{obs} under stable conditions are larger than under unstable conditions due to the reduction in $\left|\frac{\Delta T}{T_*}\right|$, which was possibly caused by the limited contribution of energy-containing large eddy motion under stable conditions.

4.2.4.3. Comparison Between b_{obs} and $b_{similarity}$

Values for $b_{similarity}$ were similar in range to those of b_{obs} under unstable conditions (Figure 4.1, section 3), suggesting that b_{obs} has a universal range from 0.52 to 0.60 when turbulence is well organized. The dependency of $b_{similarity}$ on $(z\text{-}d)/L$ was similar to that of b_{obs} under both unstable and stable conditions, although $b_{similarity}$ under the stable conditions had a wider range than those of b_{obs}. This consistent dependency of b_{obs} and $b_{similarity}$ on $(z\text{-}d)/L$ suggests the dependency of b_{obs} on $(z\text{-}d)/L$, because the independently derived $b_{similarity}$ showed a similar dependency on $(z\text{-}d)/L$.

The fact that b_{obs} and $b_{similarity}$ are the lowest at the KEW site among the three sites under both unstable and stable conditions may be attributed to the effect of complex terrain (Figure 4.1). The Monin-Obukhov similarity theory is violated at the KEW site due to the effect of the complex terrain, especially when winds from the south come over the ridge (Ueyama et al., 2004). Since most data under stable conditions were observed with winds from the south at the KEW site, turbulent transfer under stable conditions may especially differ from those at a homogeneously flat terrain. When winds come over the ridge, σ_w increased by flow separation from the surface (Kaimal and Finnigan, 1994; Ueyama et al., 2004). Transport efficiency could be improved and could make ΔT larger and b_{obs} smaller with high σ_w, as explained in section 4.2. Consequently, the increase of σ_w may be due to the complex terrain suppressing the increase in b_{obs} and $b_{similarity}$ at the KEW site (Figure 4.1a,d).

Discrepancy in the turbulent intensity ($\frac{\sigma_w}{u_*}$ and $\frac{\sigma_T}{|T_*|}$) among the observations and the

universal functions (Equations (4.6) to (4.9)) resulted in differences between b_{obs} and $b_{similarity}$ under both unstable and stable conditions. Under unstable conditions, overestimation of $\frac{\sigma_w}{u_*}$ and underestimation of $\frac{\sigma_T}{|T_*|}$ by the universal function are cancelled out, and b_{obs} and $b_{similarity}$ were very similar at all sites (Figure 4.4).

On the other hand, the discrepancies for w and T did not balance under stable conditions (Figure 4.4). The values of $b_{similarity}$ were larger than those of b_{obs} under stable conditions (Figure 4.1), because the observed $\frac{\sigma_T}{|T_*|}$ was larger than those expected from the universal function (Figures 4.4b,d,f). At the TMK site, values of $b_{similarity}$ under stable conditions were especially larger than those of b_{obs} (Figure 4.1c,f), because the universal function for $\frac{\sigma_w}{u_*}$ was lower than those from observations (Figure 4.4e). The underestimation of the universal function made $b_{similarity}$ larger than b_{obs} because the denominator in Equations (4.3) and (4.4) decreased. The reason why the discrepancies for w and T balanced under unstable conditions and did not do so under stable conditions could not be identified. However, the standard deviation of the observed $\frac{\sigma_T}{|T_*|}$ under the stable conditions was larger than the standard deviation under the unstable conditions at the three sites (Figure 4.4b,d,f), and therefore the observed $\frac{\sigma_T}{|T_*|}$ could not be expressed well as a universal function.

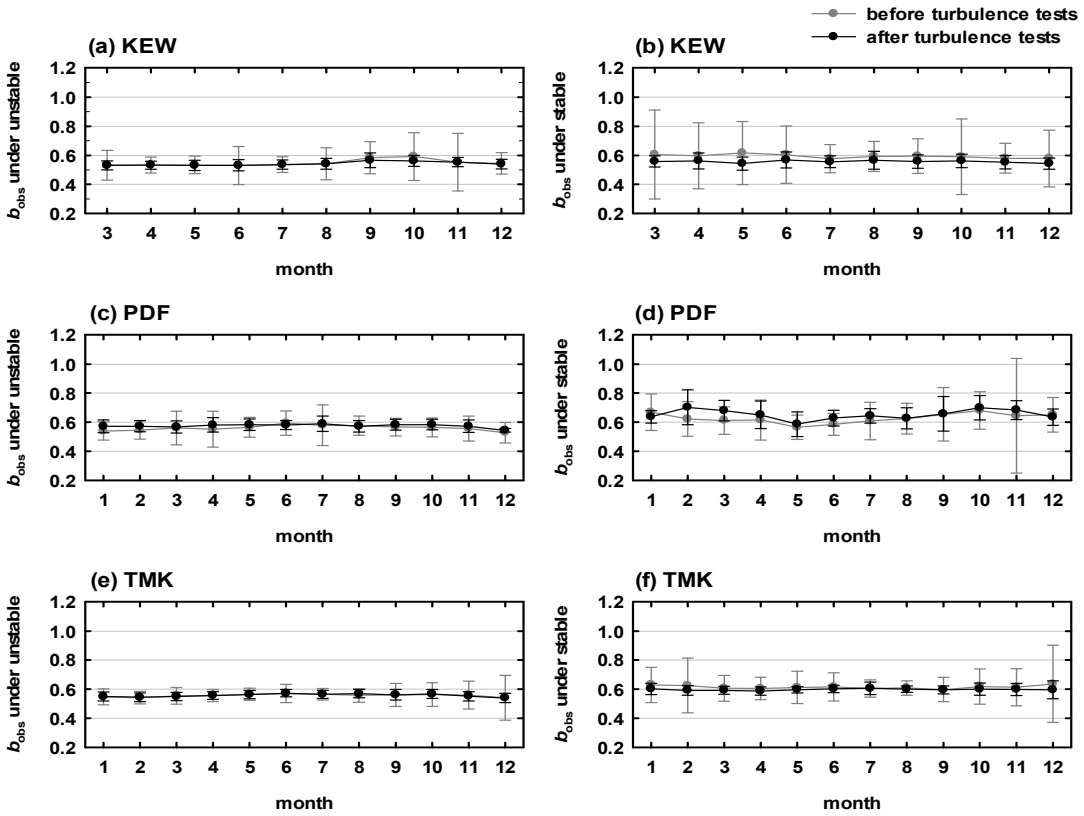

Figure 4.3 Seasonal variations in b_{obs} under unstable conditions ($(z\text{-}d)/L < 0$) at KEW (a), PDF (c), and TMK (e), and those under stable conditions ($0 < (z\text{-}d)/L$) at KEW (b), PDF (d), and TMK (f). Gray circles and error bars represent monthly means and one standard deviation for b_{obs} before the integral turbulence characteristics tests, and black circles and error bars represent those for b_{obs} after the turbulence tests.

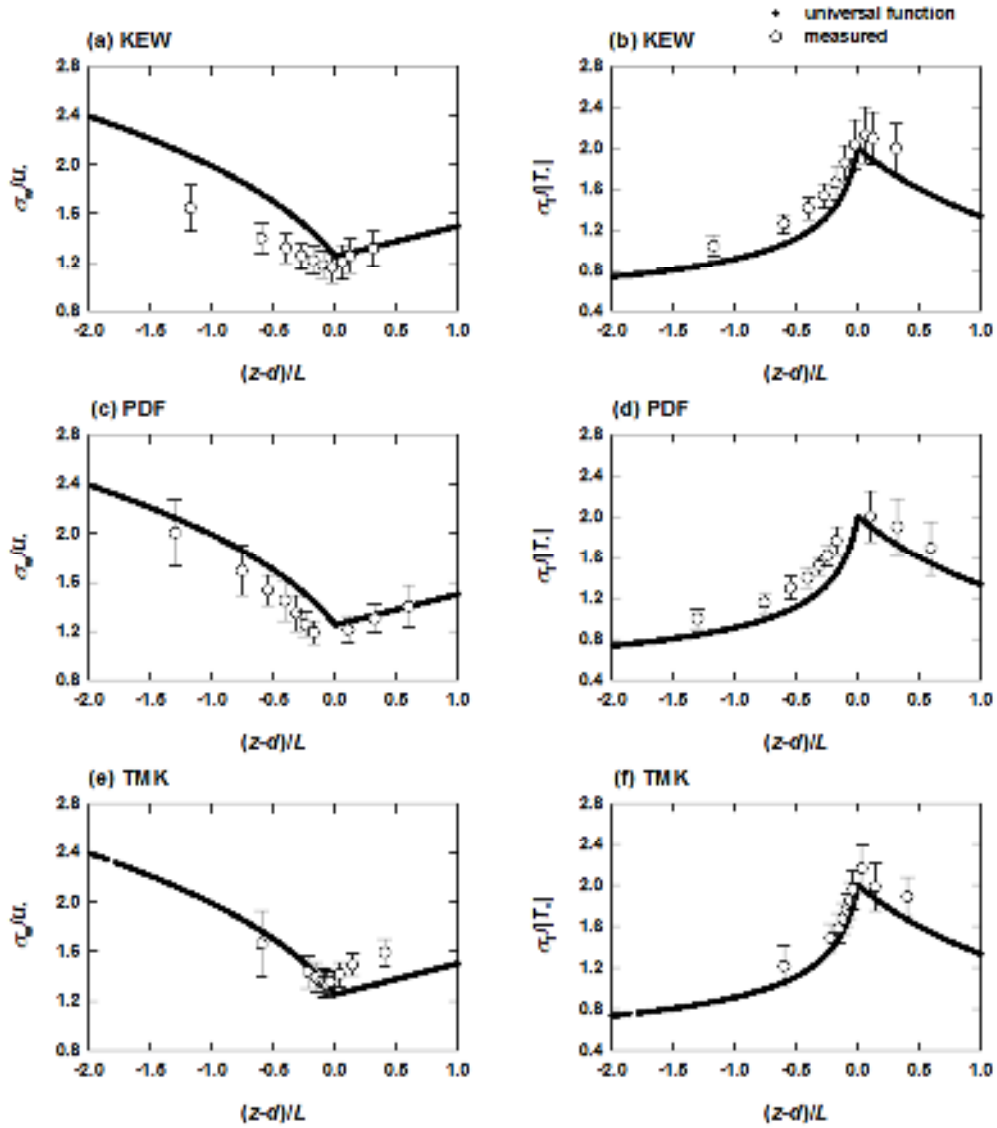

Figure 4.4 Comparison of the curves for $\frac{\sigma_w}{u_*}$ as a function of (*z*-*d*)/*L* based on empirical observation and the Monin-Obhkov similarity theory at KEW (a), PDF (c) and TMK (e), and those for $\frac{\sigma_T}{|T_*|}$ at KEW (b), PDF (d) and TMK (f). Black lines represent the universal functions of integral turbulence characteristics, equations (4.6)–(4.9) and white circles represent empirical observations. Error bars represent standard deviations of the empirical observations.

4.2.5. Conclusions

The empirical coefficient *b* of the REA method was derived from observations and the Monin-Obukhov similarity theory using data from long duration monitoring at three forest sites. No seasonal variations in b_{obs} were observed at either the evergreen or the deciduous forest sites. The median values of b_{obs} and $b_{similarity}$ under unstable conditions had the same range of between 0.52 and 0.60 among the three sites, which had almost the same z/h. On the other hand, values of b_{obs} under stable conditions were significantly different between the sites and ranged from 0.55 to 0.63. The value of *b* increased under calm conditions, such as stable conditions or low σ_w, probably due to a lower contribution of the large eddy motion. Such calm conditions mainly occurred at nighttime. As a result, if a constant value for *b* is used for the REA method, nighttime fluxes would be underestimated. I therefore recommend determining constant *b* for unstable conditions for each site and considering changes in *b* associated with atmospheric stability to minimize errors in REA fluxes.

Appendix

Based on the Monin-Obukhov similarity theory (Kaimal and Finnigan 1994), the relationship of $\frac{\sigma_w}{u_*}$ and $\frac{\sigma_T}{|T_*|}$ with $(z\text{-}d)/L$ can be represented using the following equations:

$$\frac{\sigma_w}{u_*} = 1.25\left(1 - 3\frac{(z-d)}{L}\right)^{\frac{1}{3}} \quad \text{for} \quad \left(-2 \le \frac{(z-d)}{L} \le 0\right) \quad (Eq.\ 4.6)$$

$$\frac{\sigma_w}{u_*} = 1.25\left(1 + 0.2\frac{(z-d)}{L}\right) \quad \text{for} \quad \left(0 \le \frac{(z-d)}{L} \le 1\right) \quad (Eq.\ 4.7)$$

$$\frac{\sigma_T}{|T_*|} = 2(1 - 9.5\frac{(z-d)}{L})^{-\frac{1}{3}} \text{ for } \left(-2 \le \frac{(z-d)}{L} \le 0\right) \quad (Eq.\ 4.8)$$

$$\frac{\sigma_T}{|T_*|} = 2(1 + 0.5\frac{(z-d)}{L})^{-1} \text{ for } \left(0 \le \frac{(z-d)}{L} \le 1\right) \quad (Eq.\ 4.9)$$

$$\overline{w'T'} = -T_* u_* \quad (Eq.\ 4.10)$$

$$b_{obs} = \frac{T_* u_*}{-\sigma_w\left(\overline{T^+} - \overline{T^-}\right)} \quad (Eq.\ 4.11)$$

$$\sigma_w = u_* 1.25(1 - 3\frac{(z-d)}{L})^{\frac{1}{3}} \quad \left(-2 \le \frac{(z-d)}{L} \le 0\right) \quad (Eq.\ 4.12)$$

$$|T_*| = \frac{\sigma_T}{2(1 - 9.5\frac{(z-d)}{L})^{-\frac{1}{3}}} \quad \left(-2 \le \frac{(z-d)}{L} \le 0\right) \quad (Eq.\ 4.13)$$

Substituting Equation (4.10) in Equation (4.3) results in Equations (4.11). For conditions -2 < (*z*-*d*)/*L* < 0, Equation (4.4) can be derived by substituting Equations (4.12) and (4.13) in Equation (4.11). Equation (4.5) can be derived in a similar manner for conditions 0 < (*z*-*d*)/*L* < 1.

References

Amiro, B.D., Barr, A.G., Black, T.A., Iwashita, I., Kljun, N., McCaughey, J.H., Morgenstern, K., Murayama, S., Nesic, Z., Orchansky, A.L., Bland, W.L. (2006) Carbon, energy and water fluxes

at mature and disturbed forest sites, Saskatchewan, Canada. Agric. For. Meteorol., 136, 237–251.

Ammann, C., Meixner, F.C. (2002) Stability dependence of the relaxed eddy accumulation coefficient for various scalar quantities. J. Geophys. Res., 107, 4071.

Andreas, E.L., Hill, R.J., Gosz, J.R., Moore, D.I., Otto, W.D., Sarma, A.D. (1998) Stability dependence of the eddy-accumulation coefficients for momentum and scalars. Boundary-Layer Meteorol., 86, 409–420.

Aubinet, M., Grelle, A., Ibrom, A., Rannik, U., Moncrieff, J., Foken, T., Kowalski, A.S., Martin, P. H., Berbigier, P., Bernhofer, C., Clement, R., Elbers, J., Granier, A., Grunwald, T., Morgenstern, K., Pilegaard, K., Rebmann, C., Snijders, W., Valentini, R., Vesala, T. (2000) Estimates of the annual net carbon and water exchange of European forests: The EUROFLUX methodology. Adv. Ecol. Res., 30, 113–174.

Baker, J.M., Norman, J.M., Bland, W.L. (1992) Field-scale application of flux measurement by conditional sampling. Agric. For. Meteorol., 62, 31–52.

Baker, J.M. (2000) Conditional sampling revisited. Agric. For. Meteorol., 104, 59–65.

Baldocchi, D.D., Bowing, D.R. (2003) Modelling the discrimination of $^{13}CO_2$ above and within a temperate broad-leaved forest canopy on hourly to seasonal time scales. Plant, Cell and Environ., 26, 231–244.

Beverland, I.J., Moncrieff, J.B., O'Neill D.H., Hargreaves K.J., Milne, R. (1996) Measurement of methane and carbon dioxide fluxes from peatland ecosystems by the conditional-sampling technique. Q. J. R. Meteorol. Soc., 122, 819–838.

Bowling, D.R., Baldocchi, D.D., Monson, R.K. (1999) Dynamics of isotopic exchange of carbon dioxide in a Tennessee deciduous forest. Glob. Biogeochem. Cycles, 13, 903–922.

Bowling, D.R., Turnipseed, A.A., Delany, A.C., Baldocchi, D.D., Greenberg, J.P., Monson, R.K. (1998) The use of relaxed eddy accumulation to measure biosphere-atmosphere exchange of

isoprene and other biological trace gases. Oecologia, 116, 306–315.

Businger, J.A., Oncley, S.P. (1990) Flux measurement with conditional sampling. J. Atmos. Ocean. Tech., 7, 349–352.

Foken, T., Wichura, B. (1996) Tools for quality assessment of surface-based flux measurements. Agric. For. Meteorol., 78, 83–105.

Gao, W. (1995) The vertical change of coefficient *b*, used in the relaxed eddy accumulation method for flux measurement above and within a forest canopy. Atmos. Environ., 29, 2339–2347.

Hamotani, K., Monji, N., Yamaguchi, K. (2001) Development of a long-term CO_2 flux measurement system using REA method with density correction. J. Agric. Meteorol., 57, 93–99.

Hamotani, K., Uchida, Y., Monji, N., Miyata, A. (1996) A system of the relaxed eddy accumulation method to evaluate CO_2 flux over plant canopies. J. Agric. Meteorol., 52, 135–139.

Hattori, S. (1985) Explanation on derivation process of equations to estimate evapotranspiration and problems on the application to forest stand. Bull. For. & For. Prod. Res. inst., 332, 139–165.

Hignett, P. (1992) Correction to temperature measurements with a sonic anemometer. Boundary-Layer Meteorol., 61, 175–187.

Hirano, T., Segah, H., Harada, T., Limin, S., June, T., Hirata, R., Osaki, M. (2007) Carbon dioxide balance of a tropical peat swamp forest in Kalimantan, Indonesia. Glob. Chang. Biol., 13, 412–425.

Hirano, T., Hirata, R., Fujinuma, Y., Saigusa, N., Yamamoto, S., Harazono, Y., Takada, M., Inukai, K., Inoue, G. (2003) CO_2 and water vapor exchange of a larch forest in northern Japan. Tellus, 55B, 244–257.

Hirata, R., Hirano, T., Saigusa, N., Fujinuma, Y., Inukai, K., Kitamori, Y., Takahashi, Y., Yamamoto, S. (2007) Seasonal and interannual variations in carbon dioxide exchange of a temperate larch forest. Agric. For. Meteorol., 147, 110–124.

Hirata, R., Saigusa, N., Yamamoto, S., Ohtani, Y., Ide, R., Asanuma, J., Gamo, M., Hirano, T., Kondo, H., Kosugi, Y., Li, S., Nakai, Y., Takagi, K., Tani, M., Wang, H. (2008) Spatial distribution of carbon balance in forest ecosystems across East Asia. Agric. For. Meteorol., 148, 761–775.

Kaimal, J.C., Finnigan, J.J. (1994) Atmospheric boundary layer flows, their structure and measurement. Oxford University Press, New York 289 pp.

Kaimal, J.C., Gaynor, J.E. (1991) Another look at sonic thermometry. Boundary-Layer Meteorol., 56, 401–410.

Katul, G.G., Finkelstein, P.L., Clarke, J.F., Ellestad, T. G. (1996) An investigation of the conditional sampling method used to estimate fluxes of active, reactive, and passive scalars. J. Appl. Meteorol., 35, 1835–1845.

Kondo, F., Tsukamoto, O. (2008) Evaluation of Webb correction on CO_2 flux by eddy covariance technique using open-path gas analyzer over asphalt surface. J. Agric. Meteorol., 64, 1–8.

Kosugi, Y., Takanashi, S., Tanaka, H., Ohkubo, S., Tani, M., Yano, M., Katayama, T. (2007) Evapotranspiration over a Japanese cypress forest. I. Eddy covariance fluxes and surface conductance characteristics for 3 years. J. Hydrol., 337, 269–283.

McMillen, R.T. (1988) An eddy correlation technique with extended applicability non-simple terrain. Boundary-Layer Meteorol., 43, 231–245.

Oncley, S.P., Delany, A.C., Horst, T.W. (1993) Verification of flux measurement using relaxed eddy accumulation. Atmos. Environ., 27, 2417–2426.

Park, C., Schade, G.W., Boedeker, I. (2010) Flux measurements of volatile organic compounds by the relaxed eddy accumulaton method combined with a GC-FID system in urban Houston, Texas. Atmos. Environ., 44, 2605–2614.

Pattey, E., Desjardins, R.L., Westberg, H., Lamb, B., Zhu, T. (1998) Measurement of isoprene emissions over a black spruce stand using a tower-based relaxed eddy-accumulation system. J.

Appl. Meteorol., 38, 870–877.

Pattey, E., Desjardins, R.L., Rochette, P. (1993) Accuracy of the relaxed eddy-accumulation technique, evaluated using CO_2 flux measurements. Boundary-Layer Meteorol., 66, 341–355.

Sakabe, A., Hamotani, K., Kosugi, Y., Ueyama, M., Takahashi, K., Kanazawa, A., Itoh, M. (2012) Measurement of methane flux over an evergreen coniferous forest canopy using a relaxed eddy accumulation system with tuneable diode laser spectroscopy detection. Theor. Appl. Climatol., 109, 39–49.

Takanashi, S., Kosugi, Y., Tanaka, Y., Yano, M., Katayama, T., Tanaka, H., Tani, M. (2005) CO_2 exchange in a temperate Japanese cypress forest compared to that in a cool-temperate deciduous broadleaved forest. Ecol. Res., 20, 313–324.

Tsai, J., Tsuang, B., Kuo, P., Tu, C., Chen, C., Hsueh, M., Lee, C., Yao, M., Hsueh, M. (2012) Evaluation of the relaxed eddy accumulation coefficient at various wetland ecosystems. Atmos. Environ., 60, 336–347.

Ueyama, M., Takai, R., Takahashi, Y., Ide, R., Hamotani, K., Kosugi, Y., Takahashi, K., Saigusa, N. (2013) High-precision measurements of the methane flux over a larch forest based on a hyperbolic relaxed eddy accumulation method using a laser spectrometer. Agric. For. Meteorol., 178–179, 183–193.

Ueyama, M., Hamotani, K., Nishimura, W.: A technique for high-accuracy flux measurement using a relaxed eddy accumulation system with an appropriate averaging strategy. J. Agric. Meteorol., 65, 315–325 (2009)

Ueyama, M., Tosa, R., Doke, T., Hamotani, K., Monji, N. (2004) Feature of wind profile in and above a forest canopy in a complex terrain. J. Agric. Meteorol., 60, 25–32.

Webb, E.K., Pearman, G.I., Leuning, R. (1980) Correction of flux measurements for density effects

due to heat and water vapour transfer. Quart. J. Roy. Meteorol., 106, 85–100.

Wyngaard, J.C., Moeng, C.H. (1992) Parameterizing turbulent diffusion the joint probability density. Boundary-Layer Meteorol., 60, 1–13.

CHAPTER 5

Measurement of methane flux over an evergreen coniferous forest canopy using a relaxed eddy accumulation system with tuneable diode laser spectroscopy detection

5.1. Introduction

Long-term CH_4 flux measurements in forested areas have been mostly performed using chamber methods. While chamber methods are useful for understanding the processes controlling CH_4 fluxes on small spatial scales (usually less than 1 m^2) in Chapter 2 and 3, the small footprint of the measurement creates a difficult scaling problem (Denmead, 1994) when estimating landscape-scale fluxes in heterogeneous terrain such as forests. Moreover, the occasional measurements of manual chambers restrict the time resolution. These inherent limitations of chamber methods have made it difficult to evaluate CH_4 dynamics in whole forest ecosystems, as CH_4 fluxes from forest soils have wide spatial and temporal variations. CH_4 fluxes in forest ecosystems could have wide-ranging spatio-temporal variations both emission and absorption sides, especially in the forest ecosystems which have wide spatio-temporal range in soil water status, such as Asian monsoon forests under warm and humid climate, or boreal and tropical peat forests. Scaling up of CH_4 fluxes in those types of forests and understanding CH_4 dynamics as a whole ecosystem would be difficult only with chamber methods. In addition, both open and closed chambers disturb natural environmental conditions during the measurement by affecting airflow, radiant energy receipt, and energy transfer to the atmosphere (Denmead, 1994). Consequently, CH_4 exchanges estimated by the chamber method could contain biases and uncertainties if up-scaled to stand, watershed, and regional scales.

Micrometeorological methods such as the eddy covariance (EC) method are ideally suited for

continuous ecosystem-scale flux measurements integrated over a larger area without artificial disturbance. Although the EC method has been widely used for ecosystem-scale flux measurements, it has not been used until very recently for CH_4 measurements because it requires a fast-response and high-precision gas analyzer. Recent technological advances in the application of tuneable diode laser spectroscopy (TDLS) to *in situ* field measurements open the possibility of long-term EC measurement of CH_4 in a variety of ecosystems. Previously, a limited number of CH_4 EC measurements have been obtained in peatlands (Hendriks et al., 2008; Schrier-Uijl et al., 2009), rice paddy fields (Simpson et al., 1994), and prairies (Kim et al., 1998a, b). The lack of long-term CH_4 flux observations in forest ecosystems restricts our understanding of ecosystem-scale CH_4 dynamics. However, measuring CH_4 exchange over forest ecosystems is still challenging compared to measurements in the above source areas because of the small fluxes in forests (Smeets et al., 2009). According to previous EC measurements in wetlands and farmlands, the precision of the CH_4 concentration measurements was 2.9 ppb at 10 Hz using a Quantum Cascade Laser Spectroscopy (QCLS) analyzer (QCL-TILDAS-76; Aerodyne Research Inc., Billerica MA, USA) (Kroon et al., 2007). Recently, the open path sensor is available for the CH_4 EC measurement with the precision of < 5 ppb at 10 Hz (McDermitt et al., 2011). However, those precisions are still insufficient to measure small CH_4 fluxes at forest ecosystems if the CH_4 fluxes measured by chamber techniques (Itoh et al., 2005, 2007, 2009) assumed to be representative to the ecosystem-scale exchange.

Although the state-of-the-art CH_4 analyzers could be insufficient for the EC measurements, those analyzers are available for CH_4 flux measurements by using a micrometeorological relaxed eddy accumulation (REA) method (Businger and Oncley, 1990; Hamotani et al., 1996, 2001). The REA method can take longer time for CH_4 concentration measurements, thus a laser signal can be averaged to optimize the instrumental sensitivity, and higher precision of TDLS CH_4

analyzer was achievable. The flux, calculated by the REA method, is equal to the difference in the mean concentrations of the trace gas of interest associated with updraft and downdraft, multiplied by the standard deviation of the vertical wind velocity and an empirical coefficient. In Chapter 4, I have investigated the uncertainty in REA flux calculations introduced by the coefficient *b*.

In this chapter, I employed an REA method (Businger and Oncley, 1990; Hamotani et al., 1996, 2001) with a TDLS CH_4 analyzer for long-term observation of CH_4 fluxes from a temperate evergreen coniferous forest site. My goal was to examine whether the REA method is applicable to (1) measure CH_4 fluxes over the forest canopy, (2) reveal the amplitude and seasonal variations in CH_4 fluxes, and (3) examine the response of CH_4 fluxes to rainfall. This is the first report showing the seasonal cycle of ecosystem-scale CH_4 fluxes in a temperate forest.

5.2. Methods

5.2.1. Site Description

The observations were made in a coniferous forest in the Kiryu Experimental Watershed, (KEW; area: 5.99 ha) in Shiga Prefecture, Japan. A meteorological observation tower is located in a small catchment within KEW (Figure 5.1). The forest consists of 50-year-old Japanese cypress (*Chamaecyparis obtusa* Sieb. et Zucc.). Mean tree height was approximately 16.8 m in 2007. The annual mean air temperature and precipitation measured at the meteorological station shown in Figure 5.1 from 2002 to 2009 were 13.3°C and 1,576 mm yr^{-1}, respectively. The site has a warm temperate monsoon climate with a wet summer. Rainfall occurs throughout the year with two peaks in summer due to the Asian monsoon; the early summer ‘Baiu’ front season and the late summer typhoon seasons. The entire watershed is underlain by weathered granite with considerable amounts of albite.

Canopy fluxes of heat, water, and CO_2 have also been measured at this site at 29-m above the

ground, using the EC method (e.g., Takanashi et al., 2005; Kosugi et al., 2007; Kosugi and Katsuyama, 2007; Ohkubo et al., 2007). Takanashi et al. (2005) reported that the CO_2 flux for 92% of the daytime flux and 81% of the nighttime flux originated from the forest area according to an analytical footprint model by Schuepp et al. (1990). The trend in wind direction at this site did not change seasonally but had diurnal variations. The daytime wind direction was from all directions, whereas the night-time wind direction was mainly from the south (Kosugi et al., 2007). Some wetlands were located in riparian zones along streams within the flux footprint area, which were either always submerged or periodically submerged. The streams and the main wetland areas (approximately 10^0-10^2 m^2) are shown in Fig. 1. The riparian zones and wetlands were distributed in both the north and south directions within the flux footprint area. The size of these areas could slightly increase after rainfall. Notably, an express highway was opened approximately 400 m south of the tower in February of 2008. During night-time, this highway was always inside of the flux footprint. The paddy fields were situated several km north to west of the tower, although these area were mostly out of the flux footprint (Takanashi et al., 2005). CH_4 fluxes from wetlands and water-unsaturated soils were investigated using a chamber method with a gas chromatograph analyzer (Itoh et al., 2005, 2007, 2009). Comparisons of the CH_4 fluxes from the previous chamber data and the present REA data will be described later.

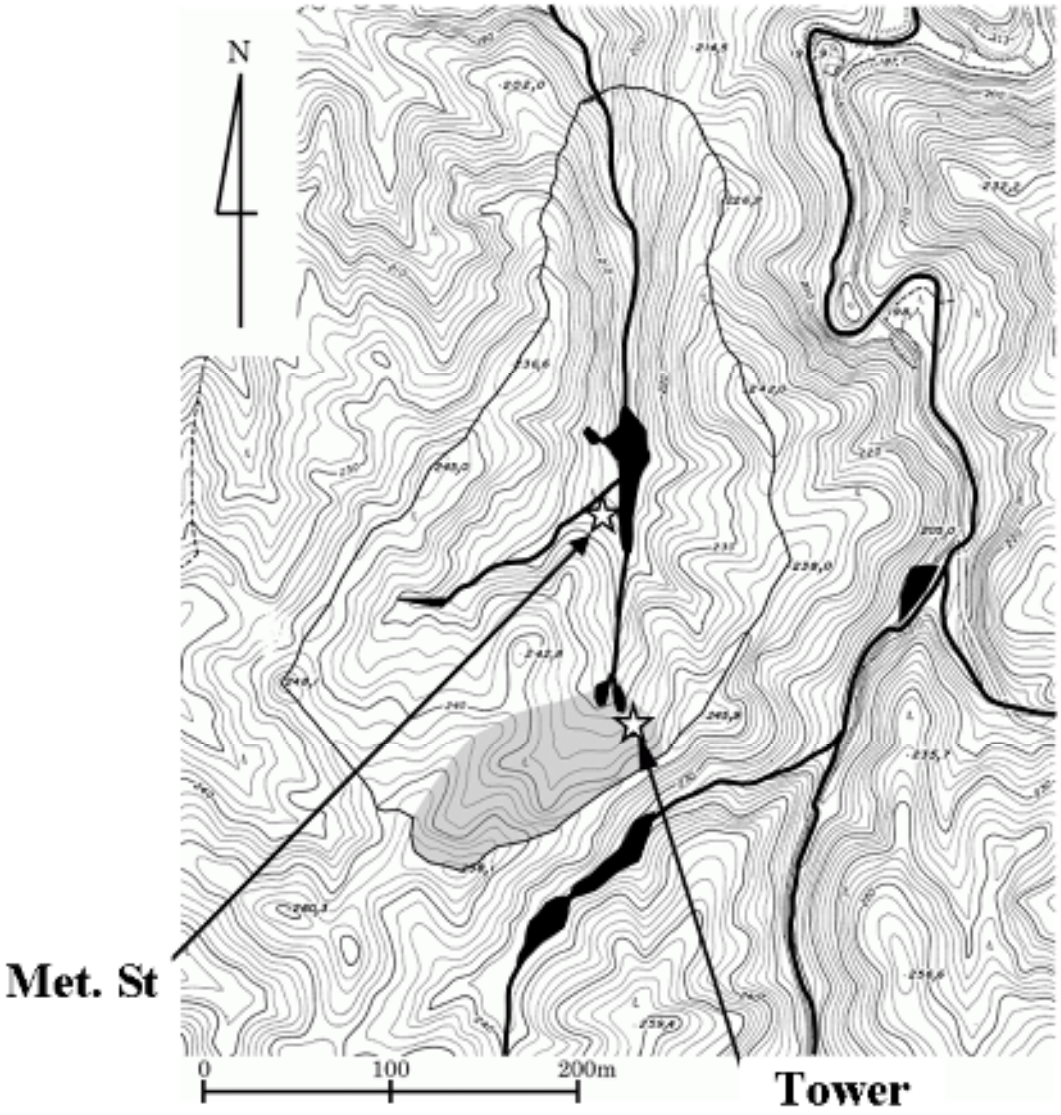

Figure 5.1 Topographic map of the observation site. Precipitation was recorded at the indicated meteorological station. The streams are shown as bold lines, and riparian zones are located along the streams. The main wetland areas are in black.

5.2.2. Measurements

The CH_4 flux was measured using the REA method (Businger and Oncley, 1990; Hamotani et al., 1996, 2001). Although the REA method is theoretically the same as the EC method, it does not require a fast response from the gas analyzer compared to the EC method. Compared to

wetlands, forest canopies are more challenging sites for conducting CH_4 flux measurements by the EC method. This is because the emission and absorption of CH_4 are both relatively small over forest canopies, and TDLS analyzers may not always be precise enough to detect the fluxes. The greatest benefit of applying the REA method is that sufficient precision in CH_4 concentration TDLS measurements is achievable by signal averaging over a longer duration. The precision of the TDLS CH_4 analyzer (FMA-200; Los Gatos Research, Mountain View, CA, USA) is 3 ppb at 10 Hz rate, 1 ppb at 1 Hz rate and 0.1 ppb at 100 s rate according to the catalog specifications. Moreover, the REA method can save electronic consumption and minimize the possible noises induced by the pressure drift of the measurement cell of the TDLS CH_4 analyzer, because the REA method with lower sampling frequency can measure CH_4 fluxes without a high-power vacuum pump. The another advantage of the REA method is that it does not require any corrections such as high frequency attenuation for closed-path EC method or WPL correction (Webb et al., 1980) for open-path EC methods, which could obscure the observed small flux values at the forest ecosystems. One possible disadvantage of the REA method involves the switching speed of the valve system, which may lead to the loss of high frequency information, however those effects can be negligible at measurements over tall forest canopies, such as in my forest (Ueyama et al., 2009). Equation 5.1 expresses CH_4 flux (F_{CH4}, nmol m^{-2} s^{-1} (Subsequently, I use this abbreviation only for CH_4 flux measured by the REA method). This equation can also be used to calculate CO_2 flux (F_{CO2}, μmol m^{-2} s^{-1}):

$$F_{CH4} = \sigma_w \left(\overline{S_{CH4}^{+}} - \overline{S_{CH4}^{-}} \right) \rho_a b \qquad (Eq.\ 5.1)$$

where σ_w is the standard deviation (SD) of the vertical wind velocity (w, m s^{-1}), $\overline{S_{CH4}^{+}}$ and

$\overline{S_{CH4}^{-}}$ are the 30-minute mean CH_4 mole fractions (ppmv) associated with updraft and downdraft, respectively, and ρ_a (mol m^{-3}) is molar air density. The coefficient *b* was empirically determined from EC data using air temperature given by *Eq*. 5.2:

$$b = \frac{\overline{w'T'}}{\sigma_w\left(\overline{T^+} - \overline{T^-}\right)} \qquad (Eq.\ 5.2)$$

where $\overline{T^+}$ and $\overline{T^-}$ are 30-min mean fast-response temperature data associated with updraft and downdraft, respectively. I determined *b* to be 0.59, which is the average of 16,576 values obtained from *Eq*. 5.2 and the standard error was 0.04. The sensible heat flux and air temperature data used here was all data measured from August 2009 to August 2010 by the sonic anemometer (SAT-550; Kaijo Corp., Tokyo, Japan) mounted on top of the 29-m-tall tower. The term *b* was applied to both F_{CO2} and F_{CH4}. The value of *b* is relatively constant over a wide range of atmospheric stability (Bowling et al., 1998). In Chapter 4, I confirmed that dependence of *b* on atmospheric stability was relatively weak at KEW.

My REA system consists of a sonic anemometer (SAT-550; Kaijo Corp.) to measure wind speed and direction, two diaphragm pumps (CV-201, Enomoto Co., Tokyo, Japan), four reservoirs (CCK-20; GL Science, Tokyo, Japan) to accumulate sampled gas, a CO_2/H_2O gas analyzer (LI-840; Li-Cor Inc., Lincoln, NE, USA), a CH_4 gas analyzer (Baer et al. 2002; Hendriks et al., 2008) (FMA-200; Los Gatos Research) and a data logger (CR1000; Campbell Scientific, Logan, UT, USA). The sonic anemometer was mounted on top of the 29-m-tall tower and the air inlets were set directly below the sonic anemometer. Air samples for updraft and downdraft were pulled through DK tubes (inner tube: 4 mm in diameter and coated with aluminium) to the reservoirs by two diaphragm pumps at a constant flow rate (0.7 l min^{-1}). The frequency of switching the pumps

was 10 Hz. One pump worked only for updraft and the other worked only for downdraft. Updraft or downdraft was determined by the difference between the instantaneous and adjacent 15-min moving average of *w*. Air flow was switched using the solenoid valves (CKD USB3-6-3-E; CKD Corp., Aichi, Japan) and controlled by the CR1000 data logger. To sequentially determine the flux every half hour, I prepared two sets of sampling reservoirs: one pair of reservoirs accumulated air during 0–30 min and the other pair accumulated air for the next 30–60 min. After accumulating in the reservoirs for 30 min, the air in the reservoirs was pulled a diaphragm pump into the CH_4 analyzer at a flow rate of approximately 0.7 l min^{-1}, and the air in each reservoir was analyzed for 2 min. Three filters were inserted in the gas sample line to protect the CH_4 analyzer from dust and insects. Before entering the CO_2/H_2O and the CH_4 analyzers, the sampled air was dried using a gas dryer (PD-50T-48; Perma Pure Inc., Toms River, NJ, USA). Dilution by water vapour, which could not be completely removed by the drying system, was corrected for using the H_2O concentration measured with the CO_2/H_2O analyzer. I confirmed that the gas dryer did not alter the CH_4 mixing ratio within measurement uncertainties. Data were recorded at 10 Hz by the CR1000 data logger and stored on a compact flash card using a compact flash module (CFM100, Campbell Scientific). A 10-s moving average filtered the high frequency noises for the CO_2/H_2O analyzer and a 1-s moving average was used for the CH_4 analyzer. Volumetric soil water content (VWC) at a depth of 0–30 cm was measured with a CS616 water content reflectometer (Campbell Scientific) at four different points around the tower on the water-unsaturated forest floor, and soil temperatures were measured with a thermistor (RT-10,11,12; ESPEC Mic Corp., Kanagawa, Japan) at depths of 2 cm near the tower. Precipitation was measured with a tipping bucket rain gauge at an open screen site near the tower. Air temperature above the canopy was measured with a ventilated temperature and humidity sensor (HHP45AC; Vaisala, Helsinki, Finland) at a height of 29 m above the ground.

In this chapter, I compared CO_2 fluxes measured by the REA and EC methods in order to examine the validity of my REA system. An open-path CO_2/H_2O analyzer (LI-7500; Li-Cor) was used to measure CO_2 flux by the EC method. The double-rotation method was applied to the sonic anemometer velocities (McMillen, 1988), and the Webb, Pearman, Leuning (WPL) correction for the effect of air density fluctuations (Webb et al., 1980) was applied to CO_2 flux using the EC method. Details of the EC measurements have been described by Kosugi et al. (2007) and Okubo et al. (2007b).

5.2.3. Data analysis

Hendriks et al. (2008) described the specifications of the CH_4 analyzer used in this study in detail. To examine the accuracy and precision of the CH_4 analyzer, calibration experiments were performed on site using a standard CH_4 gas cylinder (Takachiho, Tokyo, Japan, 1773 ppb CH_4 in synthetic air) several times during the course of this study. The typical SD for determining the CH_4 mixing ratio was 0.4 ppb with a 30-s moving average within a 3-min standard gas flow period, which is the same condition used for calculating the reservoirs concentrations with the REA method; the reservoir concentrations were averaged for 30 s and analyzed within 2 min. No significant drift in the measurement accuracy of the CH_4 analyzer was observed during the entire observation period (less than 6 ppb). I also examined the detection limit of CO_2 and CH_4 fluxes in my REA system by storing the same air in reservoir pairs and measuring the concentration difference in each pair. This check mode was performed during 1 day of every month.

I performed a *t*-test (significance level: 0.05) for the CH_4 concentration difference between updraft and downdraft to examine whether there was a statistical difference between the mean values. F_{CH4} assumed to be zero by the *t*-test (21.8% of all available data) is shown as grey circles in Figs. 3 and 5. All CO_2 and CH_4 fluxes collected with the REA method were rejected when CO_2 flux data collected with the EC method did not meet the stationary criteria (Foken and Wichur,

1996; Aubinet et al., 2000). I also rejected CO_2 and CH_4 fluxes collected during night-time under highly stratified conditions, using a previously examined friction velocity threshold of 0.3 m s^{-1} for the CO_2 flux data (Takanashi et al., 2005). The total amount of F_{CH4} data rejected by these criteria accounted for 66% of the entire data series.

The data analyzed in this chapter were recorded between 1 August 2009 and 31 August 2010. Data were missing from 11 to 20 August 2009, from 16 June to 22 July 2010, and from 10 December 2009 to 17 February 2010 due to instrumental malfunctions.

5.3. Results

5.3.1. Validity of the CH_4 fluxes collected with the REA system

Before application to F_{CH4} measurement, I validated my REA system by comparing F_{CO2} measured by the EC and REA method for daytime (Figure 5.2a) and nighttime periods (Figure 5.2b). The CO_2 fluxes by the EC and REA methods were highly correlated for both daytime with a slope of 0.95, $r^2 = 0.72$ and the root mean square error (RMSE) of 3.7 μmol m^{-2} s^{-1} (Figure 5.2a) and nighttime with a slope of 0.81, $r^2 = 0.45$ and the RMSE of 3.4 μmol m^{-2} s^{-1} (Figure 5.2b). Although the slopes of the linear regression showed a slightly smaller value than 1.0, the observed data both in the daytime and nighttime were mostly scattered around the 1:1 line and the F_{CO2} measured by the REA method did not show obviously higher or lower values than those by the EC method (Figure 5.2a, b). The F_{CO2} measured by the EC and the REA methods had worse correlation in the night-time than daytime (Figure 5.2b).

The F_{CH4} detection limit obtained from the check mode with my REA system showed a diurnal variation because it depended on turbulent intensity (i.e., σ_w in *Eq*. 5.1 is larger in the daytime than in the night-time) The night-time (0:00–6:00 and 18:00–24:00) and daytime (6:00–18:00) F_{CH4} detection limits averaged for all 14 check mode days were 4.2 ± 3.7 and 7.4 ± 5.9 nmol m^{-2} s^{-1}, respectively, and the detection limits did not change seasonally.

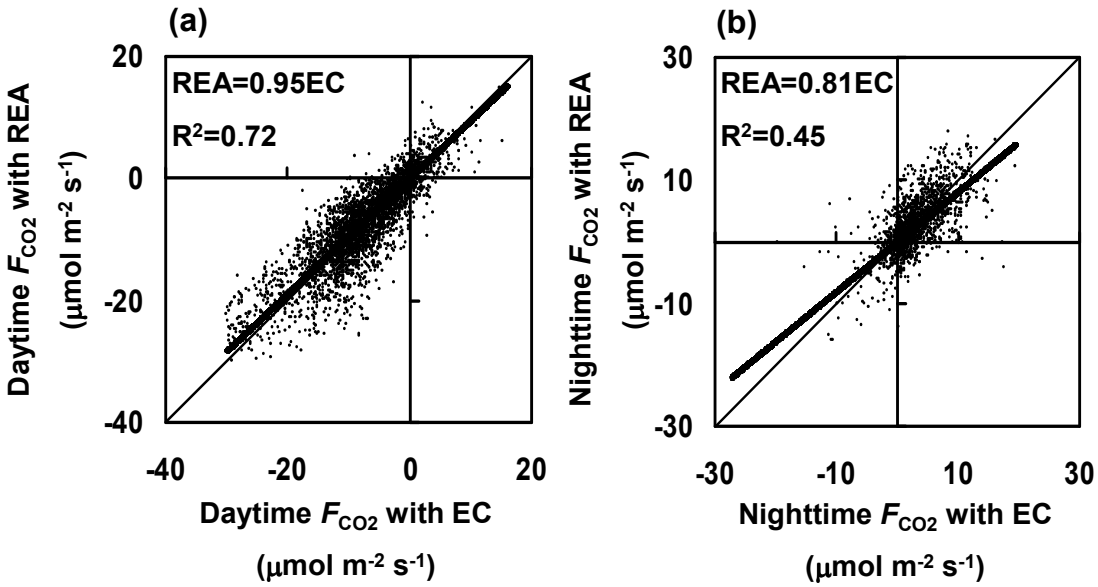

Figure 5.2 Comparison between CO_2 fluxes obtained by the REA and EC methods at the half-hourly time scale in the (a) daytime (0600-1800 h) and (b) nighttime (0000-0600 and 1800-2400 h). The thin and bold lines represent 1:1 and linear regression, respectively. The linear regression equation and r^2 obtained from analysis of all data are shown.

5.3.2. Amplitude and seasonal variations in CH4 flux and its response to rainfall

Figure 5.3 shows the seasonal variations in (a) instantaneous F_{CH4}, (b) air and soil temperature, and (c) precipitation and VWC. The average and SD of F_{CH4} was 5.9 ± 11.5 nmol m^{-2} s^{-1} for the summer of 2009 (August and September), 5.3 ± 10.4 nmol m^{-2} s^{-1} for the fall of 2009 (October and November), 2.2 ± 10.9 nmol m^{-2} s^{-1} for the winter of 2009 (December, February, and March), -10.0 ± 14.3 nmol m^{-2} s^{-1} for the spring of 2010 (April, May, and June), and -4.7 ± 15.3 nmol m^{-2} s^{-1} for the summer of 2010 (July and August). This site had a heterogeneous topography, and some riparian zones and wetlands were distributed both in the north and south directions within the flux footprint area. However, the wind direction at this site did not change seasonally. I confirmed that

both daytime and night-time F_{CH4} from the north or south was not particularly larger than those from other wind directions by analysing F_{CH4} for each wind direction (Figure 5.4). F_{CH4} seasonally shifted from emission in the summer and fall of 2009 to absorption in the spring of 2010. Then the absorption weakened and changed to emission in the summer of 2010 (Figure 5.3a). The diurnal patterns changed seasonally. In the summer and fall of 2009, F_{CH4} showed clear diurnal variation with an emission peak around noon (Figures 5.5a, b and 6a, b). Large emission was observed in the fall of 2009 during sequential rain events for several days (Figure 5.5b). The emission decreased with a decrease in air temperature (Figure 5.6a, b), and then F_{CH4} became almost zero in winter (Figures 5.5c and 6c). F_{CH4} remained relatively small until the spring of 2010 (Figure 5.5d). Then, F_{CH4} gradually shifted to exhibit a clear diurnal variation with an absorption peak around noon, which was an opposite pattern compared to the previous summer (Figure 5.5e and 6d). The magnitude of peak CH_4 absorption increased with air temperature. Maximum CH_4 absorption was observed in June, when the absence of rain lasted 17 days and VWC decreased. After intense rainfalls in late July 2010, the CH_4 absorption rate gradually decreased and seemed to shift to emission.

I detected evidence for short-term F_{CH4} that rainfall was an important factor contributing to increased CH_4 emission. After rainfall on 12 September 2009, high F_{CH4} was observed on 13 September 2009 (Figure 5.5a) and similarly on 27 October and 2 November 2009 (Figure 5.5b). Averaged diurnal variations for the summer of 2009 (August and September) and the fall of 2009 (October and November) also showed that CH_4 emission increased after precipitation (Figure 5.6a, b). Even when high CH_4 absorption rates were observed around noon, rainfall contributed to weakening CH_4 absorption and/or F_{CH4} switched to emission as shown on 24 May 2010 (Figure 5.5e). Averaged diurnal variation for the spring of 2010 (April, May, and June) also showed that CH_4 absorption was weakened after precipitation (Figure 5.6d). Approximately a day after rainfall,

CH_4 emission typically increased and/or absorption decreased (Figure 5.5a, b, e). The response of F_{CH4} to rainfall was not obvious in winter (Figures 5.5c and 6c).

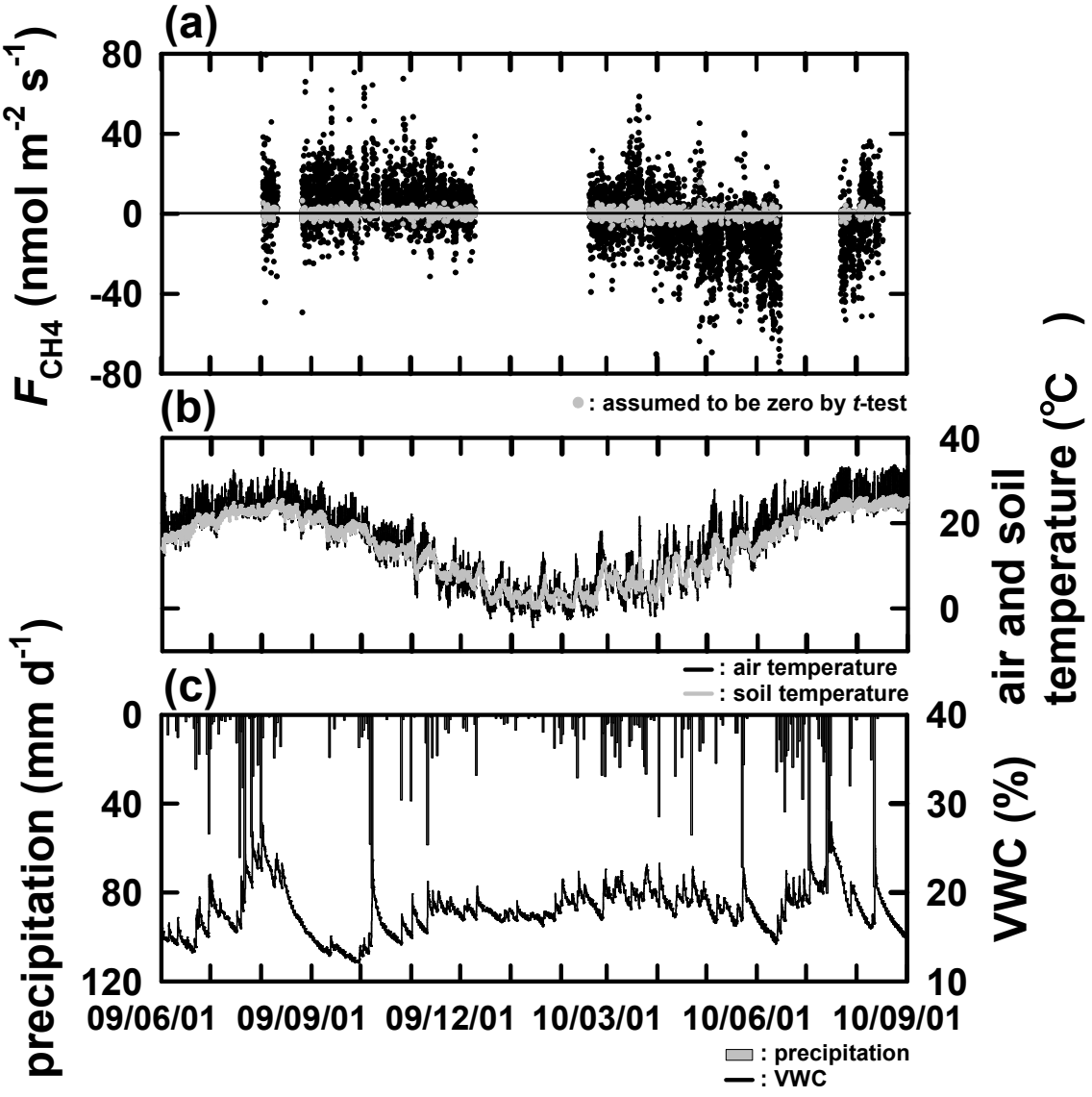

Figure 5.3 Seasonal variation in (a) instantaneous canopy CH_4 flux and CH_4 flux assumed to be zero by the *t*-test (grey circles), (b) air temperature and soil temperature (grey lines), and (c) precipitation and the volumetric soil water content (VWC) at the water-unsaturated forest floor during August 2009 and August 2010, in an evergreen Japanese cypress forest in a warm temperature climate.

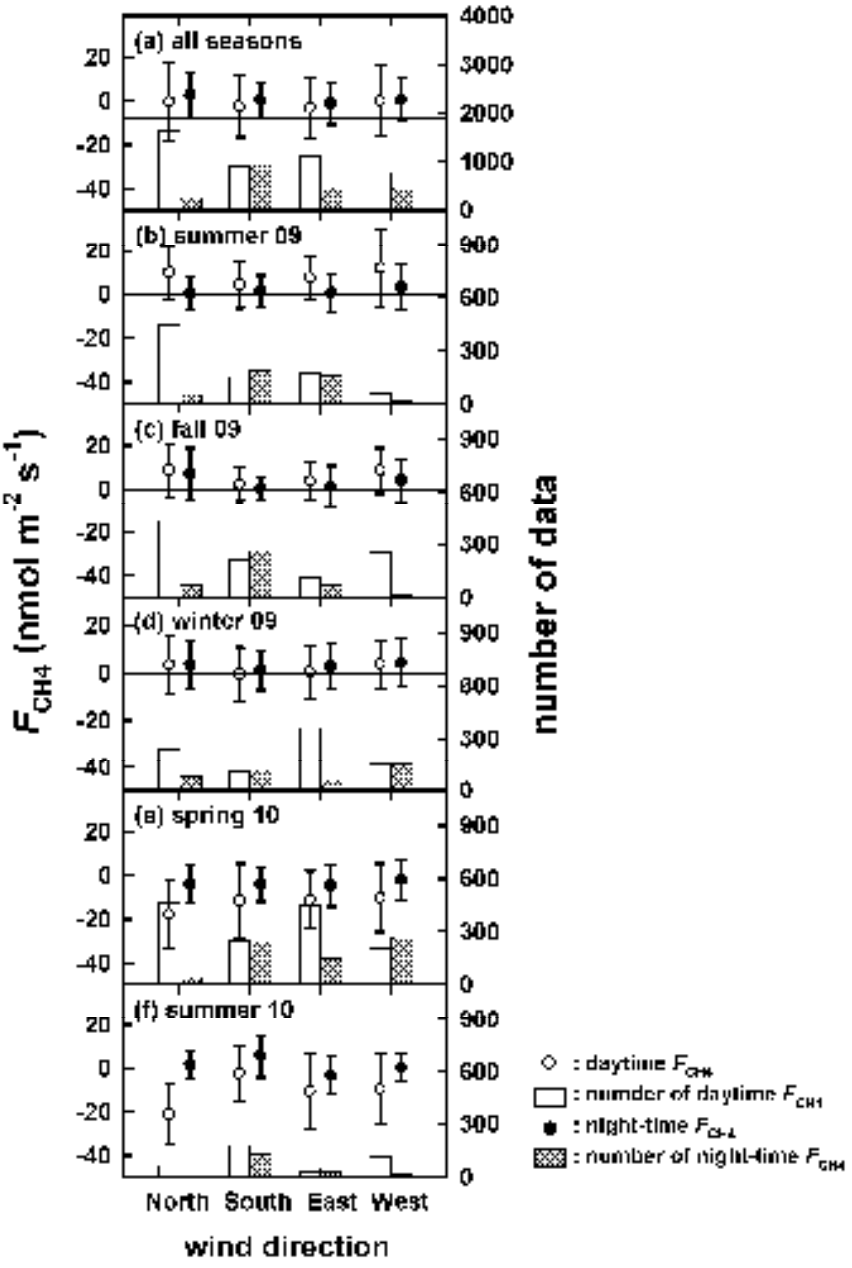

Figure 5.4 Daytime and night-time CH_4 fluxes averaged for each wind direction (north, south, east, west) in each season: (a) the sum of all seasons, (b) summer 2009, (c) fall 2009, (d) winter 2009, (e) spring 2010, and (f) summer 2010 are shown. Daytime and night-time CH_4 fluxes are shown as white and black circles. Error bars show the standard deviations. The data used for averaging seasonal CH_4 fluxes for each wind direction are shown as bars. The data for daytime and night-time are shown as white and black bars, respectively.

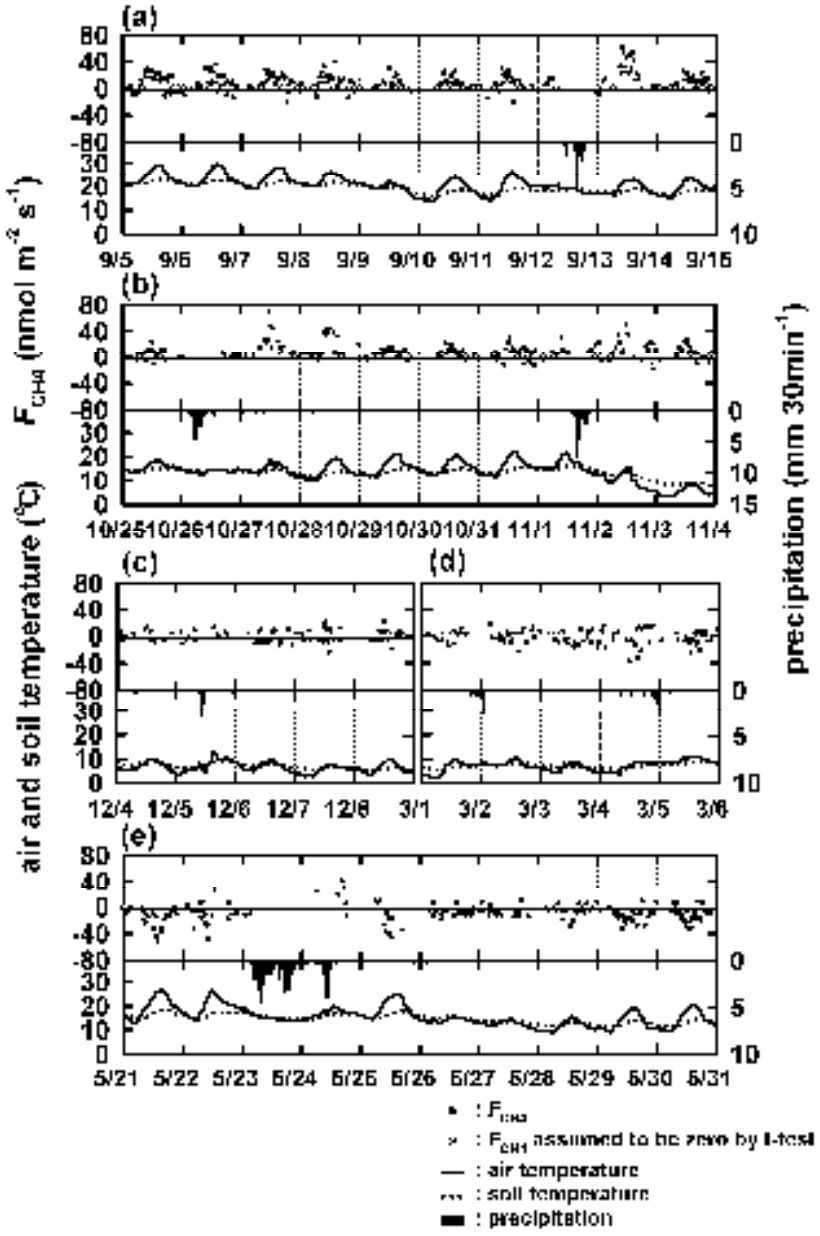

Figure 5.5 Diurnal course of instantaneous canopy CH_4 flux and CH_4 flux assumed to be zero by the *t*-test (grey circles), precipitation, and air temperature and soil temperature (dotted lines) measured in (a) summer (between 5 September and 14 September 2009), (b) fall (between 25 October and 3 November 2009), (c) winter (between 4 December and 8 December 2009 and between 7 March and 11 March 2010), (d) early spring (between 1 March and 5 March 2010), and (e) late spring (between 21 May and 30 May 2010) in an evergreen Japanese cypress forest in a warm temperature climate.

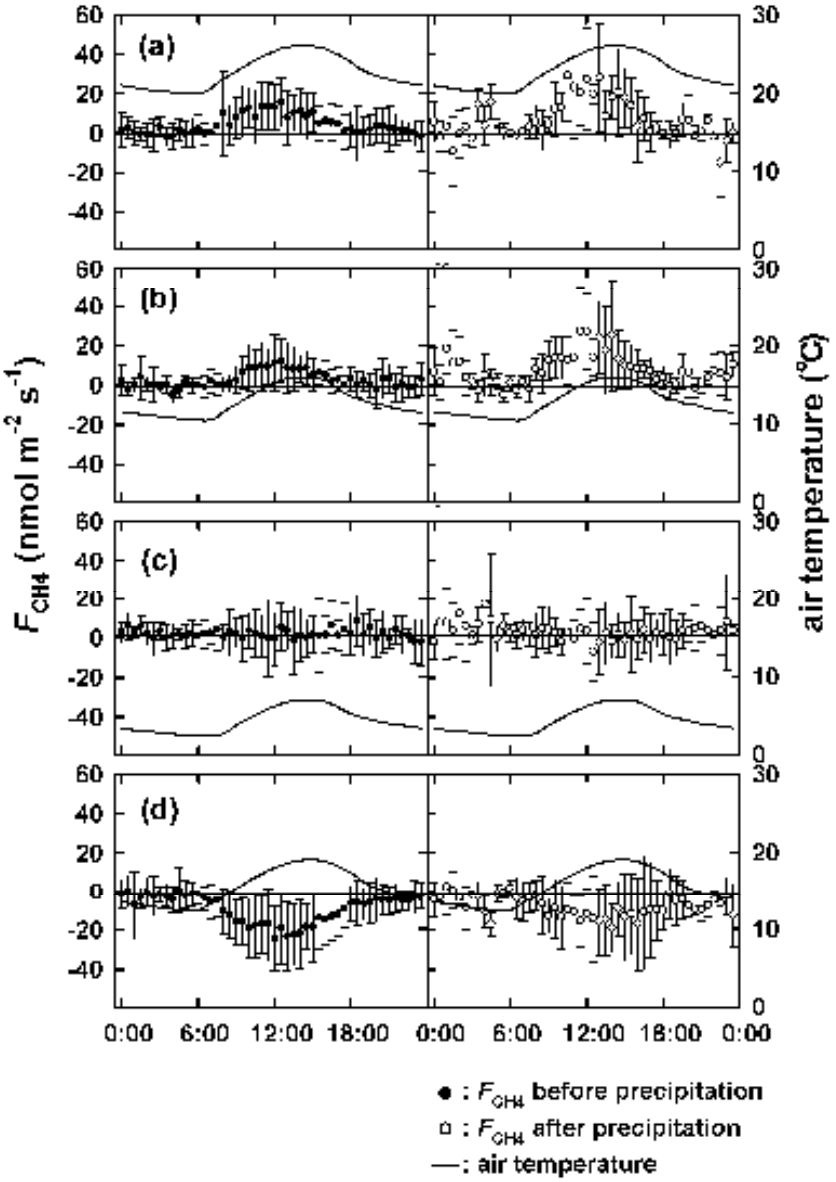

Figure 5.6 Diurnal variations of CH_4 fluxes before precipitation (black circle) and after precipitation (white circle) (in case accumulated precipitation was more than 2 mm within last 24 h) and air temperature, averaged for (a) the summer of 2009 (August and September), (b) the fall of 2009 (October and November), (c) the winter of 2009 (December, February and March), and (d) the spring of 2010 (April, May and June). Error bars show the standard deviations for CH_4 fluxes.

5.4. Discussion

5.4.1. Assignment of the REA system

From comparison of CO_2 fluxes between the REA and EC data, I concluded that my REA system generally provided a good approximation of the EC method and could thus be applied to measure F_{CH4}. One possible reason for the difference in CO_2 fluxes between the EC and REA methods is the method for determining coefficient *b* in *Eq*. (5.1); coefficient *b*, although constant in *Eq*. 5.1, might change slightly and is not constant throughout the day or year. However this is improbable, because coefficient *b* in KEW changed only 7.3% between unstable and stable conditions as shown in Chapter 4. This cannot explain the large difference in CO_2 fluxes between the EC and REA methods at night. Another possibility is that the loss of high frequency information due to the switching speed of the REA valve system might lead to an underestimation of F_{CO2} with the REA method. However, the latter possibility was thought to be less likely because turbulent transfer was significant at a lower frequency below 1 Hz at this site (Kosugi et al., 2007; Ueyama et al., 2009). More investigation is necessary to explain the difference between EC and REA methods.

The most difficult part of measuring F_{CH4} in the forest canopy is that the F_{CH4} detection limit is very close to the actual flux range. Although F_{CH4} was larger than the detection limit in summer, fall, and spring, it was smaller in winter. Spatial variability of F_{CH4} ranged approximately from -2.24 to 383.3 nmol m^{-2} s^{-1} on October 27 and 28 in 2011, and from 0.04 to 1380.63 nmol m^{-2} s^{-1} on September 19, 20, an 21, 2012 in wetlands and from -7.08 to 7.22 nmol m^{-2} s^{-1} on October 27 and 28 in 2011, and from -3.47 to 1.35 nmol m^{-2} s^{-1} on September 19, 20, and 21, 2012 in water-unsaturated forest floors as shown in the 120 multi-point measurements by chamber method in Chapter 2; some of these values are smaller than the detection limit of my REA system. I suggest that further improvements in measurement precision for the difference between upward and

downward air CH_4 concentration are required to measure F_{CH4} more precisely particularly in the winter. A possible approach to improving the precision of my REA system is to apply the hyperbolic REA method (Bowling et al., 1999), which samples air only for high turbulent transport eddies. Applying this method would allow us to increase the CH_4 concentration differences (up to a factor of 2.7; Bowling et al., 1999) and thus improve the precision of the REA system. One disadvantage of the hyperbolic REA is that the majority of air (80%) is discarded, and roughly 10% of the original volume is sampled into each of the updraft and downdraft reservoirs (Bowling et al., 2003). The information contained in the discarded air must be reconstructed through the coefficient *b*. The *b* is determined under the assumption of the scalar similarity between temperature, CO_2 and CH_4, so under some conditions large errors can result from violation of scalar similarity using the hyperbolic REA (Ruppert, 2002).

5.4.2. Amplitude and seasonal variations in CH_4 flux and its response to rainfall

At the study site, the main CH_4 sources areas (riparian wetlands) were heterogeneously distributed within the flux footprint area, as shown in Figure 5.1, and the typical wind direction (described in Section 2.1) did not change seasonally. Although there were large CH_4 sources in the north and south, daytime and night-time F_{CH4} from the north or south were not particularly larger than those from other wind directions (Figure 5.4). Although there was a difference between the F_{CH4} from the north and south in summer 2010, this was probably caused by artificial difference due to limited number of available data; F_{CH4} in summer 2010 could not be affected by wind direction. Thus, I assumed that the observed F_{CH4} seasonal variations would be mainly caused by the activity of methanogens and methanotrophs influenced by the soil temperature and water conditions but not wind direction.

Itoh et al. (2005, 2007, 2009) measured seasonal CH_4 flux variations from different parts of

the slope in a water-unsaturated forest floor and riparian wetlands at the study site using the chamber method from 2001 to 2005. They showed that CH_4 emission rates from wetlands ranged from 0 to 720 nmol m^{-2} s^{-1}, and that the emission rates increased significantly during high soil temperature and VWC periods. They hypothesised that the emission rates were large enough to turn the entire watershed into a net CH_4 source, even though the source areas were very limited (Itoh et al., 2005). The emission rates from the wetlands varied from year to year due to the hydrological conditions that changed in relation to precipitation patterns (particularly summer precipitation patterns) (Itoh et al., 2007). The reported CH_4 fluxes from the water-unsaturated forest floor at this site ranged from -1.7 to 1.4 nmol m^{-2} s^{-1} (Itoh et al., 2009). CH_4 uptake was usually observed throughout the sampling periods; however, on lower hillslopes, where groundwater constantly existed underground, weak CH_4 uptake was observed only at low soil temperature (< 15°C); these areas turned to a CH_4 source at high soil temperatures (Itoh et al., 2009). In addition, larger CH_4 emission as high as 1380.63 nmol m^{-2} s^{-1}, and higher CH_4 absorption as high as -7.08 nmol m^{-2} s^{-1} were observed in multi-point soil CH_4 flux measurements as shown in Chapter 2. Furthermore, half-hourly continuous soil CH_4 flux measurement revealed how CH_4 absorption was reduced by rainfall event seasonally and instantly. Some plots switched from acting as a sink to acting as a weak source of CH_4 or neutral following rainfall as shown in Chapter 3. The chamber measurements revealed that CH_4 fluxes in this forest were heterogeneous at both temporal and spatial scales, thus highlighting the importance of conducting continuous measurements of ecosystem-scale CH_4 fluxes integrated over a larger area to evaluate the total CH_4 budget.

Four new insights were obtained by combining the results from earlier chamber studies and this chapter. First, the ecosystem-scale F_{CH4} results by the REA method showed emission in the summer and fall of 2009, indicating that a forest ecosystem consisting mostly of a water-

unsaturated forest floor could be a CH_4 source for an entire watershed, possibly due to a large source contribution by a tiny wetland (Whalen et al., 1990; Keller and Reiners, 1994; Hudgens and Yavitt et al., 1997; Itoh et al., 2007). Another possible source was the contribution from the lower hillslopes of the water-unsaturated forest floor. Even though the soil surface was water-unsaturated, groundwater constantly existed underground and produced CH_4 under unaerobic conditions, which could have been emitted (Itoh et al., 2009). This chapter shows, for an entire watershed, that a Japanese cypress forest in a warm temperate climate could be a CH_4 source in summer and fall according to tower based measurements. Previous chamber-based studies speculated on the ecosystem-scale CH_4 dynamics from the plot-scale measurements, which might contain large uncertainties. My ecosystem-scale measurements support the results of earlier chamber measurements. I found that monthly averaged F_{CH4} in October of 2009 was 6.6 nmol m^{-2} s^{-1} and it was not far less than the average CH_4 fluxes in a peat meadow (29.7 nmol $0m^{-2}$ s^{-1}, Hendriks et al., 2008), a dairy farm (42.7 nmol m^{-2} s^{-1}, Kroon et al., 2007) and a boreal fen (80 nmol m^{-2} s^{-1}, Long et al., 2010). In rice paddies, the CH_4 flux ranged from 12.5 to 131.3 nmol m^{-2} s^{-1} in Tsukuba, Japan (Miyata et al., 2000), and 30 ± 55 nmol m^{-2} s^{-1} in California, USA (Detto et al., 2011). It is not negligible CH_4 emission from forest ecosystems, and it is important to quantify CH_4 fluxes in forest ecosystems and monitor it in the long-term. From chamber CH_4 flux measurement conducted biweekly over two years at KEW, CH_4 emission in wetland showed higher seasonal variability than CH_4 absorption in the water-unsaturated forest floor, and high CH_4 emissions were observed in summer and fall during heavy rainfall period at every plot in wetland as shown in Chapter 2. Because CH_4 flux is determined from the balance between CH_4 emission and absorption, increased CH_4 emission in wetland is suggested to influence ecosystem-scale CH_4 emission flux by the REA method during summer and fall.

Second, continuous measurements at high temporal resolution revealed that the ecosystem-

scale CH_4 emissions increased and/or absorption decreased after rainfall particularly in summer and fall of 2009. The F_{CH4} response to rainfall was caused by changes in the soil water condition because the methanogenic activities increase and methanotrophic activities decrease in anoxic environments (Le Mer and Roger, 2001). The area of the CH_4 source was broadened along the riparian zones after rainfall, and the lower hillslope part of the water-unsaturated forest floor may have switched from a sink to a source for CH_4 because the anaerobic area may also have broadened deep underground, as mentioned above. Another possibility is that CH_4 diffusion from the air to the soil may have been inhibited by rainfall causing a decline in CH_4 absorption (Bradford et al., 2001). From half-hourly continuous chamber CH_4 flux measurement at water-unsaturated forest floor at KEW, we confirmed that CH_4 absorption showed distinct depressions at the peaks of rainfall intensity. After rainfall, CH_4 absorption did not recover soon, but increased gradually due to decreased activity of methanotrophs during rainfall period with limited supply of substrate, such as CH_4 and O_2, from the atmosphere and decreased activity of methaotrophs and increased activity of methanogens in anoxic soil with increased WFPS after rainfall as shown in Chapter 3. As shown in Fig. 5a, b, e, the influence of rainfall to F_{CH4} was obvious 1 or 2 days after rainfall events, at the short time-scale. On the other hand, F_{CH4} tended to be influenced by rainfall in the seasonal time-scale as seen in the shift of F_{CH4} to emission during summer 2010 (Figure 5.3a). F_{CH4} seemed to shift from absorption to emission during about 2 weeks after intense rainfalls in late July 2010 (Figure 5.3a). These different time-scale responses of F_{CH4} to rainfall were probably caused by different processes, and should be investigated with more data. In winter, the response of F_{CH4} to rainfall appeared to be low, suggesting that less CH_4 was produced and/or absorbed in winter compared to other seasons; the activities of both methanogens and methanotrophs are low at low soil temperatures, although methanotrophs are much less temperature dependent (Dunfield et al., 1993).

Third, CH_4 absorption rates increased from spring 2010 as soil temperatures increased and VWC decreased. These results are consistent with previous chamber measurements (Itoh et al., 2009). Uptake rates increased as soil temperature increased in the lower range of temperature (<15°C) and as VWC decreased. Previous studies reported a similar activation of methanotrophs with an increase in temperature (Whalen et al., 1990; Dobbie et al., 1996; Prime and Christensen, 1997; Ishizuka et al., 2000). In contrast, methanogens function at intermediate temperature ranges from 20 to 40°C (Yamane et al., 1961), and their activity is extremely low at low temperatures (Dunfield et al., 1993). The large F_{CH4} absorption obtained in the spring of 2010 by the REA method was possibly due to the different responses of methanogens and methanotrophs to temperature. Methanotrophs might function well under conditions where methanogens are still unable to function well (i.e., low temperature) (Dunfield et al., 1993; Le Mer and Roger, 2001). In the biweekly soil CH_4 flux measurement for two years, the largest CH_4 absorption was observed in spring before intensive summer rainfall at some chambers as shown in Chapter 2. Therefore, large CH_4 absorption would be observed in spring by the REA method in dry soil condition with low antecedent rainfall. I still do not have enough information to explain the differences in F_{CH4} between fall 2009 and spring 2010 within a similar temperature range. In Chapter 2, higher CH_4 absorption was observed in spring than in fall by manual chamber measurements. This was probably due to the soil being drier in spring than it was in fall after continuous rainfall during the summer and fall months. In addition, the difference in temperature before the sampling season (summer or winter in this case) might have affected both methanogenic and methanotrophic activities during these periods. Longer duration observational data are needed to help clarify the seasonal F_{CH4} variation in forest ecosystems.

Finally, the CH_4 absorption rates in spring 2010 (monthly averaged F_{CH4} from April to June of 2010 ranged from -5.1 to -18.3 nmol m^{-2} s^{-1}) were larger than the range measured by manual

chamber method (-7.08 to 7.22 nmol m^{-2} s^{-1}; Chapter 2) at the water-unsaturated forest floor at this site. Although the CH_4 fluxes obtained by the REA and chamber measurements cannot be compared directly, one possible explanation involves the detection limit of my REA system (4.2 ± 3.7 nmol m^{-2} s^{-1} in the night-time and 7.4 ± 5.9 nmol m^{-2} s^{-1} in the daytime), which may not be sufficient to detect the range of CH_4 uptake rates obtained by the chamber method for the water-unsaturated forest floor (-7.08 to 7.22 nmol m^{-2} s^{-1}). The other possible reason is that the chamber method is not always an excellent tool for investigating representative CH_4 flux over a large watershed. An unobserved area that is consuming CH_4 more effectively than estimated previously might exist at the study site. It was suggested that further detailed studies are required to clarify whether spatial heterogeneity is sufficient to explain such discrepancies or whether there are systematic methodological differences between the measurement techniques (Miyata et al., 2000). In a forest ecosystem, the soil water status has a heterogeneous distribution. Therefore these results suggest that ecosystem-scale measurements using micrometeorological methods are important to evaluate total CH_4 exchange and its impact on the environment, and further studies using simultaneous micrometeorological and chamber-based measurements of CH_4 fluxes are necessary for a comparison.

5.5. Conclusions

This chapter is the first report of continuous measurements of ecosystem-scale F_{CH4} in an upland forest using the REA method with a TDLS CH_4 analyzer. My observations revealed how the entire forest ecosystem complexly switched between being a CH_4 sink or a source on hourly, diurnal, and seasonal scales. As micrometeorological methods provide spatially integrated fluxes with high temporal resolutions, measuring F_{CH4} with these methods is particularly important to investigate the CH_4 dynamics in forest ecosystems. In this chapter, I demonstrated that the REA method is applicable for measuring CH_4 flux over a large representative area. Further longer-term

observations with improvement of the system are needed to evaluate the controlling factors for methanogens and methanotrophs activity in the CH_4 dynamics of forest ecosystems. A combined approach between conventional chamber and micrometeorological methods is particularly important to evaluate the total CH_4 exchange, its impact on the environment, and the detailed processes involved.

References

Aubinet, M., Grelle, A., Ibrom, A., Rannik, U., Moncrieff, J., Foken, T., Kowalski, A.S., Martin, P.H., Berbigier, P., Bernhofer, C., Clement, R., Elbers, J., Granier, A., Grunwald, T., Morgenstern, K., Pilegaard, K., Rebmann, C., Snijders, W., Valentini, R., Vesala, T. (2000) Estimates of the annual net carbon and water exchange of forests: the EUROFLUX methodology. Adv. Ecol. Res., 30, 113–175.

Baer, D.S., Paul, J.B., Gupta, M., O'Keefe, A. (2002) Sensitive absorption measurements in the near-infrared region using off-axis integrated cavity-output spectroscopy. Appl. Phys., B75, 261–265.

Bowling, D.R., Pataki, DE., Ehleringer, J.R. (2003) Critical evaluation of micrometeorological methods for measuring ecosystem-atmosphere isotopic exchange of CO_2. Agric. Meteorol., 3118, 1-21.

Bowling, D.R., Delany, A.C., Turnipseed, A.A., Baldocchi, D.D., Monson, R.K. (1999) Modification of the relaxed eddy accumulation technique to maximize measured scalar mixing ratio differences in updrafts and downdrafts. J. Geophys. Res., 104, 9121-9133.

Bowling, D.R., Turnipseed, A.A., Delany, A.C., Baldocchi, D.D., Greenberg, J.P., Monson, R.K. (1998) The use of relaxed eddy accumulation to measure biosphere–atmosphere exchange of isoprene and other biological trace gases. Oecologia., 116, 306–315.

Bradford, M.A., Ineson, P., Wookey, P.A., Lappin-Scott, H.M. (2001) Role of CH_4 oxidation, production and transport in forest soil CH_4 flux. Soil Biol. and Biochem., 33, 1625-1631.

Businger, J.A., Oncley, S.P. (1990) Flux measurement with conditional sampling. J. Atmos. Oceanic Technol., 7, 349–352.

Denmead, O.T. (1994) Measuring fluxes of CH_4 and N_2O between agricultural systems and the atmosphere. In: Peng S, Ingram KT, Neue H-U, Ziska LH (eds) Climate change and rice. International Rice Research Institute, Manila, Philippines.

Detto, M., Verfaillie, J., Anderson, F., Xu, L., Baldocchi, D. (2011) Comparing laser-based open-and closed-path gas analyzers to measure methane fluxes using the eddy covariance method. Agri. For. Meteorol., 151, 1312–1324.

Dobbie, K.E., Smith, K.A., Christensen, S., Degorska, A., Orlanski, P. (1996) Effect of land use on the rate of methane uptake by surface soils in Northern Europe. Atmos., Environ., 30, 1005-1011.

Dunfield, P., Knowles, R., Dumont, R., Moore, T.R. (1993) Methane production and comsumption in temperate and subarctic peat soils: response to temperature and pH. Soil Biol. Biochem., 25, 321-326.

Foken, T., Wichura, B. (1996) Tools for quality assessment of surface-based flux measurements. Agric. For. Meteorol., 78, 83–105.

Hamotani, K., Uchida, Y., Monji, N., Miyata, A. (1996) A system of the relaxed eddy accumulation method to evaluate CO_2 flux over plant canopies. J. Agric. Meteorol., 52(2), 135–139.

Hamotani, K., Monji, N., Yamaguchi, K. (2001) Development of a long-term CO_2 flux measurement system using REA method with density correction. J. Agric. Meteorol., 57(2), 93–99.

Hendriks, D.M.D., Dolman, A.J., van der Molen, M.K., van Huissteden, J. (2008) A compact and stable eddy covariance set-up for methane measurements using off-axis integrated cavity output spectroscopy. Atmos. Chem. Phys., 8, 431–443.

Hudgens, D.E., Yavitt, J.B. (1997) Land-use effects on soil methane and carbon dioxide fluxes in near Ithaca, New York. Ecoscience., 4(2), 214-222.

Ishizuka, S., Sakata, T., Ishizuka, K. (2000) Methane oxidation in Japanese forest soils. Soil Biol. Biochem., 32, 769-777.

Itoh, M., Ohte, N., Katsuyama, M., Koba, K., Kawasaki, M., Tani, M. (2005) Temporal and spatial variability of methane flux in a temperate forest watershed. J. Japan Soc. Hydrol. Water Resour., 18, 244–256. (in Japanese with English abstract).

Itoh, M., Ohte, N., Koba, K., Katsuyama, M., Hayamizu, K., Tani, M. (2007) Hydrologic effects on methane dynamics in riparian wetlands in a temperate Forest catchment. J. Geophys. Res., 112(G1):G01019.

Itoh, M., Ohte, N., Koba, K. (2009) Methane flux characteristics in forest soils under an East Asian monsoon climate. Soil Biol. Biochem., 41, 388–395.

Keller, M., Reiners, W.A. (1994) Soil-atmosphere exchange of nitrous oxide, nitric oxide, and methane under secondary succession of pasture to forest in the Atlantic lowlands of Costa Rica. Global Biogeochem. Cycles., 8(4), 99-409.

Kim, J., Verma, S.B., Billesbach, D.P. (1998a) Seasonal variation in methane emission from a temperate Phragmites-dominated marsh: effect of growth stage and plant-mediated transport. Global Change Biol., 5, 433–440.

Kim, J., Verma, S.B., Billesbach, D.P., Clement RJ (1998b) Diel variation in methane emission from a midlatitude prairie wetland: significance of convective throughflow in Phragmites australis. J. Geophys. Res., 103, 28,029–28,039.

Kosugi, Y., Katsuyama, M. (2007) Evapotranspiration over a Japanese cypress forest. II. Comparison of the eddy covariance and water budget methods. J. Hydrol., 334, 305–311.

Kosugi, Y., Takanashi, S., Tanaka, H., Ohkubo, S., Tani, M., Yano, M., Katayama, T. (2007)

Evapotranspiration over a Japanese cypress forest. I. Eddy covariance fluxes and surface conductance characteristics for 3 years. J. Hydrol., 337, 269–283.

Kroon, P.S., Hensen, A., Jonker, H.J.J., Zahniser, M.S., van't Veen, W.H., Vermeulen, A.T. (2007) Suitability of quantum cascade laser spectroscopy for CH_4 and N_2O eddy covariance flux measurements. Biogeosciences., 4, 715-728.

LeMer, J., Roger, P. (2001) Production, oxidation, emission and consumption of methane by soils: a review. Eur. J. of Soil Biol., 37, 25–50.

Long, K.D., Franagan, L.B., Cai, T. (2010) Diurnal and seasonal variation in methane emissions in a northern Canadian peatland measured by eddy covariance. Global Change Biol., 16, 2420–2435.

McDermitt, D., Burba, G., Xu, L., Anderson, T., Komissarov, A., Riensche, B., Schedlbauer, J., Starr, G., Zona, D., Oechel, W., Oberbauer, S., Hastings, S. (2011) A new low-power, open-path instrument for measuring methane flux by eddy covariance. Appl Phys., B102, 391-405.

McMillen, R.T., (1988) An eddy correlation technique with extended applicability to non-simple terrain. Boundary-Layer Meteorol., 43, 231–245.

Miyata, A., Leuning, R., Denmead, O.T., Kim, J., Harazono, Y. (2000) Carbon dioxide and methane fluxes from an intermittently flooded paddy field. Agri. For. Meteorol., 102, 287–303.

Ohkubo, S., Kosugi, Y. (2007) Amplitude and seasonality of storage fluxes for CO_2, heat and water vapor in a temperate Japanese cypress forest. Tellus., 60B, 11–20.

Ohkubo, S., Kosugi, Y., Takanashi, S., Mitani, T., Tani, M. (2007) Comparison of the eddy covariance and automated closed chamber methods for evaluating nocturnal CO_2 exchange in a Japanese cypress forest. Agric. For. Meteorol., 142, 50–65.

Prime, A., Christensen, S. (1997) Seasonal and spatial variation of methane oxidation in a Danish spruce forest. Soil Biol. Biochem., 29, 1165-1172.

Ruppert, J. (2002) Eddy sampling methods for the measurement of trace gas fluxes, Diploma thesis,

95pp, University of Bayreuth.

Savage, K., Moore, T.R., Crill, P.M. (1997) Methane and carbon dioxide exchanges between the atmosphere and northern boreal forest soils. J. Geophys. Res., 102:29279–29288.

Schrier-Uijl, A.P., Veenendaal, E.M., Leffelaar, P.A., van Huissteden, J.C., Berendse, F. (2009) Methane emissions in two drained peat agro-ecosystems with high and low agricultural intensity. Plant Soil., doi:10.1007/s11104-009-0180-1.

Schuepp, P.H., Leclerc, M.Y., MacPherson, J.I., Desjardins, R.L. (1990) Footprint prediction of scalar fluxes from analytical solutions of the diffusion equation. Boundary-Layer Meteorol., 50, 335–373.

Silver, W.L., Lugo, A.E., Keller, M. (1999) Soil oxygen availability and biogeochemistry along rainfall and topographic gradients in upland wet tropical forests soil. Biogeochemistry., 44, 301–328.

Simpson, I.J., Thurtell, G.W., Kidd, G.E., Lin, M., Demetriades-Shah, T.H., Flitcroft, I.D., Kanemasu, E.T., Nie, D., Bronson, K.F., Neue, H.U. (1994) Tunable diode laser measurements of methane fluxes from an irrigated rice paddy field in the Philippines. J. Geophys. Res., 100, 7283–7290.

Smeets, C.J.P.P., Holzinger, R., Vigano, I., Goldstein, A.H., Röckmann, T. (2009) Eddy covariance methane measurements at a Ponderosa pine plantation in California. Atmos. Chem. Phys., 9, 8365–8375.

Takanashi, S., Kosugi, Y., Tanaka, Y., Yano, M., Katayama, T., Tanaka, H., Tani, M. (2005) CO_2 exchange in a temperate Japanese cypress forest compared to that in a cool-temperate deciduous broadleaved forest. Ecol. Res., 20, 313–324.

Ueyama, M., Hamotani, K., Nishimura, W. (2009) A technique for high-accuracy flux measurement using a relaxed eddy accumulation system with an appropriate averaging strategy. J. Agric. Meteorol., 65(4), 315–325.

van den Pol-van Dasselaar, A., van Beusichem, M.L., Oenema, O. (1998) Effects of soil moisture content and temperature on methane uptake by grasslands on sandy soils. Plant Soil., 204, 213-222.

Wang, F.L., Bettany, J.R. (1997) Methane emission from Canadian prairie and forest soils under short term flooding conditions. Nutr. Cycling Agroecosyst., 49, 197–202.

Webb, E.K., Pearman, G.I., Leuning, R. (1980) Correction of flux measurements for density effects due to heat and water vapour transfer. Q., J. R. Meteorol., 106, 85–100.

Whalen, S.C., Reeburgh, W.S., Sandbeck, K.A. (1990) Rapid methane oxidation in a landfill cover soil. Appl Environ Microbiol., 56(11), 3405-3411.

Yamane, I., Sato, K. (1961) Effect of temperature on the formation of gases and ammonium nitrogen in the water-logged soils. Sci. Rep. Res. Inst. Tohoku Univ. D(Agr)., 12, 31-46.

CHAPTER 6

Summary and conclusions

I examined the CH_4 dynamics in a temperate Asian monsoon forest, which included an area of wetland within the watershed. In order to reveal the spatially and temporally variable CH_4 dynamics, I combined plot-scale CH_4 flux measurements using chamber methods and ecosystem-scale CH_4 flux measurements using a micrometeorological method. The combined approach enabled the examination of ecosystem-scale CH_4 fluxes with an understanding of variability in CH_4 fluxes at each compartment level, thereby clarifying processes that determine variability in ecosystem-scale CH_4 fluxes.

In Chapter 2, I used manual chamber measurements to determine the general spatial and temporal variability of CH_4 fluxes in the wetland and within the water-unsaturated forest floor. This showed that the wetland had a greater spatial and temporal variability of CH_4 fluxes than the forest floor. It is therefore suggested to be necessary to accurately consider the effect of any wetland areas when evaluating the CH_4 budget within forests. It has been suggested that CH_4 emissions from wetlands have a greater influence on seasonal variations of ecosystem-scale CH_4 fluxes, than CH_4 absorption by the forest floor. The CH_4 fluxes at KEW exhibited large spatial variability with reference to both emission and absorption, compared to those in wetlands or forest floors reported in North America and Europe. In the wetland, hotspots of CH_4 emissions were observed during summer and fall immediately after intensive precipitation. In the water-unsaturated forest floor, seasonal variations of CH_4 fluxes were not simply associated with temperature variations. However, some measurement plots showed an increase in CH_4 absorption in spring before intensive summer rainfall, and this is considered to be related to the relatively dry soil environment in spring, whereas a reductive environment would be established by the

intensive rainfall occurring in fall. The result of this chapter suggested that it is necessary to investigate the CH_4 dynamics of each compartment, such as the water-unsaturated forest floor and the anaerobic wetland, to reveal comprehensive CH_4 fluxes in forests.

In Chapter 3, I described the environmental responses of CH_4 fluxes at a half-hourly time resolution, by using automated chamber measurements on the water-unsaturated forest floor. I found that the highest CH_4 absorption flux was observed within the summer; however, the CH_4 absorption flux was greatly weakened by summer intensive rainfall, but recovered and peaked after rainfall as the soil water content decreased. The seasonal variation could not be detected using the biweekly manual measurements presented in Chapter 2. The relationship between CH_4 absorption fluxes and soil temperature varied more than that of CO_2 within each plot because CH_4 absorption fluxes were strongly affected by the soil water content. Notably, the relationship between CH_4 absorption flux and soil temperature, or CH_4 absorption flux and soil water content, differed depending on the physical conditions of the soil, such as soil water content and organic matter content. Over short time intervals (30 min), the responses of CH_4 and CO_2 fluxes to rainfall were also different depending on the physical soil conditions that influences gas diffusivity and the balance of activity between methanotrophs and methanogens. The response also changed depending on the amount of rainfall. Therefore, when evaluating the expected CH_4 absorption flux in forests, it is important to consider the responses of CH_4 fluxes to rainfall, particularly in the Asian monsoon climate. The Asian monsoon rainfall was found to strongly influence temporal variations in CH_4 fluxes, and the differences in flux response to environmental factors among plots caused large variability in the annual budgets of CH_4 fluxes. Simultaneous measurements of CO_2 fluxes would thus provide useful information when considering the controlling factors affecting complex CH_4 fluxes in terms of gas diffusivity and microbial activity. In this chapter, I revealed the environmental responses particular to CH_4 fluxes, which are evidently different from

CO_2 fluxes.

In Chapter 4, I investigated the validation of the coefficient *b*, which results in uncertainties in the relaxed eddy accumulation (REA) method. The consistency of *b* for temperature was investigated using a one-year dataset obtained at three forest sites in East Asia: a temperate evergreen coniferous forest, a tropical evergreen broadleaf forest, and a cool-temperate deciduous coniferous forest. I also introduced a new expression for *b*, similarity *b*, to investigate the nature of *b*, where similarity *b* is based on scalar similarity using the integral turbulence characteristics. Both observational and similarity *b* were found to increase with increasing atmospheric stability under stable conditions, and the values of b_{obs} under stable conditions were significantly different between the sites. The value of *b* increased under calm conditions such as stable conditions, or with a low standard deviation of vertical wind velocity, probably due to a lower contribution of the large eddy motion. Such calm conditions mainly occurred at nighttime. As a result, if a constant value for *b* were to be used for the REA method, nighttime fluxes would be underestimated. Consequently, the chapter recommended that it is important to determine the coefficient *b* for unstable conditions for each site and then consider changes in *b* associated with atmospheric stability, in order to minimize errors in the REA method.

In Chapter 5, I showed an ecosystem-scale CH_4 flux using the REA method. The observations revealed how the entire forest ecosystem complexly switched between being a CH_4 sink or source on hourly, diurnal, and seasonal scales. The Japanese cypress forest switched seasonally between being a sink and source of CH_4, probably because of competition by methanogens and methanotrophs, which are both influenced by soil conditions (e.g., soil temperature and soil moisture). At hourly to daily timescales, the CH_4 fluxes were sensitive to rainfall, probably because CH_4 emissions increased, and/or absorption decreased during and after rainfall. The observed ecosystem-scale fluxes showed complex behaviors beyond those expected from

previous plot-scale measurements. As micrometeorological methods provide spatially integrated fluxes with high temporal resolutions, using such methods to measure CH_4 flux is particularly important when investigating CH_4 dynamics in forest ecosystems. Chapter 5 suggested that forest ecosystem-scale CH_4 fluxes can be compared between various ecosystems. Although the range in the temperate forest was smaller than that of the wetlands or paddy fields, it was not negligible. Temperature has a great influence on CH_4 fluxes in ecosystems such as wetlands and rice paddies. In general, increasing temperatures accelerate CH_4 production in relation to the methanogenic bacteria in the soil, and enhance CH_4 transport from soil, by promoting ebullition through an increase in bubble volume and repartition of CH_4 to gaseous phase, as well as promoting plant-mediated transport through greater pressurized ventilation, and consequently CH_4 bulk flow in the aerenchyma. Compared to such ecosystems, the CH_4 dynamics in the forest have a complex relationship with temperature, because both CH_4 emissions and absorption are considered to occur within a forest, and increasing temperature enhances both activities. The two-directional CH_4 dynamics mean that it is difficult to understand CH_4 dynamics in forests, and longer observation times are needed to clarify this. In Chapter 5, I demonstrated that the REA method is applicable for measuring CH_4 flux over a large representative area. However, an improvement of the system and longer-term observations are required to evaluate the controlling factors for methanogens and methanotrophs activity in the CH_4 dynamics of forest ecosystems.

A combined approach using chamber and micrometeorological methods is particularly important when evaluating the ecosystem-scale CH_4 exchange and the detailed processes involved. The manual and automated chamber measurements used in this study indicated that there was considerable heterogeneity in CH_4 fluxes both spatially (hotspots) and temporally (hot moments), which had a substantial influence when up-scaling when compared to the result using the REA methods. Ecosystem-scale CH_4 flux using the REA method showed sporadic CH_4 emissions

seasonally from summer to fall, and in relation to meteorological events, such as after rainfall in most cases. In chamber measurements, high CH_4 emissions were observed in the wetland from summer to fall (see Chapter 2), and the CH_4 absorption showed a distinct depression at the peaks of rainfall intensity on the water-unsaturated forest floor (see Chapter 3). Recovery of CH_4 absorption was slow on the water-unsaturated forest floor after rainfall. As the CH_4 flux is determined from the balance between CH_4 emission and absorption, the increased CH_4 emission in the wetland and/or the decreased CH_4 absorption on the water-unsaturated forest floor were suggested to influence the ecosystem-scale CH_4 emission flux. In addition, a large, ecosystem-scale CH_4 absorption was observed in spring 2010, related to an increase in soil temperatures and a decrease in soil water content. Chamber measurements also showed that the largest CH_4 absorption was also observed in the spring with a low antecedent rainfall, as shown in Chapter 2. In a forest ecosystem, the soil water status has a heterogeneous distribution, and therefore it was suggested that micrometeorological measurements are important to evaluate total CH_4 fluxes, and further studies using simultaneous micrometeorological and chamber-based measurements of CH_4 fluxes are necessary for a comparison.

This is the first report showing a consistency between measurements of plot-scale CH_4 dynamics using chamber measurements and ecosystem-scale CH_4 dynamics using REA measurements. The results show that a temperate Asian monsoon forest acts as a CH_4 source seasonally on an ecosystem-scale, through the CH_4 fluxes occurring in the wetland or on the water-unsaturated forest floor in response to changing soil temperatures and/or the soil water status. These results are meaningful in considering the role of forest ecosystems in relation to global CH_4 budgets.

ACKNOWLEDGEMENTS

Many people have contributed to this work and supported me during my doctoral research. First, I would like to acknowledge Prof. Makoto Tani and Assistant Prof. Yoshiko Kosugi in the laboratory of Forest Hydrology, Kyoto University who providing countless hours of guidance and support to help me complete my research. Prof. Tani taught me the significance to proceed field work and the attitude to struggle with understanding the complex relationship between forest ecosystem and environment. Assistant Prof. Kosugi provided me the basis for the entire research, many discussions on the experimental design and encouragement. I was always inspired by her diligent and enjoying attitude to researches.

I would like to appreciate Prof. Kanehiro Kitayama and Prof. Shigeto Kawashima for providing their valuable comments on my manuscript.

I would like to thank Dr. Ken Hamotani who have provided invaluable assistance and advice for his exceptional knowledge and experiences on micrometeorological flux measurement technique, relaxed eddy accumulation method. I wish to acknowledge valuable suggestions and encouragement from Dr. Yoshinobu Harazono for his significant knowledge and experience of the overall field of micrometeorology. I would like to appreciate Dr. Kenshi Takahashi for coping with technical problems on CH_4 analyzer and providing me many creative advices throughout my research. I am deeply grateful to Dr. Masahito Ueyama who gives me constructive comments and warm encouragement. Without his persistent help, this dissertation would not have materialized. I would like to express special acknowledgement to Dr. Masayuki Itoh for supporting my field studies and providing valuable advices throughout my research. I express my gratitude to Prof. Takashi Hirano and Dr. Ryuichi Hirata for providing their data and many constructive advices. I would like to give special thanks to Dr. Akira Miyata, Dr. Masayoshi Mano, and Dr. Keisuke Ono for providing suggestive advices and taking time to discuss my research.

I would like to specially thank Dr. Hiroki Iwata, Mr. Akito Kanazawa, Ms. Mioko Ataka, and Ms. Chika Okumi, who assisted my field research and provided suggestive comments. I would like to thank the members like a family of Laboratory of Forest Hydrology, Kyoto University for guidance and huge help. Special thanks to Ms. Michiko Fukuda, Dr. Masanori Katsuyama, Dr. Kazuho Matsumoto, Dr. Motonori Okumura, Dr. Natsuko Yoshifuji, Dr. Kenji Tsuruta, Dr. Mai Kamakura, Dr. Shinjiro Ohkubo, Dr. Naoki Makita, Mr. Shuhei Kanemitsu, Mr. Satoshi Nishimoto, Ms. Michiko Shimizu, Mr. Koichiro Majima, Mr. Kenta Iwasaki, Mr. Megumi Yajima, Mr. Jun Tsuruta, Mr. Ryuhei Nagano, Ms. Kana Takaki, Mr. Hiroyuki Yamamoto, Mr. Yotaro Tanaka, Ms. Rie Takagi, Mr. Syohei Komatsu, Ms. Emi Kawai and Mr. Shimpei Yamamoto for their support during my field and lab works.

Finally, I would like to thank the countless people who provided emotional support during my doctoral research. The utmost thanks go to my parents and my family for their encouraging attitude toward my research work.

Ayaka Sakabe